Incorporation of silver nanoparticles and eucalyptus oil onto electrospun hemp/PVA nanofibres and their antibacterial activity

A Dissertation submitted to the Faculty of Applied and Computer Sciences,

Vaal University of Technology, in fulfilment of the requirement for the degree of Magister Technologiae: Chemistry.

by

Student Name: Ms Lebogang Mogole

Student Number: 217240682

Supervisor :

Prof. Makwena Justice Moloto (VUT, Department of Chemistry)

Co-supervisors:

Dr. Elvera Viljoen (VUT, Department of Chemistry)

Dr. Wesley Nyaigoti Omwoyo (Maasai Mara University)

Academic year 2021

DECLARATION

I, Lebogang Mogole, student number 217240682, declare that this research is my own. It has been submitted in partial fulfilment for the degree of Magister technologiae Chemistry in the faculty of Applied and Computer Sciences at the Vaal University of Technology. It has not been submitted for any degree or examination in any other university.

Signature ……. Date……..

DEDICATION

I dedicate this dissertation to my dear parents,

Caroline Gaolebale Mogole and Pule Abel Mogole

CONFERENCE PRESENTATIONS

1. Oral presentation: Mogole L, 3rd VUT interdisciplinary research and postgraduate conference (Vaal University of Technology) (17/8/2018), Antioxidant activity and α-amylase inhibition study using different extracts of *Eriobotrya japonica*
2. Poster presentation: Mogole L, 43rd National convention of the South African chemical institute held at the CSIR-ICC in Pretoria, South Africa (12/2018): Antioxidant activity and α-amylase inhibition study using different extracts of *Eriobotrya japonica*
3. Mogole L, 9th annual DAAD South Africa conference; Science communication, (9/2019), Johannesburg: Incorporation of silver nanoparticles and *Eucalyptus* oil into PVA/CNC polymer fibres and their antibacterial activity.

LIST OF PUBLICATIONS

Publications

1. L. Mogole, W N Omwoyo, F M Mtunzi, Phytochemical screening, anti-oxidant activity, and α-amylase inhibition study using different extracts of loquat (*Eriobotrya japonica*) leaves, doi.org/10.1016/j.heliyon.2020.e04736, 6 (8),2020.

Manuscripts under preparation

2. L. Mogole, M. J. Moloto, W. N. Omwoyo, E. L. Viljoen, Synthesis of silver nanoparticles from aqueous extracts of *Citrus sinensis* peels to be submitted to,, Journal of nanoparticles synthesis".
3. L. Mogole, M. J. Moloto, W. N. Omwoyo, E. L. Viljoen, Hemp generated cellulose nanocrystals and their polyvinyl alcohol blended fibres using electrospinning technique, to be submitted to the journal,, Polymers and Fibres".

ABSTRACT

The world is continuously losing the battle against superbugs (resistant bacteria towards commonly used antibiotics), hence there is an urgent need to develop novel antibacterial agents. In this study, green synthesized silver nanoparticles (AgNPs) and eucalyptus oil, were incorporated into the polymer blend fibres of polyvinyl alcohol (PVA) and cellulose nanocrystals (CNC's). Various techniques were used to characterize the AgNPs, PVA/CNC polymer fibres, and PVA/CNC incorporated with AgNPs/eucalyptus oil. The morphology of AgNPs synthesized using an increasing concentration of the *Citrus sinensis* peels (CSP) extract was obtained from transmission electron microscopy (TEM). AgNPs synthesized using 1 and 2 % m/v (CSP) were agglomerated and whereas those synthesized using 3 % m/v of the extract were spherical with an average particle size 10 ± 1.2 nm. UV/Visible absorption spectra for all the synthesized AgNPs exhibited a surface plasmon resonance (SPR) peak at around 400 nm which is a characteristic peak of silver. Significant shifts in the absorption peaks or maxima were observed to signify changes in the shape and size of the nanoparticles.

Scanning electron microscopy (SEM) was used to study the morphology of the fabricated polymer fibres. The Addition of CNC's to PVA resulted in an increase in fibre diameter due to an increase in viscosity of the solution. An increase in the concentration of silver nanoparticles and the eucalyptus oil in the PVA/CNC resulted in a decrease in fibre diameter due to an increase in conductivity of the material. The fibres with AgNPs were smooth while the ones with the eucalyptus oil were beaded. X-ray diffraction (XRD) showed the presence of the AgNPs in the polymer fibres and Fourier transform infrared (FTIR) showed the presence of the functional groups that are available in the eucalyptus oil. The antibacterial efficiency of the PVA/CNC incorporated with AgNPs, eucalyptus oil, and the mixture of AgNPs and the eucalyptus oil was investigated using *S. aureus* and *K. pneumoniae*. All the materials showed significant inhibition of the growth of the selected bacterial strains. PVA/CNC polymer fibres incorporated with AgNPs showed higher antibacterial activity compared to PVA/CNC polymer fibres incorporated with eucalyptus oil.

ACKNOWLEDGEMENTS

All the glory belongs to God who enabled me to complete this research, for giving me health and protecting me. I would like to acknowledge everyone who contributed and made the completion of this thesis a success.

I would like to express my sincere gratitude to my supervisor Prof M.J Moloto and co-supervisors, Dr. E L Viljoen and Dr. N W Omwoyo for the continuous support, guidance, and patience during the time of conducting experiments in the laboratory and writing of the thesis. My academic twin sister; Miss B.D Mabaso thank you for walking this journey with me, working overnight in the laboratory, and pulling each other up whenever things didn't make sense. Prof F.M Mthunzi, Dr. S.B Sibokoza, Mr. P.M Ngoy, and Mr. Z Nate thank you for all the contributions and academic advice.

A special thank you to my colleagues in C108, Miss P Mthombo, Miss M.C Qhubu, and Miss Z Nqaba for creating a supportive and friendly working environment. I am also thankful to the nanotechnology research group and Nanotechnology Catalysis Adsorption and Phytochemistry (NCAP) group for the guidance and support throughout this research.

The completion of experiments in the laboratory and writing of the thesis required more than academic support and I have many people to thank. My parents, Mrs. C.G Mogole and Mr. A.P Mogole thank you for your endless love, sacrifice, prayers, and supporting me in chasing my dreams. My one and only sister Miss M.N Mogole, thank you for planting a seed and believing in me. My friend, Miss L.G Mooketsi for always being available whenever I needed to vent even about the things you had no idea about.

Lastly, I would like to acknowledge the National Research Foundation (NRF) and the Vaal University of Technology (VUT) research directorate for the financial support, Chemistry department for providing equipment I needed to conduct my research and complete my thesis, department of biotechnology at the Vaal University of Technology, more especially Mr. H.D. Mokgope and Mr. G Mohlala for their assistance with the antimicrobial studies and Mr. Hennie Venter for supplying us with hemp fibres.

Table of Contents

LIST OF ABBREVIATIONS

AgNPs	:	Silver nanoparticles
ASE	:	Accelerating solvent extraction
ATP	:	Adenosine triphosphate
CNC’s	:	Cellulose nano-crystals
CSP	:	*Citrus sinesis* peels
CVP	:	*Chuonminshen violaceum polysaccharides*
EO	:	Eucalyptus oil (EO)
FCC	:	Face centered cubic
FTIR	:	Fourier transform infrared spectroscopy
FWHM	:	Full width at half maximum
INT	:	p-iodonitrotetrazolium chloride
K.p	:	*Klebsiella pneumoniae*
MH	:	Mueller-Hinton
MAE	:	Microwave assisted extraction method
MIC	:	Minimum inhibition concentration
PVA	:	Poly(vinyl alcohol)
RSM	:	Response surface methodology
SEM	:	Scanning electron microscopy
Sa	:	*Staphylococcus aureus*
SPR	:	Surface plasmon resonance
TEM	:	Transmission electron microscopy
TGA	:	Thermo-gravimetric analysis
UAE	:	Ultrasonic assisted extraction
UV-vis:	:	Ultraviolet-visible absorption spectroscopy
XRD	:	X-ray diffraction

LIST OF FIGURES

LIST OF TABLES

LIST OF SCHEMES

OUTLINE OF DISSERTATION

This dissertation consists of four chapters, where Chapter one gives the overall background of the study, literature review, rationale, and lastly, the aim and specific objectives of the study.

Chapter two provides detailed experimental procedures that were carried out to achieve the set objectives. Chapter three presents the results from various characterization techniques and their discussion. Chapter four provides the overall conclusion of the study and recommendations, respectively.

Chapter one

This chapter begins with the background study where the topic of the project is briefly described, this is followed by the literature reviews that surveys various studies that relate to the specific project and this includes studies that were based on the synthesis of nanoparticles (silver nanoparticles), The combination of metal nanoparticles (silver nanoparticles) and natural products (essential oils) as potential antibacterial agents with improved properties, the incorporation of both the nanoparticles and essential oil into polymer fibres to minimise the toxicity of the materials while providing controlled release of the metals nanoparticles/essential oils at effective levels. This chapter also consists of the rationale, aim, and specific objectives of the study.

Chapter two

Chapter two begins with a list of reagents that were utilised in conducting experiments, followed by the various techniques that were used to characterize the resultant samples. Specific methods that were used to extract bioactive compounds from *Citrus sinensis* peels and the synthesis of silver nanoparticles are described in this chapter. Furthermore, the fabrication of polymer nanofibres incorporated with silver nanoparticles and eucalyptus oil using the electrospinning technique is explained. Lastly, the antibacterial activity methods are covered.

Chapter three

This chapter presents the experimental results and discussion for each objective. The chapter begins with quantification of the bioactive compounds from the *Citrus sinensis* peels and the characterization of silver nanoparticles. This is followed by the characterization of the electrospun nanofibres. Lastly, the antibacterial efficiency of all the synthesised nanomaterials is discussed.

Chapter four

This chapter gives the overall conclusion of the research and recommendations for future work.

CHAPTER ONE

1.1 INTRODUCTION

1.1.1. BACKGROUND

The resistance of pathogenic bacteria towards commonly used antibiotics is increasing at an alarming rate worldwide. The resistant bacteria do not only increase the morbidity and mortality rate, but the treatment is also not cost-effective (Cavassin *et al*., 2015). Novel strategies and methods are required to overcome this problem. Silver containing systems and especially their nanoparticles are considered the strongest alternatives due to their previously reported interesting antibacterial activity against a broad spectrum of pathogenic bacteria at low concentrations and this is due to their unique chemical and physical properties and also the fact that they have a high surface to volume ratio (Hashim *et al.*, 2020; Vilela *et al.*, 2017). A stronger antibacterial activity can be achieved through the combination of metal nanoparticles and other antibacterial agents such as natural antimicrobials (Prasad *et al*., 2017). Essential oils are derived from non-woody parts of the plants through hydro-distillation. They contain a mixture of various compounds, mainly terpenoids and aromatic groups such as phenols, esters, aldehydes, and ketones. Throughout history, essential oils have been used as fragrances, condiments and in medicine, they are also used as antimicrobial agents and also used as a repellent for insects (Kaliamurthi *et al*., 2019). Eucalyptus oil (EO) is amongst the most traded essential oils in the world and this is due to its antibacterial, antiviral, and antifungal activity and also its long use against the effects of colds, influenza, other respiratory infections, rhinitis, and sinusitis through history (Sadlon & Lamson, 2010).

Direct application of either silver nanoparticles, eucalyptus oil, or their combination have some drawbacks. Silver nanoparticles have been reported to be toxic when exposed to them for a long time at high concentration and also the problem with the use of essential oils, is their high volatility and high sensibility towards light and oxygen which decreases their biological use thus multiple application is required to maintain its activity (Wu *et al*., 2015). The incorporation of silver nanoparticles and eucalyptus oil into polymer fibres will provide controlled release of both the silver nanoparticles and eucalyptus oil, at an effective level and this is due to the unique structure of polymer fibres, a high porosity, high surface to volume ratio, and many others (Dias Antunes et al., 2017; Ravindra et al., 2010; Syafiq et al., 2020).

Polyvinyl alcohol (PVA) is a semi-crystalline polymer known for its biocompatibility, biodegradability, excellent solubility in water, good spinnability, and ability to interact with a wide range of hydrophilic materials, and hence it has large industrial application (Augustine *et al*., 2018b). PVA is often combined with other polymers or fillers to enhance its performance and barrier properties. Cellulose nanocrystals are promising composite reinforcements to produce polymer composite with physicochemical properties (thermal, mechanical, and optical) even when added in small amounts (Ahmed *et al*., 2004). The main advantages of cellulose nano-crystals are low density, recyclable, positive ecological effects, and their high abundance in nature (Börjesson & Westman, 2015). The source of the cellulose controls the structure and size of the isolated cellulose nano-crystals and the functional groups present on the cellulose nanocrystals (CNC). Cellulose nanocrystals (CNCs) are derived from cellulose, which is one of the most abundant biopolymers that can be found in plants such as hemp, flex, and sugarcane bagasse (Slavutsky & Bertuzzi, 2014; Symington et al., 2009).

Different techniques such as chemical vapour deposition, phase separation, sol-gel method, thermal oxidation, and electrospinning can be used to incorporate metal nanoparticles into synthetic and natural polymers. However, the electrospinning technique is considered the best technique because it is simple, efficient, and cost-effective to set up, thus makes it more versatile compared to the other techniques (Kim *et al*., 2019; Leidy & Ximena, 2019). Schematic diagram 1:1 below shows the electrospinning set-up. An electric field is applied to a polymer solution that is held together by its surface tension in the capillary tube. The application of the electric field induces a charge on the surface of the liquid. An opposite force to the surface tension is formed due to the mutual repulsion. An increase in the intensity of the electric field results in the elongation of the surface of the solution to a conical shape. The polymer solution is released from the tip of the Tyler cone when the applied electric field reached a point in which the surface tension force is overcome by the repulsive force, As the jet is released from the tip, it travels in the air to the collection screen where it will form a non-woven mat from the continuous fibres (Doshi & Reneker., 1995).

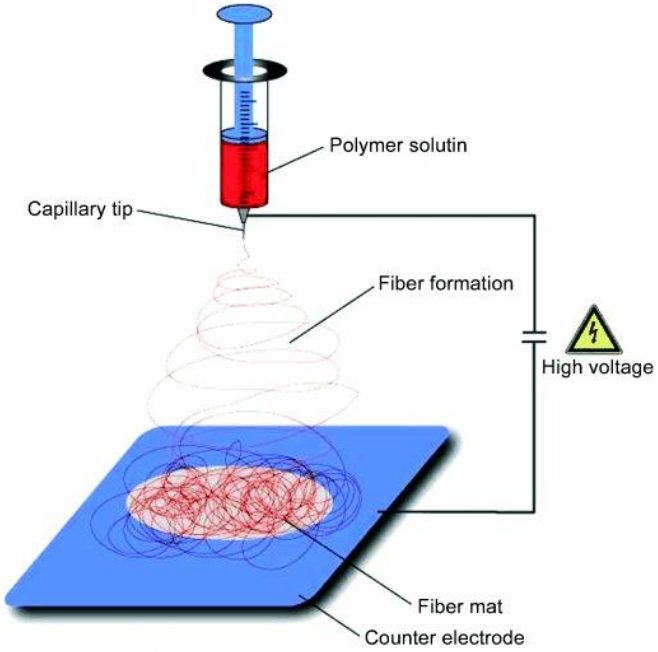

Scheme 1.1: Electrospinning set-up (Greiner & Wendorff, 2007).

1.2 LITERATURE REVIEW

1.2.1. Properties of silver nanoparticles

The science that deals with the preparation of materials in their nanoscale (1-100 nm) is known as nanotechnology (Sharma *et al*., 2009a). Metal-based nanoparticles are used in a broad range of applications from daily life products such as textiles, food products, and personal care products. Nanomaterials provide solutions to environmental and technological changes in areas such as water treatment, medicine, solar energy conversion, and catalysis. Decreasing the size of the material to its nanoscales improves its optical, electrical, and biological properties thus justify its use in different fields such as physics, medicine, organic and inorganic chemistry. Silver, platinum, and gold metallic nanoparticles have been reported to have health benefits compared to their bulk material. These materials are used in catalysis and sensor technology (Govindrao *et al*., 2019; Thomas *et al*., 2019).

Silver nanoparticles specifically are extensively applied in many fields due to their unique properties such as thermal, electrical conductivity, and antimicrobial activities (Logeswari *et al*., 2013; Mochochoko *et al*., 2013). Silver nanoparticles have a surface plasmon resonance absorption in the ultravioletvisible region, when the free electron in the conduction band of the metal nanoparticles interact with light at a certain wavelength, an oscillation of electron occurs

in resonance and that results in the surface plasmon resonance band. Factors such as the size of the nanoparticles, chemical surroundings, the dielectric constant, and the species absorbed on the surface of the silver nanoparticles cause the surface plasmon band to shift. A shift in the higher wavelength (Red-shift) has been related to the presence of nanoparticles with bigger particle diameter while a shift in the lower wavelengths (Blue-shift) is due to a decrease in the diameter of the particle size. Further on change in absorption or wavelength provides information about the particle size, shape, and other inter particles properties (Smitha *et al*., 2008; Vasileva *et al*., 2011; Yeshchenko *et al.*, 2012).

1.2.2. Synthesis of nanoparticles

Top-down and bottom-up are the two strategies that can be used to synthesize nanoparticles. The top-down method involves the breaking down of bulk material into nano-sized materials while the bottom-up approach involves the development of molecular structure into the nanometer range using atoms and molecules. The major drawback with synthesizing nanoparticles through the top-down approach is that the synthesized nanoparticles may have defects on their surfaces which may influence both the physical and chemical properties of the nanoparticles (Thakkar *et al*., 2010). Different methods such as chemical reduction, electrochemical changes, photochemical reductions, and biological can be used to prepare nanoparticles. The selection of the method of preparation of nanoparticles is of importance since factors such as the interaction between the metal ion and the reducing agent as well as the interaction between the nanoparticles and the stabilizing agent influence the size, shape, stability, Physico-chemical properties, and yield of the synthesized nanoparticles (Barberia-roque *et al*., 2019; Ibrahim, 2015).

Physical methods used to prepare nanoparticles such as milling and the use of a furnace are expensive since they require a high amount of energy. For example (Darezereshki *et al*., (2011) synthesized zinc oxide (ZnO) nanoparticles by decomposition of the precursor $ZnCO_3$ at 825 °C for one hour which was prepared by mixing $ZnSO_4$ and Na_2CO_3 at 70 °C for 45 minutes. In another study, Hosseinpour-mashkani & Ramezani, (2014) synthesized AgNPs and Ag_2O by decomposition of silver salicylate complex at 400 °C for three hours which was prepared by mixing $AgNO_3$ and salicylate. Jeevanandam *et al*., (2010) also synthesized silver nanoparticles through the decomposition of silver acetate in diphenyl ether in the presence of oleylamine and oleic acid, the reaction was carried out for 5 hours at 120 °C.

Furthermore, chemical methods using complex organic capping molecules are not eco-friendly since they often require toxic chemicals as starting material and also release toxic or hazardous chemicals, leaving the environment devastated (Ren *et al*., 2019). Chemical reduction is the commonly used method to prepare nanoparticles. The method uses chemicals such as citrate, borohydride, and ascorbate as reducing agents. With this method, silver ion (Ag^{+}) in the solution is reduced to silver nanoparticles (Ag^{0}) with a diameter in the nano range. Borohydride ion is considered a strong reducing agent and often results in the synthesis of smaller nanoparticles. However, the generation of nanoparticles with a larger diameter is also uncontrollable. Citrate ion on the other hand is a weak reducing agent which results in slower reaction rates with better size distribution. The chemical reduction method often requires stabilizers to prevent agglomeration of nanoparticles (Luty-błocho *et al*., 2011).

1.2.3. Green synthesis of silver nanoparticles

Green chemistry has received significant attention from researchers because of the growing need to develop environmentally friendly material that focuses on the elimination or minimization of the usage of toxic chemicals. A method is considered "green'' depending on three aspects, the first one is the kind of solvent that was used, whether water was used or an organic solvent. The second one is, the type of reducing agent used (chemical or biological) and the third aspect covers the capping/stabilizing agent used (Li *et al*., 2007).

The biological synthesis of nanoparticles involves the use of fungi, bacteria, yeast, and viruses. Biological synthesis is regarded as safe, cost-effective, sustainable, and environmentally friendly. Biological microorganisms such as enzymes and bacteria can act as both reducing agents and stabilizing agents (Narayanan & Sakthivel, 2010; X. Zhang *et al*., 2011). The method is environmentally friendly but chemically complex. Biological synthesis has drawbacks which include culturing of microbes which is time-consuming. Further on, controlling the shape, size, and crystallinity of the biologically synthesized nanoparticles is difficult and the method is slow (Narayanan & Sakthivel, 2010). Kumar & Mamidyala, (2011) synthesized silver nanoparticles using the supernatant culture of *Pseudomonas aeruginosa*. The method required the pre-preparation of the *Pseudomonas aeruginosa* which took 72 hours. The synthesis reaction took 8 hours. TEM results showed the successful synthesis of the silver nanoparticles. Syed & Ahmad, (2012) synthesized platinum nanoparticles using the fungus *Fusarium oxysporum* and according to their method, 5 days was required to grow the fungus,

and this was followed by preparation of the subculture which required an additional 5 days to complete. The synthesis reaction was carried out for 96 hours. X-ray photon spectroscopy confirmed the successful synthesis of platinum nanoparticles with Pt, C, O and N as prominent elements.

The use of plant extracts has not been fully explored. Various plants have been used to synthesize silver nanoparticles. The plant extracts play a dual role in the synthesis of nanoparticles, firstly as reducing agents and secondly as stabilizers. Stabilization occurs to maintain distance between the particles, thereby avoiding aggregation which would result in fusion and finally forming bigger particles. In general, stabilization provides steric hindrance or electrostatic repulsion. This specific study will focus on the green synthesis of silver nanoparticles. This method is considered cost-effective. Plants are known for their intrinsic biological activity such as their antioxidant, antibacterial, antifungal, and anti-hypoglycaemic activity and it has been reported that the biological may also manifest in the final synthesized nanoparticles (Bar *et al*., 2009a; Ruíz-baltazar *et al*., 2019).

1.2.4. Effect of experimental parameters on the synthesis of silver nanoparticles

Experimental conditions such as time, temperature, pH, the concentration of the reducing agent, stabilizing agent, and precursor affect the stability, size, and morphology of the synthesized nanoparticles. Irrespective of whether the nanoparticles were physically and chemically synthesized.

(a) The effect of pH

The pH of the resultant solution, after mixing the metal precursor and the reducing agent/capping agent is one of the critical factors in controlling the shape and size of the synthesized nanoparticles. pH induces the reactivity of the leaf extract with silver ions and it has been reported to influence the yield, stability, and synthesis rate (Iravani & Zolfaghari, 2013). Abdel-halim & Al-deyab, (2011) studied the effect of pH on the formation of silver nanoparticles. Briefly, silver nanoparticles were synthesized using hydroxypropyl cellulose as both a reducing agent and stabilizing agent. The pH was adjusted using sodium hydroxide and sulphuric acid to pH 4, 7, 10, and 12.5. According to the UV-vis spectra, there were changes in the absorption spectra as the pH changes and the SPR band started to appear at pH 10 and maximum intensity was recorded at pH 10 with a narrow peak. No distinct peak was observed at pH 4 and 7 thus acidic conditions are not suitable for the synthesis of silver nanoparticles.

Mochochoko *et al*., (2013) also studied the effect that pH has on the synthesis of silver nanoparticles at different pH, 4, 7, and 11. It was observed that, as the pH increased the surface plasmon band became narrower, indicating that alkaline solution favours the synthesis of silver nanoparticles and according to the TEM images, the smallest nanoparticles in diameter (2.68 nm) was obtained at pH 11. Acidic environments promote the agglomeration of nanoparticles (Jorge de Souza *et al*., 2019). Further on, according to many other studies, it was found that as the pH increased, the colour of the reaction mixture turned brown which signified successful synthesis of the silver nanoparticles. In summary, lower pH/acidic mediums promote the formation of larger nanoparticles since the aggregation of the nanoparticles is favoured over nucleation. While higher pH/basic mediums promotes the formation of smaller nanoparticles as higher pH facilitates the nucleation and subsequent formation of a large number of nanoparticles with a smaller diameter.

(b) The effect of quantity of the plant extracts as reducing and a capping agent.

The quantity of the plant extract used affects the synthesis of the nanoparticles and also the characteristics of the synthesized nanoparticles. The concentration of the biological extract used, either plants or microorganisms is directly related to the phytochemicals present which can act as both the reducing and capping agent (Sadhasivam *et al*., 2020). Bar *et al*., (2009b) synthesized silver nanoparticles using plant extract of latex of *Jatropha curcas*. The effect that the increasing concentration of the plant extract (1,2 and 3 % m/v) on the synthesis of silver nanoparticles was studied, According to the UV-vis spectra, 3% m/v of the latex extract gave a more distinct and narrow SPR band. El Raey *et al*., (2019) synthesized silver nanoparticles using plant extracts of *Acalypha wilkesiana* flowers. The volume of the plant extract added to the silver nitrate solution was varied from 100 µL to 400 µL while the concentration of AgNPs and the volume were kept constant. The UV-vis spectrum of all the samples showed an SPR band at 446-462 nm which shows the successful synthesis of silver nanoparticles. According to the TEM images, the nanoparticles were separated from each other and were found to be mainly spherical. Nesrin *et al*., (2020) synthesized silver nanoparticles using *Rhododendran penticum* extracts of water and ethyl alcohol, according to the UV-vis spectra of AgNPs synthesized using water extract of the plant had and an SPR band at 431 while the AgNPs synthesized using ethyl alcohol showed an SPR band at 439 nm. The difference in the absorption band showed variation in particle size, further on according to the TEM images, the AgNPs synthesized using water extract of the plant showed good particle distribution of 12-19 nm while the particle size of AgNPs synthesized using ethyl alcohol had a particle distribution

of 16-40 nm. Hajji *et al*., (2017) studied the effect that different volumes (0.1, 1, and 5 mL) has on the synthesis of silver nanoparticles using Chitosan/PVA composite as a reducing agent and a stabilizing agent. The XRD results showed peaks at 2θ 43.18º, 44.14º and, 73.6º which can be indexed to characteristic Bragg diffraction planes (111), (200), and (311) of the face centred cubic crystalline structure of silver nanoparticles. The FTIR spectra of AgNPs showed characteristic peaks of both chitosan and PVA however with decreased intensities and a shift in the frequency. The change in frequency and wavenumbers shows possible interaction between the CS/PVA blend and the AgNPs.

1.2.5. Citrus sinensis

Among the different plants used *Citrus sinensis* peels are an attractive source of many biological compounds, such as phenols. Approximately 140 million of citrus fruits are produced annually worldwide, thus considered one of the important fruits. *Citrus sinensis,* commonly known as the orange fruit, accounts for about 70 % of the produced citrus species. *Citrus sinensis* is often consumed as fresh fruits or used to make orange juice, and after consumption, the peels which contribute to about 50 % of the mass of the fruit are discarded (Abbate *et al*., 2012; Balasundram *et al*., 2006).

Organic compounds found in plants, such as phenols, flavonoids alkaloids, and steroids can aid in the synthesis of nanoparticles. Orange peels also contain compounds such as phenolic and flavonoids that have been reported to have human health benefits such as antimicrobial and antioxidant activity (Gorinstein *et al*., 2001). The following compounds can also act as potential reducing and capping agents for the synthesis of stabilized silver nanoparticles (Behravan *et al*., 2019; Garriga *et al*., 2019). Flavonoids found in Citrus plants are known for their broad spectrum of biological effects including anticancer, antiviral, antifungal, and antibacterial activities. Flavonoids can also function as antioxidants. Dhanavade *et al*., (2011) extracted biological active compounds from *Citrus aurantuium* (lemon) using acetone, methanol, and ethanol and tested their antibacterial activity against *Micrococus aureus*, *Pseudomanas aeruginosa*, and *Salmonella typhimurium*. The results showed that all the extracts gave significant antibacterial activity. Kaviya *et al*., (2011) synthesized silver nanoparticles using the extracts of *Citrus sinensis* peels at 25 and 60 ℃. As the metal precursor ($AgNO_3$) was added to the plant extracts the colour of the solution changed to brown due to the excitation of the surface plasmon vibrations. According to the UV-vis spectra, the wavelength decreased from 445 nm to 425 nm as the temperature was raised from 25 ℃ to 60

℃ which shows higher temperature favours the formation of smaller nanoparticles. The TEM results support the UV-vis spectroscopy results since smaller nanoparticles with the particle of 10 nm were observed at 60 ℃, while at 25 ℃ the average particle size was 35 nm.

1.2.6. Extraction methods

During the extraction of bioactive compounds from plants, selective solvents and extraction methods are used to separate medicinally active portions in plants. The main objective of extraction is to separate the soluble plant metabolites from the insoluble residue. Biologically active compounds occur in low concentrations thus selection of a suitable extraction technique, solvent, and optimisation of various parameters is essential. Ideal extraction techniques are those that give a higher percentage yield of the desired compounds at shorter extraction times, using minimum solvents and energy, thus minimising costs. The technique should also be environmentally friendly, safe, and reliable to use (Barba *et al*., 2016). The fundamental step in the investigation of bioactive compounds from plants is extraction; this involves steps such as rinsing the plant with water to remove dust, drying of the plant material at room temperature or freeze-drying, and, grinding of the plant material.

(a) Soxhlet extraction method

The Soxhlet extraction method operates at low pressure and solvents boiling point. The technique is quite selective; it is usually used for the recovery of oil and fatty constituents. The principle of the Soxhlet extraction method involves filling the boiling flask with a suitable solvent as seen in the Schematic diagram 1.2. below, followed by loading the crushed plant material into the thimble. Upon heating, of the boiling flask, the solvent will evaporate passing through the left sidearm of the extractor, cooling down to suitable temperature while condensing in the condenser. The condensate will then drip into the thimble. As soon as the level of the solvent reaches the siphon arm, it is discharged back into the flask through the siphon sidearm and the cycle begins again (Luque-García & Luque De Castro, 2004). The method requires quite a large solvent volume and takes a longer time, thus it is considered expensive since it also uses electricity. Prolonged extraction time and excessive temperature result in the degradation of significant components, hydrolysis, and oxidation of compounds (Luque de Castro & García-Ayuso, 1998). Sati *et al*., (2018) investigated the antimicrobial, antioxidant, and yield of the ginkgo plant using the Soxhlet and maceration extraction methods. The soxhlet extraction method was found to be more effective compared to maceration. Xu *et al*., (2017) optimised and compared the ultrasonic-assisted extraction (UAE) and Soxhlet-

assisted extraction of natural antioxidants from the flowers of *Limonium sinuatum*. The operating conditions for UAE were 60 % ethanol, 40 ℃ and the extraction time was 9.8 minutes. On the other hand, the optimum operating conditions for the Soxhlet technique were 60 % ethanol solution, 95 ℃ and the extraction time was 4 hours. The comparative study showed that the antioxidant activities of the flower extracts using UAE were significantly higher than that of the Soxhlet technique. Lopresto et al., (2014) evaluated a non-conventional method to extract D-limonene from waste lemon peels and compared it with the traditional Soxhlet extraction technique. The optimum operating conditions for the Soxhlet technique were as follows: 1:25 solid/liquid ratio, 68 °C, and the extraction time was 4 hours.Another study by (Rodríguez-Solana et al., 2014) optimised and compared accelerating solvent extraction (ASE) with the Soxhlet technique for the extraction of fennel from estragole. The optimum conditions of accelerated solvent extraction were 125 ℃, 7 minutes at three cycles. The optimum operating extraction time for the Soxhlet extraction technique was 8 hours, however, a yield of 6.60 g/kg was obtained for ASE when operated for 30 minutes and a yield of 6.99 kg was obtained for the Soxhlet technique when operated for 8 hours. ASE was considered more efficient compared to the Soxhlet technique since it requires less solvent and saves time.

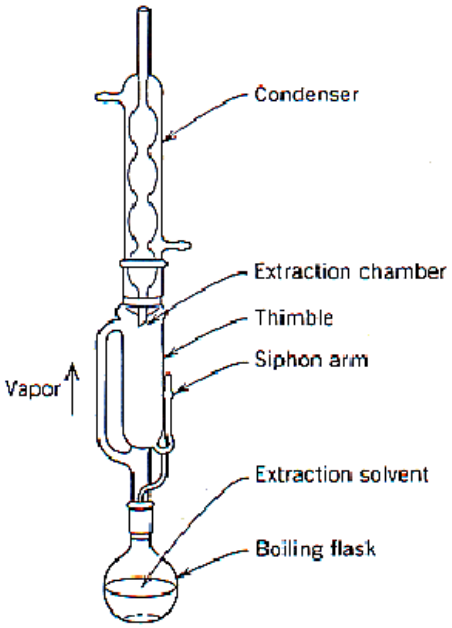

Scheme 1.2: Typical apparatus of the soxhlet extraction (Yue *et al.*, 2018).

(b) Maceration extraction method

Maceration involves soaking of the plant material usually in the form of a powder obtained from grinding in a stoppered container, containing a solvent of interest. The process involves stirring the material at desired intervals and temperature (Albuquerque *et al*., 2017). The process releases soluble bioactive compounds into the solvent by breaking the plant cell walls. The efficacy of maceration is determined by the solubility and effective diffusion (Cheok *et al*., 2012). However, this method is considered time-consuming and requires a lot of solvents (Yolmeh *et al*., 2014). Milić *et al*., (2013) optimised and compared maceration extraction method and ultrasonic-assisted extraction of resinoid from aerial parts of *Gallium mollugo* using 50 % aqueous ethanol solution at various temperatures. The optimum extraction temperature for maceration was 80 and 40 °C for ultrasonic-assisted extraction. A yield of 22 g/100 g for four hours and 25.1 g/100 g in 30 minutes was obtained for maceration-assisted extraction and ultrasonic assisted extraction, respectively. Ultrasonic assisted extraction was shown to be more effective in extracting resinoid since it gave a better yield at low temperatures and in minimum time. Another comparative study was done by (Vieira *et al*., 2017) to optimise and compare maceration and microwave-assisted extraction of phenolic compounds from *Juglans regia*. The optimum operating conditions for maceration were 112.5 minutes, 61.3 ℃ and the concentration of ethanol solution used was 50.4 %, while the operating conditions for microwave-assisted extraction were 3.0 minutes, temperature 107.5 °C and 67.9 % for the ethanol solution. Microwave-assisted extraction was shown to have a higher yield at a shorter timer compared to maceration, thus considered more efficient.

Deng *et al*., (2017) also optimised maceration and ultrasonic-assisted extraction of phenolic compounds from fresh olives. The optimum conditions for maceration were 50 ℃, 4.7 hours and the liquid-solid ratio was 24 mL/g. The optimum operating conditions for ultrasonic-assisted extraction were 47 ℃, 30 minutes and the liquid-solid ratio was 22 mL/g. A yield of 22 and 5.98 mL/g was observed for ultrasonic-assisted extraction and maceration-assisted extraction, respectively. Ultrasonic-assisted extraction exhibited higher amounts of phenolics at shorter periods, thus considered more efficient. Ćujić *et al*., (2016) optimised maceration assisted extraction of polyphenols from dried chokeberry. The optimum operating conditions were 0.75 mm size of berries, 50 percent ethanol, and the solid to liquid ratio of 1:20. The predicted values of 27.7 mg GAE/g for phenolics and 27.7 mg GAE/g were obtained for the experiment.

(c) Microwave-assisted extraction method

The principles of microwave-assisted extraction is based on two steps; the first step is known as the dielectric heating step, which involves the movement of solvent based on their dipole moments, which results in heating of the solvent. The second step is called ionic conduction and is based on the heating of a solvent as a result of ions rubbing against the solvent (Sanchez-Prado *et al*., 2015). The technique is based primarily on immersing a sample in a clear solvent and placing the mixture of the solvent and sample inside the microwave, which results in heating of the sample, then rupturing the cell wall, which increases mass transfer. The method is considered rapid, simple, economical, and efficient since it requires minimal amounts of solvent and the extraction period is quite short (Chan et al., 2014). Dong *et al*., (2016) extracted *Chuonminshen violaceum* polysaccharides (CVPs) using conventional heated reflux extraction, ultrasonic-assisted extraction, and microwave-assisted extraction (MAE). The results revealed that MAE gave the highest percentage yield of polysaccharides at a lower temperature and shorter extraction time compared to all the extraction methods. In another study, (Lefsih *et al*., (2017) extracted pectin from *opuntia ficus*- using MAE and evaluated the optimum conditions. The optimum conditions for extraction of pectin were pH 2.26, 517 W microwave power, 2 g/30.66 mL of solid to liquid ratio, and 12.56 % of pectin was recovered.

Wang *et al*., (2007) extracted pectin from apples pomace using microwave-assisted extraction method and optimised the extraction method using response surface methodology (RSM). Factors such as the duration in which the extraction takes place, pH of HCl solution, the ratio of solid to liquid, and the microwave power were varied. The optimum conditions for the extraction of pectin were as follows, time 20.8 min, pH 1.01, solid to liquid ratio 0.069, and the microwave power of 499 W. A yield of 0.315 g of pectin was extracted from 2 g of an apple. Lianfu & Zelong (2008) conducted a comparative study on the extraction of lycopene from tomatoes using microwave-assisted extraction and ultrasonic-assisted extraction. The optimum conditions for the extraction of lycopene were 98 W, 40 kHz, the solvent ratio was 10.6:1 (w/v), extraction time 367 s. In the UAE, optimum conditions were 86.5 ℃, the solvent ratio was 8.0:1 (v/w) and the extraction time was 29.1 min. A percentage yield of 97.4 and 89.4 was observed for microwave-assisted extraction and ultrasonic-assisted extraction, respectively. Microwave-assisted extraction was found to be more efficient compared to ultrasonic-assisted extraction.

(d) Ultrasonic assisted extraction method

The technique is commonly used due to its simplicity, decreased processing time, less energy, small solvents amount, and the possibility of handling multiple samples at the same time (Chemat *et al*., 2017). The technique is based on the removal or recovery of organic compounds from a permeable solid matrix by means of a solvent, which is energised by sound energies. (Vinatoru, 2001). The recovery of the bioactive compounds from the plant extract using UAE is affected by several elements such as solvent type, solvent ratio, pH, extraction time, and ultrasound power (Khan et al., 2010). Bayar et al., (2017) extracted pectin from *Opuntia ficus-indica* using the ultrasonic-assisted extraction method. The optimum conditions obtained were 70 minutes, 70 ℃, pH 1, 5, and 30 mL/g for sonication time, temperature, pH, and water material ratio respectively. A percentage yield of 18.4 % was obtained.

Heleno *et al*., (2016) also optimised the ultrasound-assisted extraction method for the extraction of mycosterols from *Agaricus bisporus* L by RSM and compared it to conventional Soxhlet extraction. About 4 g of the plant material was extracted in 150 mL of different solvents (limonene, hexane, ethanol) for 4 hours (12 cycles) using the Soxhlet extraction method, for UAE the sound power between 100-500 W was applied at a frequency of 20 kHz. 3,0 g of the plant material was extracted in 100 mL of the three different solvents. The optimum conditions for the extraction of ergosterol using UAE were 15 minutes and 375 W. This method was considered more efficient compared to the Soxhlet. Hammi *et al*., (2015) also optimized UAE of antioxidants compounds from Tunisian Zizphus lotus fruit using RSM. High phenolic content was observed at the operating conditions of 25 minutes, 63 ℃, and 67 mL/g for the extration time, temperature, and solvent ratio respectively.

(e) Decoction extraction method

Decoction is a method used to extract bioactive compounds by boiling the plant material to dissolve chemicals of the material which may include stems, roots, and the bark of the tree. In this process, the plant material is boiled in a specified volume of water for a defined time followed by filtering or straining. Decoction involves first the mashing of the plant material to allow maximum dissolution and the boiling of the extract essential oil, volatile organic compounds, and other various compounds. This procedure is suitable for water-soluble and heat-stable constituents Poonam *et al*., (2011). Jovanović *et al*., (2017) evaluated the influence of different techniques and conditions on the extraction of polyphenolic compounds from *Serpylli herba*. Maceration, decoction, and ultra-assisted extraction were used. Ethanol was

used as a solvent for all three techniques. A greater yield was obtained using UAE. According to the total phenol yield, the efficiency of the extraction method for all variables was ranked in the following order UAE > Decoction > Maceration. Martins *et al*., (2015) evaluated and compared the antioxidant and antibacterial properties of thyme using decoction, infusion, and hydroalcoholic extraction methods. Decoction showed the highest concentration of polyphenolic compounds followed by infusion and hydroalcoholic extracts.

1.2.7. Incorporation of nanoparticles into polymer fibres

Apart from all the excellent antibacterial activity that silver provides towards a broad scope of bacteria, Silver induces serious health-related problems. Silver nanoparticles can be oxidised to produce silver ions (Ag^{+}) which can be toxic to both humans and the environment. The direct and excessive contact to silver may result in allergic reactions, cause skin problems and in more adverse case, it can be carcinogenic when used in animals, silver nanoparticles promotes the production of the reactive oxygen species thus causing oxidative stress in human being. Since AgNPs are also used in water treatment, their release into the aquatic ecosystem results in the accumulation of the metal nanoparticles in fish tissues, mainly in the intestine, liver, and gill (Minghetti & Schirmer, 2016).

The incorporation of silver nanoparticles into polymer fibres prevents direct contact of the skin to silver nanoparticles and provides controlled release of the nanoparticles (Ng *et al*., 2013). Bakhsheshi-Rad *et al*., (2020) also reported that the incorporation of nanoparticles into polymer fibres is a promising method to prevent the growth of microbes on the surface of materials. Further on, the incorporation of nanoparticles into polymer fibres improves the mechanical, physical, thermal, and antibacterial properties of the fibres. Thus these polymer fibres are used in many fields such as biotechnology, energy, sensors, and optoelectronics (Islam *et al.*, 2020). Two different approaches can be used to produce polymer fibres incorporated with nanoparticles using the electrospinning method. In the first approach, nanoparticles are dispersed into the polymer solution and the resultant solution is electrospun to fabricate fibres. The second approach involves dissolving the metallic precursor and the polymer in one solution and electrospinning the resultant solution. Deniz *et al*., (2011) incorporated gold (Au) nanoparticles into PVP polymer fibres using laser ablation. The SEM images showed uniform diameter polymer fibres without beads. TEM images showed the presence of gold nanoparticles dispersed homogenously with the average diameter in the range of 5-20 nm. A similar study was conducted by Bai *et al*., (2007) where different concentrations

(0.024, 0.04, and 0.07%) of gold nanoparticles were incorporated into PVA fibres. The SEM images showed that as the concentration of the Au NPs increased, the diameter of the fibres decreased due to an increase in conductivity (038 ms/nm to 0.75 ms/cm). In contrast Selvaraj *et al*., (2018) Incorporated AgNPs into Casein-Peo polymer solution and electrospun the solution to fabricate fibres. The SEM images show that the addition of silver nanoparticles into the Casein-Peo polymer solution increased the diameter of the fibres.

Similarly, Sekar *et al*., (2018) incorporated Fe-doped ZnO into PVA polymer fibres as potential antibacterial agents. Neat PVA fibres were found to have a smooth surface with a diameter in the range of 120-150 nm. The addition of the Fe-doped ZnO at increasing concentrations (4 - 12%) resulted in the formation of beaded fibres with a rough surface and this was due to the aggregation of the nanoparticles in fibres. The diameter of the fibres was found to increase as the concentration of the nanoparticles increased. Yang *et al.*, (2013) reported that the aggregation of nanoparticles in fibres occurs when the attractive interaction forces (Van der Waals forces) outcompetes the repulsive interaction and forces, such as steric hindrance and electrostatic forces. Aktürk *et al*., (2019) synthesized AgNPs using starch as both a reducing and capping agent. The AgNPs were incorporated into PVA at increasing concentrations (5, 7.5, and 10 %) and electrospun to fabricate fibres. According to the SEM images, all the fibres has a smooth surface with no beads. There was no significant difference in the diameter of the fibres before and after the addition of the AgNPs. The disk diffusion method was used to test the fibres antimicrobial activity against gram-positive bacteria *S. Aureus* and gram-negative *E. coli*. No antibacterial activity was observed for plain PVA fibres while those incorporated with the AgNPs gave more antibacterial activity against gram-positive bacteria. Jatoi., (2020) also evaluated the antimicrobial activity of polyurethane (PU) fibres incorporated with Zinc and silver (Ag-Zn) composite nanoparticles. The SEM images demonstrated regular beadles fibres for both the neat PU and after the addition of the nanoparticles. The addition of the Ag-Zn composite to the polymer solution resulted in a decreased diameter of the fibres due to higher conductivity of the AgNPs. The polymers fibres with the AgNPs exhibited antimicrobial activity against gram positive *S. aureus* and *B. subtilis* and gram-negative *E. coli*.

1.2.8. Fabrication of polymer nanofibres using the electrospinning technique

Nanofibres are favoured among many other nanostructures that have been recently developed, and this is because nanofibers can be easily produced from both natural and synthetic polymers. The functional properties of the nanofibers can be manipulated during the synthesis step.

Nanofibres are further known for their excellent physicochemical properties, such as high porosity, large surface to mass ratio and their superior mechanical performance thus can be exploited for a wide variety of applications.

Various processing techniques, such as chemical vapour deposition, sol-gel method, phase separation, drawing, and electrospinning can be used to produce fibres from a polymer solution. Electrospinning is considered the best and has proved to be simple, efficient, and a versatile method due to its cost-effective setup. Electrostatic spinning, commonly known as electrospinning is a fibre spinning technique that uses a high voltage electric field to produce fibres in the nanoscale from a polymer solution (Kim *et al*., 2005). The electrospinning technique was first introduced in 1934 by Formhals and Gastel and was applied in many industries around the 1990s (Rezaei *et al*., 2015). A typical electrospinning technique is made up of a pump, high voltage, power supply, a collector, and a syringe as shown in the schematic diagram (Scheme 1.1) in page 16. Different parameters such as ambient conditions (humidity and temperature), properties of the polymeric solution (viscosity, surface tension, and conductivity), hydrostatic pressure in the needle, and the electric potential at the tip of the needle influence the diameter of the fibres produced through electrospinning technique. The reduced diameter of fibres is desired since it comes with improved mechanical properties, large surface area, and flexible functionalities thus have many applications. Nanofibers have a large surface area, small pore sizes, and also have a diameter that is about 100 nm (Subbiah *et al*., 2004).

(a) Ambient conditions

Humidity and temperature are ambient parameters that also influence both the morphology and diameter of the fibres. The influence that humidity has on the morphology of the fibres, greatly depends on the composition of the polymer solution. Humidity can also be used to control the rate at which the solvent that was used to prepare the polymer evaporates. Low humidity promotes the fabrication of polymer fibres with bigger diameter and this is because, at low humidity, the solvent evaporated quickly from the polymer, solidifying the polymer as soon as it leaves the needle thus leading to the polymer jet experiencing the induced voltage for a short period. With high humidity, solidification of the polymer occurs more slowly which allows the jet to experience voltage-induced stretching for a long period, resulting in polymer fibres with a thinner diameter (Medeiros *et al*., 2008; Pelipenko *et al*., 2013). The temperature influences the rate at which the solvent evaporates and also the viscosity of the solution. Increasing the temperature increases the rate at which the solvent evaporates while decreasing the viscosity

of the solution thus results in the formation of fibres with a decreased diameter (Haider *et al.*, 2018).

(b) Effect of Solution parameters (Viscosity and concentration)

One of the important parameters when electrospinning a polymers solution is viscosity. The viscosity is important since it describes the entanglement of the polymer molecule chains. Low viscosity which means minimum entanglement of polymer molecule chains often results in the formation of beads or drops instead of fibres. On the other hand, high viscosity results in no formation of fibres, since no polymer jets will be ejected from the needles thus optimum viscosity is one of the requirements for electrospinning. The concentration of the polymer solution is also one of the critical parameters when electrospinning. A low concentration of polymers has been observed to result in the formation of beads while a high very concentration results in the formation of fibres with large diameters.

The formation of beads or droplets mainly depends on the surface tension of the polymer solution. A lower electric field is required to electrospun a solution with lower surface tension, while a solution with higher surface tension requires a high electric field. Droplets are formed when a solution of high surface tension is electrospun and this is because the jet is unstable and spray out to prevent the electrospinning process to take place. Bhardwaj & Kundu, (2010) stated that the electrospinning of a polymer solution with lower conductivity results in fibres with large diameters due to shorter stretching of the electrified jet. Polymer solutions with high conductivity often result in the formation of polymer nanofibres with decreased diameters. Different studies have been conducted to investigate the influence of electrospinning parameters on the diameter and length of polymer nanofibres. The effect of concentration on the conductivity and viscosity of the electrospun polyacrylic acid (PAA) nanofibers was investigated by (Kim *et al*., 2005). Scanning Electron Microscopy (SEM) was used to evaluate the morphology of all the electrospun fibres and it was observed that no fibres were synthesized when 1 M of NaCl was added to PAA solution and all the other synthesized polymer fibres of PAA gave beaded structures. The smallest diameter was observed with the polymer fibres that had 0.01 M NaCl while larger diameters was observed with polymer fibres that had no NaCl. It was further observed that an increase in the concentration of NaCl in the polymer solution decreased the viscosity and conductivity of the solution. In all SEM images beaded structures were observed and this is mainly due to low wt. % of polyacrylic acid prepared which is related

to low viscosity. Consequently, it was imperative to optimise the concentration of PAA to avoid the formation of beads.

Another study evaluated the effect of different solvent ratios of ethanol and water on the electrospinning of polyacrylic acid solution (Ding *et al*., 2005). Polyacrylic acid dissolved in plain water (0/100) gave beaded fibres with an average diameter of 1.1 um and conductivity of 149.2 ms/m. Plain ethanol gave fibres with a diameter of 2 um and the mixture of water and ethanol (50/50) gave fibres with a diameter of 6.7 um with no beads on the fibres. The beaded fibres were due to high conductivity and low viscosity, the introduction of ethanol to the water solution increased the viscosity and decreased the conductivity thus nanofibers with no beads were formed.

(c) Effect of Process parameters (Applied voltage and flow rate of the polymer solution)

In the electrospinning technique given in Schematic diagram 1.1, the polymer solution in the metal needle experiences current that flows from the high voltage supplier, this results in the polymer solution forming a spherical shaped droplet at the tip of the needle which later deforms to form polymer fibres at a critical voltage. While the morphology of the fabricated fibres depends on the strength of the applied voltages other studies also reported that various polymers have different critical voltages (Haider *et al*., 2018; Sill & von Recum, 2008).

Many studies have brought about different theories with regards to the relationship between the strength of the voltage applied and the diameter of the resultant polymer fibres. Some studies suggested that an increase in voltage increases the power in which the polymer solution is ejected from the needle. Thus results in the formation of fibres with a diameter that is large. In contrast, other studies suggested that an increase in voltage resulted in decreased fibre diameter and this is because when the voltage is increased, electrostatic repulsive forces on the fluid jet, leads to intense stretching of the polymer solution (Bhardwaj & Kundu, 2010). Other studies, such as those conducted by Tan *et al*., (2005) have reported that applied voltage does not have any influence on the diameter of the electrospun fibres. The effect of applied voltage on the morphology of the fabricated poly(ethylene oxide) fibres was studied. It was observed that a lower voltage of 5 kV resulted in the formation of irregular beaded fibres, the voltage between 10-17.5 kV, resulted in thicker fibres and 20 kV resulted in polymer fibres with a reduced diameter. Awal *et al.*, (2011) also conducted a study on the influence that applied voltage has on the fabrication of 6 % nylon polymeric fibres and they reported that an increase

in the applied voltage results in fibres with a reduced diameter. The rate at which a polymer solution flows out of the metallic needle tip has an influence on the morphology of the polymer fibres. Even though various polymers require different flow rates to fabricate the desired beaded free polymer, a minimum flow rate is recommended to maintain a balance between the leaving polymeric solution and replacement of that solution with a new one during jet formation. Also low flow rates allows the solvent sufficient time for evaporation. High flow rate results in the formation of bigger drops at tip of metallic needle thus resulting in the formation of polymer fibres with an increased diameter and beads (Zargham *et al*., 2012).

1.2.9. Blending of PVA with natural fibres using the electrospinning technique

Petroleum-based polymers such as polystyrene, polyethylene terephthalate, and polypropylene have been used throughout history in everyday human activities however they often leave the environment devastated through plastic pollution and global warming. Presently, both the industrial and scientific communities are focusing on the development and application of biodegradable and renewable materials (Kargarzadeh *et al*., 2017). Polyvinyl alcohol (PVA) has gained considerable attention from various industries: food, medical, and cosmetics this is due to its desirable properties, such as non-toxicity, biocompatibility, biodegradability, wide availability, and low cost. PVA given in *Figure 1.1* below is a water-soluble, hydrophilic, semi-crystalline polymer with good thermal and chemical stability (Augustine *et al*., 2018b; Jiang *et al*., 2011). Apart from its great properties, PVA has its setbacks such as its high solubility in water, thus its outstanding properties are compromised when it comes in contact with water. It also has defects like poor decomposition temperature, high glass transition temperature, and low elongation at break (Popescu *et al.,* 2018). Nevertheless, many studies have reported on the blending of polymers with fillers or reinforcing agents to improve their physical properties (Zou *et al*., 2020). Nanofillers offer enhances mechanical, thermal, and water barrier properties of the polymer due to their enormous advantages such as a high surface area and high surface energy (Ali *et al*., 2017). Panichpakdee *et al*., (2019) electrospun a polymer blend of natural rubber latex (NRL) with PVA at different ratios and evaluated the change in diameter of the electrospun fibres. Firstly, according to the SEM images, pure electrospun PVA mats were found to be smooth with no beads. The polymer blends ratio of NRL/PVA were as follows: 10:90, 70:30, 50:50 and 70:30 and all their surfaces were found to be rough which implies phase separation between the NRL and the PVA. The average diameter increased as the concentration of the NRL increased in the blend. The viscosity polymer solutions also increased as the concentration of the NRL in the polymer blend increased. Zou *et al*., (2020)

blended polycaprolactone and chitosan using the electrospinning technique, continuous uniform fibres were produced with improved thermal stability.

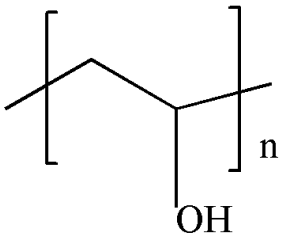

Figure 1.1: Chemical structure of polyvinyl alcohol (PVA)

(a) Natural fibres (Hemp)

Natural fibres are also known to yield composites of lighter weight and cost less compared to fibre glass reinforced polymer (Çomak *et al*., 2018; Pickering *et al*., 2016). Cellulose nanocrystals are considered an ideal reinforcing agent for polymers due to their advantages including, abundantly available, biodegradability and biocompatibility, low density, high surface area, and unique morphology abundance (Xu *et al*., 2013). Cellulose nanocrystals are derived from cellulose, which is the most abundant and renewable carbon resource in nature. Ren *et al*., (2017) observed an improvement in thermal stability of the electrospun Polyacrylonitrile polymer fibre when they incorporated both CNC's and silver nanoparticles. The fibres were uniform in size and the surface was smooth.

One of the largely used natural fibres in industries is hemp fibres scientifically known as *Cannabis sativa L.* Hemp as illustrated in Figure 1.2 is a herb that belongs to the family *Cannabaceae.* It is native to Eastern Asia but has been domesticated in many other parts of the world due to its large use in textiles (Shahzad, 2012). Hemp fibres are highly used due to their short cropping cycles and easily grows in different environments. Also, Hemp contains fibres that are considered the strongest amongst all types and this is due to its tensile strength of about 1110 MPa. Hemp fibres are considered a source of cellulose fibrils held together by pectin's (Kostic *et al*., 2008; Sair *et al.*, 2018). Natural fibres are found naturally in blends of cellulose, hemicellulose, and lignin.

Figure 1.2: Picture of the species Cannabis sativa (L) (Hemp) *(Luyckx* et al.*, 2021)*

(b) Cellulose

Cellulose shown in Figure 1.3 below is a natural polymer that is made up of repeating units of anhydro-D-glucose ($C_6H_{11}O_5$) linked together with β-1,4-glycosidic bonds by C1 and C4. As shown in Figure 1.3 each of the anhydro-D-glucose units contains about 3 hydroxyl groups. The hydrogen bonding between these hydroxyl groups plays a major role in both the physical properties and the crystalline packing of the cellulose fibrils. Cellulose can be extracted from natural fibres such as flex, bagasse, and hemp.

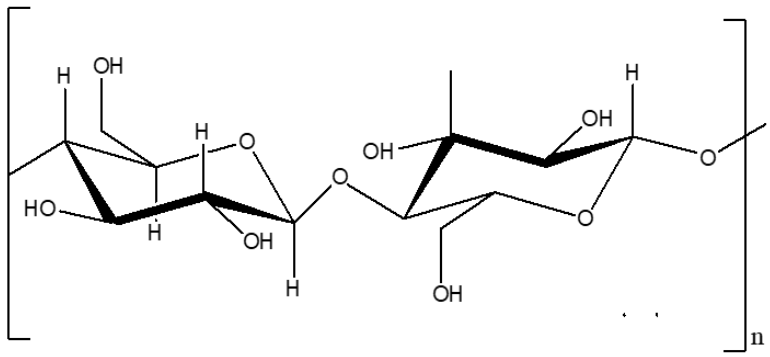

Figure 1.3: Chemical structure of cellulose

(c) Hemicellulose

Hemicellulose given in Figure 1.4 below are polysaccharides that are made of 5 and 6 carbon rings. The difference between hemicellulose and cellulose is that hemicellulose is made up of different types of sugar units where else cellulose is only made up of 1,4-β-D-glucopyranose. Hemicellulose is also considered amorphous since it's highly branched with different side groups while cellulose is a linear polymer and lastly, the degree of polymerization for hemicellulose is around 50-300 while the degree of polymerization for cellulose is about 10-100 times high than that of hemicellulose (Bhat *et al*., 2019). Hemicellulose is a link between lignin and cellulose, its hydrophilic, can be hydrolysed by acids, and is soluble in alkaline solutions

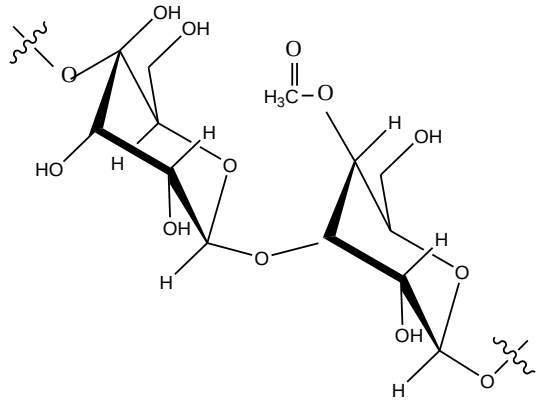

Figure 1.4: Chemical structures of hemicellulose

(d) Lignin

Lignin, Figure 1.5 are known to consist of both aromatic and aliphatic constituents with high molecular weight, thus considered complex hydrocarbon polymers. Lignin does not easily break down into its monomeric units, they are hydrophobic, insoluble in most solvents, and amorphous. The main function of lignin in the plant is to provide rigidity for protection against the wind and gravity forces, it also protects the plant from biological attack. Pectins are hetero-polysaccharides and waxes are considered the last part of the fibres and they are made up of different alcohols. The difference between hemicellulose and cellulose is that hemicellulose is made up of different types of sugar units where else cellulose is only made up of 1,4-β-D-glucopyranose.

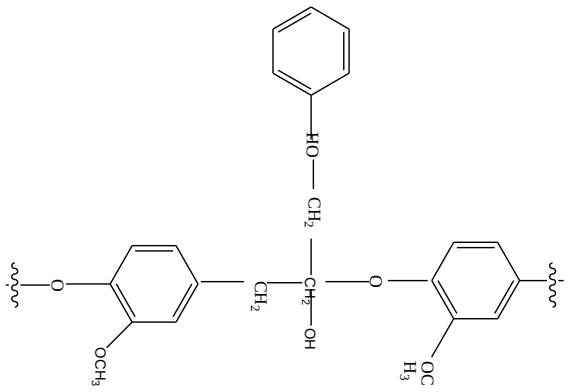

Figure 1.5: Chemical structures of lignin

(e) Extraction of cellulose from natural fibres

Natural fibres cannot be directly combined with polymers and this is due to their hydrophilic nature which results in high moisture absorption leading to high swelling and voids on the interface thus poor mechanical properties. The difference between the polarity of the natural fibres and polymer will also result in the non-uniform distribution of the natural fibres in the polymer matric. Another major drawback that limits the application of the natural fibres in their raw state, is their susceptibility to rotting and their low microbial resistance. The mentioned deficiencies of using natural fibres in their natural state can be overcome through various chemical and physical treatments that can remove the undesirable material such as the pectin, waxes, hemicellulose, and lignin while leaving behind cellulose with desirable properties. Pectin and waxes are highly soluble in hot water thus easily removed, hemicellulose can be easily hydrolysed using acid and is highly soluble in alkali solution. Lignin is not soluble in many solvents thus not easily broken down into monomeric units. Even though lignin is not hydrolysed in acid, many studies reported on the solubility of lignin using hot alkali solutions. Alkali treatment is among the many methods that can be used to treat natural fibres since both ester and the ether groups found in the lignin and hemicellulose are susceptible to the OH attack (Oriez et al., 2020). The Lignin and hemicellulose are linked together by ferulic acid and that is where the reaction takes place. According to the schematic diagram 1.3 given below, which shows the mechanism in which the alkali treatment takes place, the OH from the NaOH attacks the carbon in the ester bond of the ferulic acid, this results in the formation of a tetrahedral intermediate which quickly collapses to form a carboxylic acid when the negatively charged alkoxide is expelled by the negative oxygen. Finally, the alkoxide deprotonates the resultant carboxylic acid (Modenbach & Nokes, 2014). The treatment is based on the removal of the hydrogen bond in the network and it has two main effects on the natural fibres: It increases the

number of reactive sites by exposing cellulose to the surface and lastly it increases the roughness of the material thus proving better mechanical interlocking (Zimniewska *et al*., 2011).

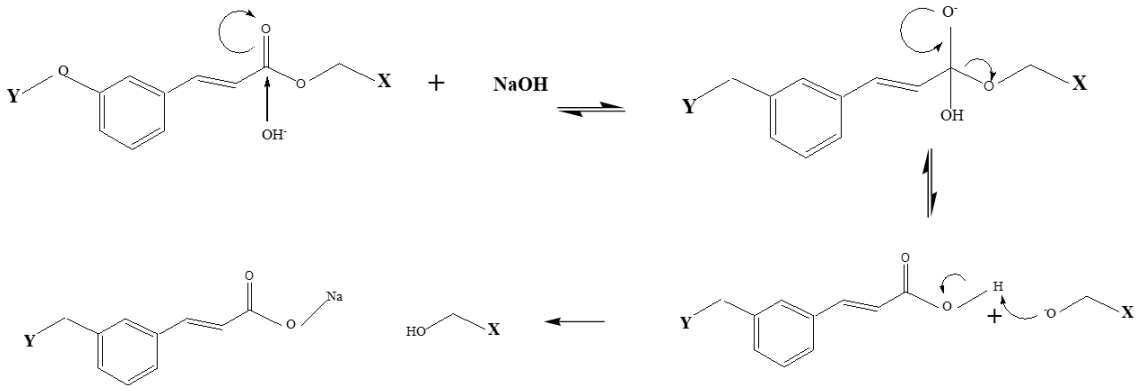

Scheme 1.3: Mechanism that illustrates the removal of lignin(Y) and hemicellulose(X) from cellulose**.**

The need for the development of environmentally friendly material is on the rise and this is because fossil fuels often leave the environment devastated. Extraction of cellulose from natural fibres, pre-treatment to remove non-cellulosic material such as lignin and hemicellulose Alkalization, and bleaching are some of the most utilized methods to remove lignin and hemicellulose. Kim et al., (2011) evaluated the spinnability of raw lignocellulosic biomass (Hemp) using ionic liquid and further evaluated the effect that lignin has on the spinnability of hemp. Various alkaline solutions were used to treat hemp to remove lignin. The two alkaline solutions were 17.5 % NaOH and 0.7 % $NaClO_2$. They found that the lignin content decreases as the treatment time increased. They also reported that further treatment also decomposed cellulose. The optimum conditions for better spinnability of hemp are 17.5 %, 0.7 %, and 5 hours for NaOH, $NaClO_2$ treatment and time respectively. Elkhaoulani *et al*., (2013) also evaluated the effect of treating Hemp fibres with sodium hydroxide and acetic acid. After treatment of the fibres, a peak which appears at 1736 cm^{-1} which corresponds to the presence of the carboxylic ester found in pectin on the surface of the untreated hemp was absent on the treated hemp further on, the peak that corresponds to the presence of lignin around the range 1268 cm^{-1} was significantly reduced in the treated hemp.

Montaño-Leyva *et al*., (2011) treated wheat straw with an alkaline solution of $NaClO_2$ and NaOH to extract cellulose and used trifluoroacetic acid to dissolve the cellulose fibres obtained after treatment. The glass transition temperature for wheat straw before treatment was 1300 ℃ and for the cellulose fibres was 1220 ℃. FTIR spectra confirmed that cellulose fibres were

successfully extracted from the wheat straws since peaks ascribed to the presence of lignin and hemicellulose disappeared after treatment. XRD also further confirmed the extraction of cellulose fibres from wheat straw since a change in the crystallinity was observed. The wheat straw gave a crystallinity of 37 % and 52 % for the cellulose nanofibres. The optimum conditions for the fabrication of nanofibres were 4 % concentration of polymer dissolved in pure TFA at a voltage of 15 kV and a flow rate of 1.5 mL/h. Kim *et al*., (2011) treated hemp fibres with NaOH and $NaClO_2$ at different rates to remove lignin and further dissolved the resultant fibres in 1-ethyl-3-methylimiazolium acetate and electrospun the polymer solution, DMF was also added to improve the spinnability of the fibres. The optimum conditions observed were treatment with 17.5% NaOH for one hour and treatment with $NaClO_2$ for 5 hours. They also found that when the lignin content was greater than 6%, it resulted in spray drying of the polymer solution due to the large drops formed on the nozzle end. Cellulose is known to contain both the amorphous and crystalline regions, acid hydrolysis of cellulose results in the hydrolysis of the amorphous region of cellulose, leaving behind the crystal regions intact often referred to as cellulose nanocrystals due to its structural stability (Spagnol *et al*., 2018)

1.2.10. Synthesis of cellulose nanocrystals

The cellulose polymers in the crystalline region, are packed together by hydrogen bonding, while in the amorphous region, the polymers are randomLy distributed. Different types of acids can be used to synthesize cellulose nanocrystals with different properties such as morphology, surface functionality, and thermal properties. Sulphuric acid has been extensively used in the synthesis of cellulose nanocrystals because it does not require a long reaction time and is simple compared to other processes. *Kassab et al*., (2020) did a comparison study where they used two different acids, namely sulphuric acid and citric/hydrochloric acid mixture to extract sulphated CNC's and carboxylated CNC respectively. The needle-like structure of cellulose nanocrystals were extracted using the two acids, however with different diameters. The crystallinity was found to be 81 and 83 % for Sulphuric acid CNC's (S-CNC's) and Citric acid CNC's (C-CNC's). The C-CNC was found to be more thermally stable. The use of C-CNC in the biomedical field is limited since they have insufficient dispersion. The stability of the colloidal suspension can maintained by mixing CNC's with water soluble polymers. The polymer chains spread throughout the aqueous solution preventing the aggregation of cellulose nanocrystals. Xing *et al.*, (2020) studied the different conditions including temperature (45 and 60 ℃), the concentration of H_2SO_4 (56 – 64 %), and time (10-20 minutes) required to

hydrolyse cellulose from eucalyptus using sulphuric acid at concentration 58 % at 45 ℃, the suspension was yellow. However, a sulphuric acid concentration above 60 % resulted in a transparent solution indicating the dissolution of cellulose or swelling. Temperature greater than 60 ℃ and concentration greater than 62 % resulted in a brownish colour due to over hydrolysis of cellulose.

1.2.11. Synergistic effect of silver nanoparticles and essential oils incorporated into polymer fibres

Some studies have reported on the combination of antibacterial agents, specifically silver nanoparticles and natural products (essential oils) to provide synergistic effects against a broad spectrum of bacterial strains. The approach is based on the combination of different antibacterial agents that exhibit antibacterial activity through different mechanisms while reducing the dosage of the individual antibacterial agents and expand the spectrum of antibacterial activity. Pei *et al.*, (2009) studied the mechanism in which carvacrol and zinc oxide nanoparticles exhibited antibacterial activity towards *Campylobacter jejuni*. Treatment with the individual antibacterial agent, either the zinc oxide or *carvavrol* generated a bacteriostatic effect while the combination of both gave enhanced antibacterial activity. carvacrol exhibited antibacterial activity by damaging the cell wall and the ZnO nanoparticles interacted with the cell wall and induce cell leakage. Patil., (2013) Evaluated the synergistic effect of silver nanoparticles synthesized using sodium citrate and cinnamaldehyde against bacterial species found in food. The combination exhibited a synergistic effect against all the tested bacterial strains. Scandorieiro *et al.*, (2016) also combined the bio-synthesized silver nanoparticles with *Origanum vulgare* essential oil and evaluated their antimicrobial activity against multi-drug resistant strains. According to their MIC results, the combination of the essential oil combined with the silver nanoparticles presented lower MIC values compared to when treated with silver nanoparticles or the essential oil individually.

1.2.12. Incorporation of eucalyptus oil into polymer fibres

The essential oils are also known as volatile oils or ethereal can be extracted from different parts of the plants such as the leaves, stem, bark, roots, and the fruits through steaming or hydro-distillation (Burt, 2004). The extracted liquid is volatile and hydrophobic and is known to contain a mixture of terpenoids particularly monoterpenes and sesquiterpenes that mainly serve as defense mechanisms for plants against pathogenic fungi and pests. Essential oils are also known to contain various aromatic esters, phenols, alcohols, aldehydes, ketones, and

oxides which determines their characteristic aroma and the odour of the plant from which the essential oil was extracted. Historically essential oils were added in food as potential preservatives and this was until their medical properties were discovered, antimicrobial, anti-hyperglycaemic and anticarcinogenic properties. They are now extensively used in aromatherapy and conventional treatment as anti-inflammatory and disinfecting agents. The use of essential oils in various fields is due to their low or no toxicity against both human beings and animals. They are also environmentally friendly since they do not persist in soil and water and are easily extractable.

Among various aromatic plants, the genus *Eucalyptus L Herit* comes from the *mitraceae* family and is represented by 700 species, distributed across the world. The plant is native to Australia where it was used traditionally to treat colds, fever, diarrhoea, toothache, and snake bites. Presently it is among the most planted species due to its extensive use in the pharmaceutical industry as an antiseptic and also as an additive in cough tablets and medicated skin creams. Eucalyptus oil is a colourless or yellow oil that can be extracted from the leaves of tall evergreen trees such as lemon (*E. citriodora*), river red gum (*E. camalulensis*), blue malle (*E. polybacteria*), and Tasmanian blue gum (*E. globulus*) (Tarabet *et al*., 2012). Among the other various complex compounds that the eucalyptus oil contains, 1,8 cineole is considered the characteristic compound of the genus since it takes up at least 70 % of the mixture. 1.8 cineole is also considered the important compound in eucalyptus oil due to its toxicity against a wide range of microbes such as bacteria and fungi (Ait-ouazzou & Conchello, 2011; Darben *et al.*, 1998). Essential oils exhibit antibacterial activity by disturbing the cytoplasm membrane, disrupting the electron flow and proton motive flow active transport, and hinders the synthesis of protein (Rafiq *et al*., 2018). El-baz *et al*., (2015) evaluated the antimicrobial activity of eucalyptus comaldulenis essential oil. The results showed that the essential oil was highly active against *Escherichia Coli, Listeria monocytogenes,* and *Candida albican*. The observed antimicrobial activity was due to the presence of eucalyptol and α- pinene which are the major compounds in the eucalyptus oil. Ghalem & Mohamed, (2008) studied the antibacterial activity of the essential oils from *E.globulus* and *E.camaldulensis*, the essential oil from the leaves of the two plants showed excellent antibacterial activity against gram-positive *S.aureus* and gram-negative *E.Coli* with *E.globulus* giving high antibacterial activity demonstrated by the larger zone of inhibition. Mulyaningsih *et al.,* (2011) also studied the antibacterial activity of *E.globulus, E.radiata,* and *E.citriodora* against multidrug-resistant bacteria, all the plants exhibited minimum antibacterial activity against gram-negative bacteria. *E.globulus* showed

higher antibacterial activity once more, compared to all the plants and this can be related to the high content of 1.8 cineole which has been reported to be in the plant as compared to the other plants.

Despite their numerous benefits, the application of essential oil has been limited and this is because of their instability in the presence of oxygen, light and temperature influences, high volatility, and their unpleasant aroma. Incorporation of the Essential oils into polymer fibres will prevent the oxidation of the oil from taking place and also reduce the rate of evaporation while releasing the oil slowly at effective levels (Hafsa *et al*., 2016; Wu *et al.*, 2015). Nanofibres are preferable for encapsulation because they have a high surface area and high porosity thus provides a controlled release. Ardekani *et al.*, (2019) reported the inhibition of *S. aureus, P. aeruginosa,* and *C. albican* when they evaluated the antibacterial activity of *Zataria Multiflora* essential oil incorporated into electrospun PVA polymer fibres. Rieger & Schiffman, (2014) also observed significant antimicrobial activity when they incorporated Cinnamaldehyde into chitosan blended with poly(ethylene oxide). Liakos *et al.*, (2017) reported on the antibacterial activity of electrospun cellulose-based polymer fibres incorporated with essential oils.

1.2.13. Antibacterial activity

60 years ago antibiotics were referred to as miracle drugs. The excessive use of these miracle drugs resulted in most pathogenic bacteria becoming resistant. The emergence of resistance of pathogenic bacteria to antibacterial agents is considered a major threat to public health since only fewer antibacterial agents are effective. Some bacterial infections are almost untreatable with the current antibiotics. Drug-resistant bacterial infections cause mortality and morbidity in patients. The rise in resistant pathogenic bacteria has been activity driven by human activity through the extensive use or misuse of antibiotics in humans, veterinary and also through agriculture (Andersson, 2003; Gullberg *et al*., 2011; Magiorakos *et al*., 2011). Bacteria can be categorised as either being gram-positive or gram-negative due to the difference in composition of their envelopes. Gram-positive bacteria such as *Staphylococcus aureus,* are known to have a thick layer of peptidoglycan which is made up of linear polysaccharides chains cross-linked by short peptides thus forming a rigid structure. The thick peptidoglycan layer acts as a cell wall that surrounds the inner plasma membrane. In contrast, gram-negative bacteria such as *Klebsiella pneumoniae* is made up of a thinner peptidoglycan layer (Worthington & Melander, 2013). The emergence and rise of antibacterial resistance affect both gram-positive and gram-

negative bacteria. *S. Aureus* and *K. Pneumonia* were selected as they are most predominant in water, air, and soil. they happen to be the most opportunistic human pathogens that can grow and reproduce causing serious illnesses in both human and animals, also these bacteria can survive in different conditions thus considered multidrug-resistant pathogens.

Bacteria can adapt easily to changes in their environment. This allows them to respond to a wide array of environmental threats including the presence of antibiotics that may threaten their existence. For microorganisms to survive they develop ways that make them resistant to antimicrobial agents (Jindal *et al.*, 2015). Factors that promote antimicrobial resistance are exposure to sub-optimal levels of antimicrobials, exposure to broad-spectrum antibiotics, exposure to microbes carrying resistant genes, Lack of hygiene in clinical environments, Use of antibiotics in food/agriculture, and lastly inappropriate antimicrobial uses. There are several resistance mechanisms that are proposed. The mechanism of resistance includes the following; drug inactivation, modification of drug binding sites, efflux pump, and porin loss (Vila *et al.*, 2007).

As the problem with resistant pathogenic bacteria towards antibiotics continuous to grow, the urgent need to develop new antibacterial bacterial agent is also increasing. Silver (silver nanoparticles) and natural products (essential oils) have been identified as potential antibacterial agents.

(a) Antibacterial activity of silver nanoparticles and essential oils

The use of silver or silver salt as antibacterial agents is an extremely old method that was used to treat open wounds and skin burns. This was due to the high reactivity of silver and its binding efficiency to proteins which allows the silver to cause changes within the cell membrane of the bacteria and nuclear membrane which results in cell disruption and cell death. Silver nanoparticles are more reactive than their bulk material and the size of nanoparticles is small, which allows the nanoparticles to penetrate the cell which results in the dis-functioning of the cell (Jazmín Silvero et al., 2018; Lee & Nagajyothi, 2011). Even though researchers have reported on the antimicrobial activity of silver nanoparticles, the mechanisms behind this phenomenon are still not completely understood. Hamedi & Shojaosadati, (2019) reported the different mechanisms of silver nanoparticles antimicrobial activity. Silver nanoparticles are reservoirs for Ag^+ ions, nanoparticles are often oxidised by oxygen from the air to form Ag^+ ions. The nanoparticles can release the Ag^+ ions that can enter the bacterial cell wall and cause cell death. Another mechanism involves biological/organic species such as carboxylic acid,

amines, thiols, and phosphate that contain elements such as sulphur, oxygen, and nitrogen can act as ligands and react with Ag^+ ions to form complexes which lead to protein denaturation and disturbs the functioning of the protein. Further on the silver has been reported to have a high affinity towards the S, O, and N elements thus gives high antimicrobial activity. The Ag^+ ions can also bind to the DNA that is negatively charged thus prevents replication. Lastly the silver ion can also induce the production of reactive oxygen species such as superoxides and hydroxyl radicals which then disturbs the cycle of cellular respiration (Siddiqi *et al.*, 2018). Rafique *et al*., (2019) reported that Ag^+ ions from $AgNO_3$ have lower antimicrobial activity compared Ag^+ ions released from AgNPs with equal concentrations.

Since ancient times, essential oils (EOs) were used in folk medicine. Besides their important roles in the protection of plants from pests, essential oils present a broad range of secondary metabolites that can inhibit or slow the growth of bacteria. The antibacterial activity of essential oils mainly depends on their chemical composition. Essential oils exhibit antimicrobial activity through the combined effect. The oil vapour that can be absorbed on the surface of the microorganisms, and also the vapour that is absorbed by the medium. They can inhibit or slow down the growth of bacteria through various mechanisms and this includes, damaging the cell wall and membrane proteins which might lead to leakage of the cell content, they can disturb the cell permeability, and also essential oils can alter the intracellular and external adenosine triphosphate (ATP) balance. The structure of various chemical compounds in essential oils and their functional groups can also induce a complete morphological change of the bacterial cells (Nazzaro et al., 2013).

1.3. RATIONALE OF THE STUDY

The world is continuously losing the battle against superbugs, Bacteria that are resistant to antibiotics. Infectious diseases are the leading cause of mortality and morbidity, claiming about 15 million deaths per year worldwide (Bhattacharya *et al.*, 2020). The antibiotic resistance crisis has been attributed to the overuse and misuse of these medications. According to the World Health Organization, the top three pathogens that directly affect human health can be categorised into three groups. ‘’Medium priority” includes bacteria such as *Streptococcus* pneumoniae and, Shigella. They are rated medium priority since they are still responsive to antibiotics, however, researchers fear soon they will become resistant. Gram-positive bacteria such as *Staphylococcus Aureus* are rated high priority and lastly gram-negative bacteria such

as *Klebsiella pneumoniae* and *Escherichia coli* are rated ‘’critical priority’’ since they can cause deadly infections in the intestinal tract. These gram-negative bacteria pose a particular threat for people with weak or not yet fully developed immune systems, including new-borns, ageing populations, people undergoing surgery and cancer treatment.

Because of the rapid increase in the number of bacteria towards commonly used bacteria and costs required for treatment. Scientists are constantly looking for new effective antimicrobial agents that can combat the problem with superbugs and treatment that is cost-effective. Metal nanoparticles have been receiving considerable attention from researchers, due to their unique biological, optical, and electrical properties which makes them applicable in many fields. Amongst other nanoparticles such as Au and Cu, Ag nanoparticles are of particular interest because of their efficient antimicrobial activity towards resistant bacteria. Silver nanoparticles have been widely used for biological applications. However, their utilization has been limited due to their toxic nature and accumulation in cells when directly applied. To overcome this problem, silver nanoparticles can be incorporated into polymer nanofibres using the electrospinning technique. Polymer nanofibres are considered a good host for volatile compounds due to their unique properties such as high porosity and high surface-to-volume area.

The use of petroleum-based polymer to produce polymer nanofibres often leaves the environment devastated and causes global warming while threatening human health. To eliminate the threats, biodegradable materials generated from renewable stock are promising materials to replace synthetic polymers. Cellulose nanocrystals are needle-like structured materials that can be prepared from cellulose. Cellulose found in natural fibres such as hemp is considered eco-friendly, renewable, and bio-compatible compared to synthetic polymers. Even with all the advantages associated with cellulose, its use has not been fully explored and this is due to its limited solubility in many solvents thus cannot be easily fabricated into polymer nanofibres. Compounding cellulose nanocrystals with other polymers such as polyvinyl alcohol makes it possible to produce fibres using the electrospinning technique. The production of bead-less fibres with smaller diameters using the electrospinning technique is crucial for various applications. Fibres formation can be affected by the following 3 main parameters: (a) ambient conditions (temperature), process parameters (applied voltage,) and lastly solution parameters (concentration). Thus, optimization of parameters is essential to produce desired fibres. Another problem that directly affects human health is the resistance of

microorganisms towards commonly used antibiotics due to the misuse and overuse of antimicrobials. Factors such as inadequate sanitary conditions, poor infection control, and inappropriate food-handling encourage the spread of antimicrobial resistance. The speed of new antibiotics development can't keep pace with the growth of bacterial drug resistance, which leads to increasingly serious antimicrobial resistance. The resistance of microorganisms often leads to increased mortality, prolonged hospitalisation, and higher medical costs.

Due to the above-mentioned problems with the resistance of bacteria towards commonly used antibiotics and the disadvantages that comes with using silver nanoparticles and essential oils in their pure state. This study will focus on the incorporation of silver nanoparticles and Eucalyptus oil into PVA/CNC composite polymer nanofibres for antimicrobial application.

1.4. AIM AND OBJECTIVES

Aim

To evaluate the antibacterial efficiency of silver nanoparticles and eucalyptus oil incorporated into PVA/CNC polymer nanofibres.

Objectives

- To analyse the total phenol and flavonoid content of aqueous extract of *Citrus sinensis* peels.
- To synthesize silver nanoparticles using *Citrus sinensis* peels extract and characterize them using TEM, XRD, UV-Vis, and FTIR spetroscopy.
- To extract cellulose from hemp fibres and to characterize the hemp fibres before and after extraction using FTIR spectroscopy, XRD, and SEM.
- To synthesize cellulose nanocrystals from the extracted cellulose and to characterize the isolated cellulose nanocrystals using FTIR, XRD, and TEM.
- To fabricate PVA/CNC polymer blend optimizing the concentration of CNC (1, 2, and 3%) and optimization of voltage (20, 25, and 30 kV).
- To incorporate different concentrations (1, 2, and 3%) of silver nanoparticles into the PVA/CNC composite polymer nanofibres.
- To incorporate different concentrations of the eucalyptus oil (1, 2, and 3%) into the PVA/CNC composite polymer nanofibres.
- To incorporate both silver nanoparticles and eucalyptus oil into PVA/CNC composite polymer nanofibers.

- To characterize the PVA/CNC composite polymer nanofibers, the PVA/CNC composite polymer nanofibres loaded with Ag nanoparticles and lastly the PVA/CNC composite polymer nanofibres loaded with eucalyptus oil for using FTIR, SEM, TEM, XRD, and thermal properties using TGA.
- To determine the efficacy of the Ag nanoparticles and the eucalyptus oil loaded polymer blends against *S. aureus* and *K. pneumoniae.*

CHAPTER TWO

2. RESEARCH METHODOLOGY

2.1. Materials and chemical reagents

Hemp fibres were collected from the Institute of Chemistry and Biotechnology, Vaal University of Technology, Sebokeng campus in the Gauteng Province of South Africa. The hemp materials were washed with distilled water, to remove impurities and oven dried at 50 °C for 24 hours. All the chemicals were of analytical grade and were all purchased from Sigma Aldrich. Sodium hydroxide pellets, silver nitrate (99.8%), sodium chlorite (0.7 %), sulphuric acid (95-97%), Folin ciocalteu reagent, gallic acid (97.5 %), aluminium chloride, ammonia (32%), quercetin (>95.5 %), methanol (99.5 %), sodium carbonate (99 %). Nutrient broth, Muller Hinton Agar, and the bacteria culture were acquired from the Department of Biotechnology laboratories, Vaal University of Technology, South Africa.

2.2. Experimental procedures

2.2.1. Preparation of plant extract from Citrus sinensis peels.

(a) Plant extract preparation

Citrus sinensis peels were collected, air dried, and ground to a fine powder using a grinder. Different concentrations (1, 2, and 3 % m/v) of the plant extract were prepared by briefly immersing the ground *citrus sinensis* peels into ultra-pure water. The mixture was boiled on the stove at 50 ℃ for approximately 40 minutes. The mixture was allowed to cool, centrifuged, and filtered using the Whattman No 1 filter paper. The supernatant was stored at 4 ℃ until the experiments were conducted.

(b) Determination of the Total Phenolic content (TPC)

The total phenolic content in the different concentrations (1, 2, and 3 % m/v) of the plant extracts of the *Citrus sinensis* was evaluated using the Folin ciocalteu reagent. Briefly, 0.5 mL of the plant extract was mixed with 0.5 mL Folin ciocalteu reagent. This was followed by adding 8.5 mL distilled water. UV-Vis spectroscopy was used to measure the absorbance at 725 nm and the results were compared to the gallic acid calibration curve (y=0.1180-0.058 r^2=0.998). The total phenolic content (TPC) was expressed as gallic acid equivalent (Cappellari et al., 2013).

(c) Determination of the Total flavonoid content (TFC)

The total flavonoid content in the increasing concentration (1, 2, and 3 % m/v) in the *Citrus sinensis* was determined using the aluminium chloride colorimetric method briefly 0.5 mL of the extract was mixed with 10% aluminium chloride prepared in methanol and this was followed by the addition of 0.1 mL of 1.0 M potassium acetate. The mixture was allowed to stand for 60 minutes and the absorbance was measured at 510 nm. Quercetin was used to prepare the calibration curve and the results were expressed as mg quercetin equivalent per g dry weight (Khaleghnezhad *et al.*, 2019).

2.2.2. Synthesis of silver nanoparticles using Citrus sinensis peels extracts

$AgNO_3$ solution (0.15 M) was prepared in 20 mL ultra-pure water. The silver nitrate solution was transferred into a 250 mL three-neck flask followed by the addition of 40 mL *Citrus sinensis* aqueous extract (1 %). Ammonia solution was added dropwise to adjust the pH to 10. The solution was allowed to stir at room temperature for 2 hours, thereafter it was centrifuged at 5000 rpm for 20 minutes. The synthesized silver nanoparticles were re-dispersed in methanol and centrifuged to remove impurities. Finally, silver nanoparticles were collected, dried at room temperature, and characterized. Silver nanoparticles capped with 2 % and 3 % *Citrus sinensis* were synthesized using the same method.

2.2.3. Extraction of cellulose

Dried hemp fibres were alkaline treated according to a method developed by (Mohamed et al., 2017) with slight modification. Briefly, 10 g of the fibres was mixed with 5 % NaOH at 80 ℃ for two hours under continuous stirring. The resultant fibres were washed with distilled water until pH 7 was achieved. The alkalization treatment was followed by the bleaching process, and this process was carried out by briefly immersing the fibres in $NaClO_2$ (0.7 %) v/v and continuously stirring the mixture for 2 hours at 80 ℃. The bleaching process was repeated

about twice until a snowy white powder was achieved, this was followed by washing with distilled water until a pH of 7 was achieved.

2.2.4. Synthesis of cellulose nanocrystals

A method developed by (Chen *et al*., 2016) was followed for the synthesis of cellulose nanocrystals from the cellulose powder that was extracted according to method 1. Briefly, 1.0 g of the cellulose powder was dispersed in 100 mL H_2SO_4 (64 %) v/v. The mixture was allowed to stir for 45 minutes at 45 ℃. The resultant solution was centrifuged to wash away the excess sulphuric acid using distilled water. The cellulose nanocrystals were washed until pH 7 was obtained.

2.2.5. Fabrication of polymer fibres

(a) Fabrication of CNC/PVA blended polymer fibres using the electrospinning technique

PVA was weighed and dissolved in water to prepare 10 % (wt/wt). The solution was allowed to stir for 25 hours at 50 ℃ until complete dissolution. The concentration of PVA was chosen according to a method by (Luzi *et al*., 2014). Different amounts of CNC (1, 2, and 3 %) that were prepared according to the method described above, ware added to the PVA solution and stirred for two hours at room temperature. The different concentrations of CNC were added to optimize the concentration. The solutions were electrospun to produce polymer nanofibres. The optimum concentration of the CNC was further used to optimize the voltage, the voltage was varied from 15-25 kV.

(b) Incorporation of Ag nanoparticles into CNC/PVA fibres using electrospinning technique

A polymer solution containing 2 % CNC and 10 % PVA was prepared by dissolving the CNC/PVA powder in distilled water. The resultant solution was stirred for 2 hours at 70 ℃ until a homogeneous solution was attained. Different concentrations of AgNPs (1,2 and 3 %) m/v were added into the polymer solution. The resultant solution was stirred until a uniform solution was achieved and electrospun using the optimum conditions.

(c) Incorporation of eucalyptus oil into CNC/PVA fibres using the electrospinning technique

A polymer solution containing 2 % wt/w CNC and 10 % wt/wt PVA was prepared by dissolving the CNC/PVA powder in distilled water. The resultant solution was stirred for 2 hours at 70 ℃ until a homogeneous solution was attained. Different concentrations of eucalyptus oil (1, 2,

and 3 % m/v) were added into the polymer solution. The resultant solution was stirred until a uniform solution was achieved and electrospun using the optimum conditions (Bonadies *et al.*, 2019).

2.2.6. Antimicrobial activity: Minimum inhibitory concentration (MIC) of Ag nanoparticles

The antibacterial activity of the synthesized silver nanoparticles using different concentrations of *Citrus sinensis* (1, 2, and 3 %) was tested against both gram-positive and gram-negative bacteria, namely *S. aureus* and *K. pneumonia* respectively. MIC was carried out to evaluate the lowest concentration of the silver nanoparticles required to prevent the visible growth of the microorganisms. Neomycin was used as positive control and water/Extract was used as a negative control. Briefly in this test, a multichannel pipette was used to pour 100 µ*l* of the prepared Mueller Hinton broth into all the wells of the 96 well plate, this was followed by the addition of 100 µ*l* silver nanoparticles (1 mg/mL) into the first row of the 96 well plate. Serial dilution of the silver nanoparticles /neomycin was done by taking 100 µ*l* of the solution in the first row and transferring it into the second row of the plate and taking the 100 ul of the solution in the second row and transferring it into the third row, this dilution was carried out until the last row of the 96 well plate to prepare decreasing concentration solution of the silver nanoparticles. 100 µ*l* of the prepared microbial *(S. aureus / K. pneumoniae*) suspension (1.0 x 10^6 Cfu/mL) was added in all the wells of the 96 well plates. Lastly 50 µ*l* of the 0.2 mg/mL of the p-iodonitrotetrazolium chloride (INT) was added also in all the wells of the plate as an indicator. The plates were incubated at 37 ℃ for 24 hours and Activity was recorded as the blue colouration (Behravan *et al.*, 2019).

2.2.6.1.Antimicrobial activity of Ag nanoparticles/Eucalyptus oil/CNC/PVA nanofibres.

The disk diffusion method was used to assess the antimicrobial activity of Ag/CNC/PVA nanofibres. A sterile cotton swab was used to apply the bacterial culture onto the agar plate containing Mueller Hinton. PVA nanofibres (no CNC), PVA/CNC nanofibres (No AgNPs), and AgNPs/CNC/PVA polymer nanofibres were placed under ultraviolet for a minute to disinfect them. The fibres were cut into small disks (5 mm) and placed onto the Petri plate containing the bacterial culture. *Neomycin* was used as a positive control. The plates were incubated over at 37 ℃ under continuous stirring. The formation of a halo around the fibres disk on the plates is referred to as the zone of inhibition and indicates the inhibition of growth against the bacteria (Alipour *et al*., 2019).

2.3.Instrumentation

An ultraviolet-visible spectrophotometer (Perkin Elmer Lambda 25) was used to study the optical properties of the synthesized silver nanoparticles. The synthesized silver nanoparticles were dispersed in double-distilled water (1.0 mg/mL) transferred into 1.0 cm pathlength cuvettes and ran at a scan range of 200 - 800 nm. The double-distilled water was also used as a blank. Fourier-transform infrared spectrometer (Perkin-Elmer Spectrum 400 FT-IR) was used to study the functional groups present in the *Citrus sinensis* peels extract and also on the synthesized Ag nanoparticles. The sample was placed on a diamond sample holder and subjected to infrared radiation the measurements were taken in the region of 500 – 4000 cm^{-1}. Transmission electron microscopy (JEOL JEM-2100) operated at 80 kV was used to study the morphology of the synthesized silver nanoparticles, the samples for TEM analysis were prepared by dispersing the silver nanoparticles in distilled water, placed on a copper grid dried under the infrared lamp. X-ray diffraction (FEI TECNAI SPIRIT) secondary graphite monochromated Co K alpha radiation (l = 1.7902 Å) was used to study the crystallinity nature of the synthesized dried powdered cellulose nanocrystals, silver nanoparticles, and polymer nanofibres. The scattered radiation was detected in the range 2θ= 10°-60°at a scan rate of 2°/min. The Segal equation given below in equation 1 was used to study the crystallinity index (CR_i) of all the isolated cellulose nanocrystals, where I_{200} represented the maximum intensity and I_{am} was the peak at 2θ=18

Equation 2.1: Crystallinity index (CrI): $=\frac{I_{200}-I_{am}}{I_{200}}$

The Scherrer equation given below was used to study the crystal size of the synthesized silver nanoparticles. Where θ is the diffraction pattern, K = 0.94 (correction factor), λ is the corrected angular width in radians at half maximum intensity.

Equation 2.2: Crystal size (W) = $\frac{k\lambda}{\beta cos\theta}$

Scanning electron microscopy (SEM, JEOL Model JSM − 6390LV) was used to study the surface morphology of the neat fibres and the fibres incorporated with the essential oil and the silver nanoparticles. The fibres were coated with platinum as a conductive material that improves images quality, placed on the sample holder and the analysis was performed at an accelerating voltage of 5 kV.

CHAPTER THREE

3.0. RESULTS AND DISCUSSION

3.1. Total phenolic and flavonoid content

The total phenolic and flavonoid content of *Citrus sinensis* extracts are shown in *Figure 3.1*. The total phenolic content ranged from 31-78 mgGAE/mg and the flavonoid content ranged between 7-32 mg QAE/mg. The highest concentration for both phenols and flavonoids was found in the 3 % m/v extract probably due to the high plant material that was immersed in water. Thus the extract can be used both as a reducing and stabilizing agent for the synthesis of silver nanoparticles compared to the 1 % and 2 % m/v. In other similar studies, Jridi *et al.*, (2019) analysed both the total phenolic and flavonoid content in the dried orange peels extracts, the results that were observed for the total phenolic and flavonoid content were 8.86 GAE/g and 6.30 GAE/g, respectively. These results are different compared to our study. The difference observed might be due to several factors such as the climate, seasons, and geographical conditions of the locations (A. F. Ahmed *et al.*, 2019).

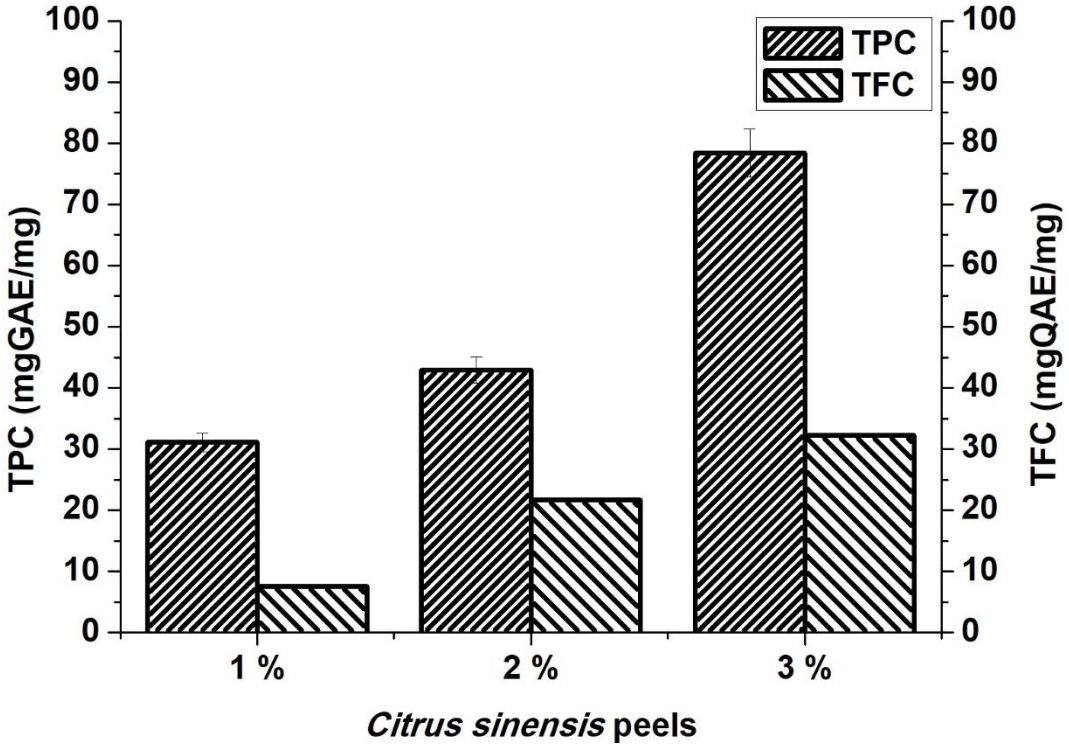

Figure 3.1: The total phenolic content in different concentrations (1, 2 and 3% m/v) of Citrus sinensis. Data are mean ± SD (n=3).

3.2. Green synthesis of Ag nanoparticles using Citrus sinensis peels extract and their antibacterial activity.

Silver nanoparticles have attracted considerable attention due to their unique optical, electronic and antibacterial activity. Various chemical and physical methods have been used to synthesize silver nanoparticles. However, these approaches may require toxic chemicals and are considered toxic to the environment. In this section, silver nanoparticles were synthesized using an increasing concentration of the aqueous extract of *Citrus sinensis* peels.

3.2.1. UV–Visible spectral analysis

UV–Vis spectroscopy was used to evaluate the formation of the silver nanoparticles. *Figure 3.2* below shows the UV-Vis spectra of silver nanoparticles synthesised using the increasing concentration (1, 2, and 3 %) of *Citrus sinensis.* A colour change of yellow to dark brown (scheme 3.2) was observed at pH 10 when both the *Citrus sinensis* and $AgNO_3$ were mixed . This illustrates the successful reduction of Ag^+ ions to produce silver nanoparticles *(Thomas et al*., 2019).

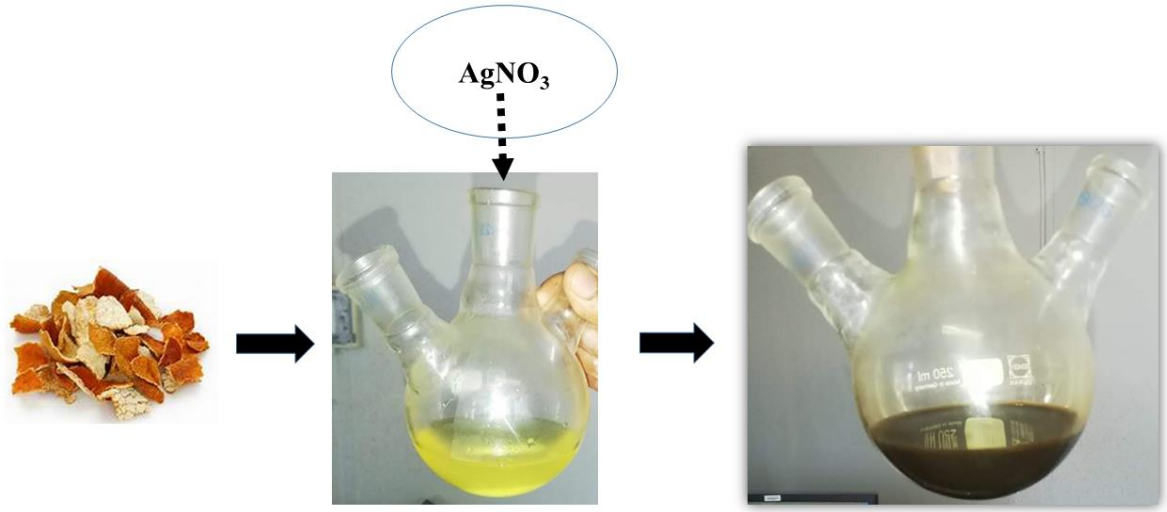

Scheme 3.1: Pictures showing the colour change of the solution when the orange peels extract is mixed with silver nitrate to form silver nanoaparticles (brown).

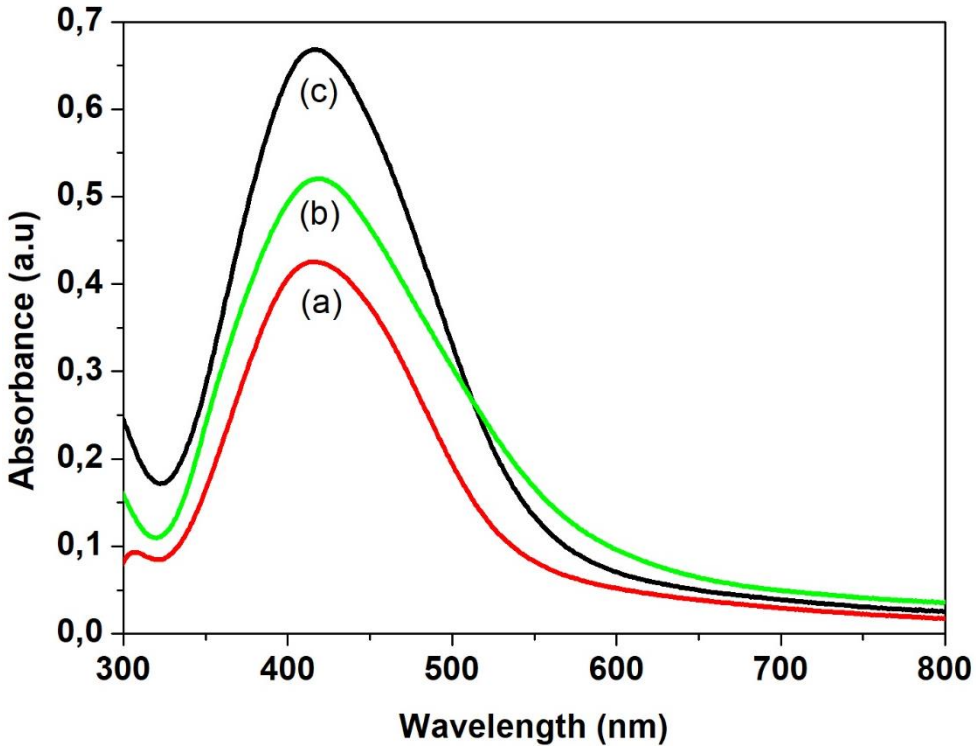

Figure 3.3: UV/Visible absorption spectra of Ag nanoparticles synthesized using three concentration of Citrus sinensis, (a) 1 %, (b) 2 % and (c) 3 % m/v for two hours at room temperature.

All the samples as shown in Figure 3.2 showed the surface Plasmon resonance (SPR) absorption band which is a characteristic for all Nobel metals including silver (Bindhu & Umadevi, 2013). The SPR peaks for the three concentrations occurred at the same wavelength of approximately 420 nm. The position of the SPR band gives more information about the shape and size of the synthesized silver nanoparticles and according to the results, the SPR bands shifted to lower wavelengths compared to the bulk material which absorbs at a wavelength of 1000 nm thus showing a decrease in particle size. Silver nanoparticles of smaller sizes are known to have a large surface-to-volume ratio thus giving the desired physical, chemical and biological properties (Chahar *et al.*, 2018).

3.2.2. FT-IR spectroscopic analysis

FTIR spectroscopy was used to investigate the presence of the different functional groups that are present in the aqueous *Citrus sinensis* peels extracts. FTIR was also used to confirm the functional groups involved in both the reduction of the silver ion and stabilization of the silver nanoparticles. *Figure 3.3* shows the FTIR spectra of the aqueous *Citrus sinensis* peels extracts and the synthesized silver nanoparticles. The band at 3400 cm^{-1} is due to the presence of O-H band of the phenolic compounds and carbohydrates, the band at 2900 cm^{-1} is due to the C-H

band of the stretching vibration of the aliphatic hydrocarbons chains, either from the methylene or methyl group from the lipids in the aqueous extract. The band at 1600 cm^{-1} is due to the C=O stretch vibration of the phenolic compounds in the aqueous extracts such as aromatic alkenes. The band at 1400 cm^{-1} is a characteristic of the amide band. The strong peak at 1100 cm^{-1} is due to the C-N stretching vibration of aromatic amines and the band at 900 cm^{-1} is attributed to the O-H bonding. The FTIR spectrum for the three different silver nanoparticles synthesized using the different concentrations of the *Citrus sinensis* peels were similar to that of the aqueous extract of *Citrus sinensis*, however, a shift in peak position was observed. A decrease in intensities of the peaks was also observed especially the OH band at 3500 cm-1.

The results described above suggests that the orange peels extract contains bio-molecles with functional groups such as the O-H and COOH. These functional groups are responsible for the reduction of the Ag^{+} to Ag^{0}, also they act as stabilizing agents (Ren *et al*., 2019). This was further confirmed by the absorption bands that appear on the FTIR spectra of the AgNPs (Chahar *et al*., 2018). The results also correspond to the results given in *Figure 3.1* where both the total phenolic and flavonoid content were quantified. Schematic diagram 3.2 given below, shows the proposed mechanism in which the silver ion (Ag^{+}) interacts with the bio-molecules. Briefly, the electron is released from an enol of a phenolic compound. The electron released during the breaking of the H from the –OH bond reduces the Ag^{+} to Ag^{0} which is the silver nanoparticles. The shift in –OH band at around 3500 cm^{-1} in the FTIR spectra confims the proposed mechanism. (Logeswari *et al*., 2015).

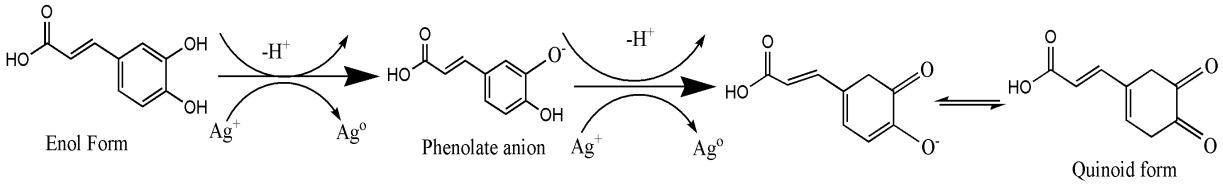

Scheme 3.2: Proposed mechanism for the synthesis of silver nanoparticles using the extract of *Citrus sinensis* peels

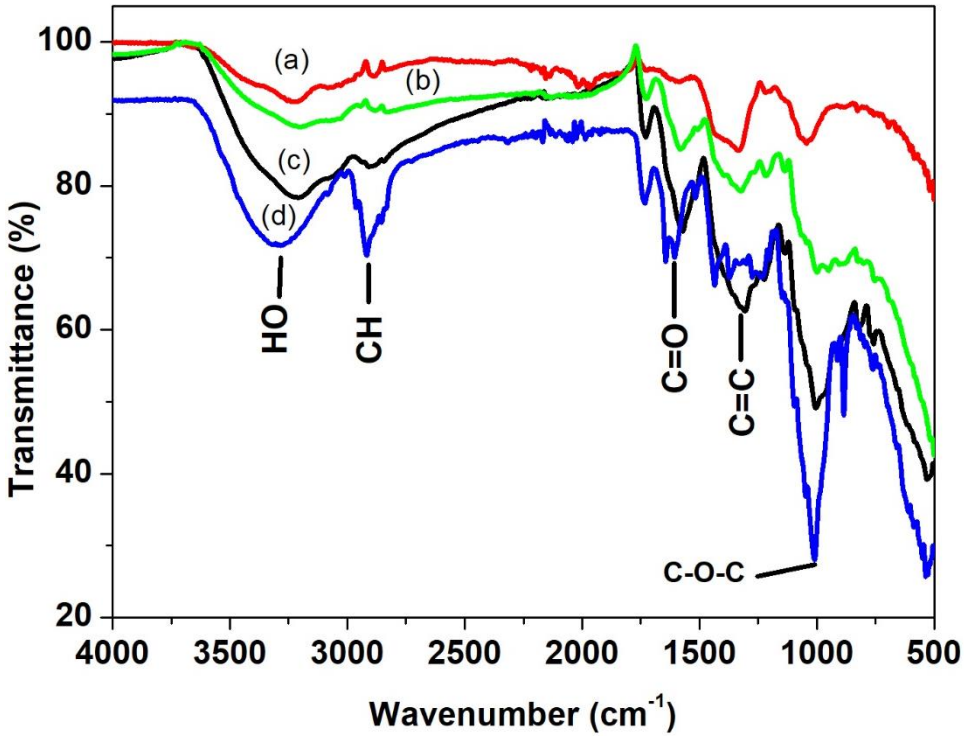

Figure 3.4: FTIR spectra of the plant extracts and silver nanoparticles synthesized using different concentration of Citrus sinensis peels extract (a) 1 %, (b) 2 %, (c) 3 % m/v and (d) *Citrus sinensis* peels extract

3.2.3. Transmission electron microscopic analysis

The morphology of the synthesized nanoparticles was evaluated using transmission electron microscopy (TEM). TEM images of the silver nanoparticles using the different concentrations of *Citrus sinensis* are presented in *Figure 3.4.* According to Figure 3.4 (A) and (B) the synthesized nanoparticles were agglomerated, with those synthesized using 1 % *Citrus sinensis* peel extract being the most agglomerated. Low concentration of the citrus sinensis peels (1 and 2 % m/v) means low concentration of the biological compound (Figure 3.1) thus the compunds are not efficient enough for the stabilization and dispersion of the nanoparticles. The silver nanoparticles synthesized using 3% *Citrus sinensis* were found to be polydispersed and spherical *Figure 3.4* (C), with a particle size distribution of 5 to 25 nm. Thus as the concentration of the *Citrus sinensis* peels increased, the agglomeration decreased. The high conentraion of the Citrus sinensis peels (3 % m/v) does not only accelerate Ag^+ but it is also more effective in preventing aggregation. The synthesized nanoparticles were found to have smaller particle sizes compared to other similar studies. Basavegowda & Rok Lee, (2013) synthesized silver nanoparticles using the *Citrus unshiu*, the average particle size was 20 nm. Majumdar *et al*., (2020) reported the synthesis of silver nanoparticles using *Citrus macroptera*

extract and their observed TEM images displayed particles with an average particle size of 16 (±2.96) nm.

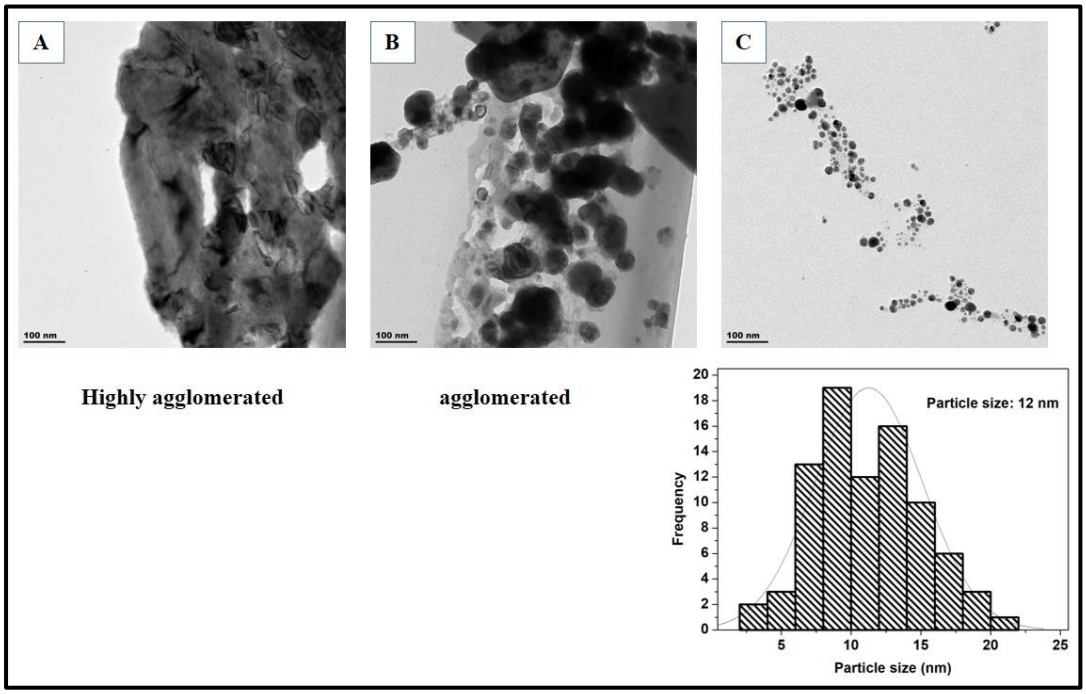

Figure 3.5: TEM images of silver nanoparticles (A, B, and C) synthesized using different concentrations of *Citrus sinensis* 1, 2, and 3 % m/v respectively and particle size distribution of silver nanoparticles synthesized using 3 % m/v Citrus sinensis peels extract.

3.2.4. XRD analysis

XRD spectroscopy was used to study the crystallinity of the synthesized nanoparticles and their structures. *Figure 3.5* shows the XRD patterns of the silver nanoparticles synthesized using the different concentrations of *Citrus sinensis*. According to Figure 3.5, four diffraction peaks with 2 theta values were observed at 38, 44, 64, and 80° respectively. The diffraction peaks can be indexed to 111, 200, 220, and 311 (JCPDS file NO. 04-0788) this proves the formation of silver nanoparticles. Samrot *et al.,* (2018) reported a similar characteristic peak when they synthesized silver nanoparticles using edible fruits. Konwarh *et al.*, (2011) also reported a similar XRD pattern when they synthesized silver nanoparticles using the *Citrus sinensis* peels extracts. The XRD patterns were further used to evaluate the crystallite sizes of the silver nanoparticles, the following sizes were observed 5.3, 5.1 and 4.9 nm for 1 %, 2 % and 3 % m/v AgNPs respectively. There is a decrease in size as the concentration is increased. Although the decrease was slight and could be influenced by the small intervals of the concentrations used. The calculated average particle size from the TEM images (*Figure 3.5*) were found to be different from the XRD sizes. This is because TEM images are obtained by placing a drop of

a sample onto the carbon film thus the drop cannot adequately represent the bulk of the sample and XRD technique is considered a bulk technique, further on nanoparticles can be polycrystalline (contain multiple crystalline domains) thus the crystalline domain does not necessarily corresponds to the particles size (Chahardoli et al., 2018).

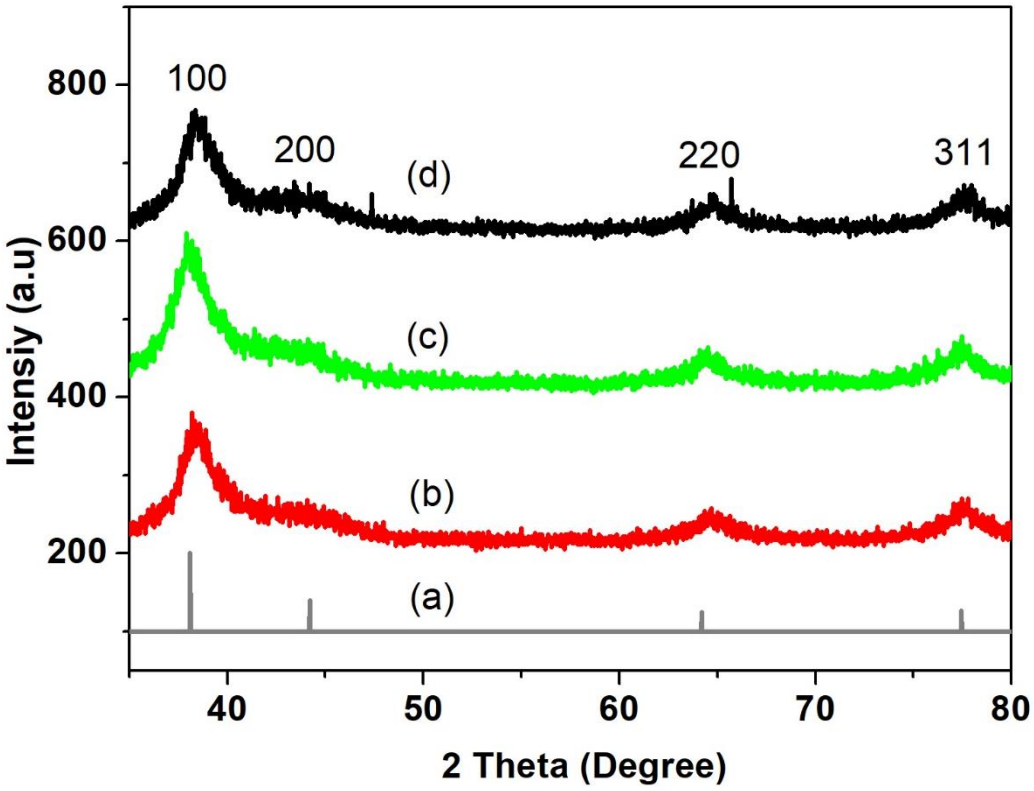

Figure 3.6: XRD diffraction patterns of silver nanoparticles synthesized using different concentrations of Citrus sinensis (a) reference spectra of silver (b) 1 %, (c) 2 % and (d) 3 % m/v.

3.2.5. Anti-bacterial activity of the synthesised nanoparticles

The antimicrobial activity of the synthesised nanoparticles was evaluated using MIC which is defined as the minimum concentration of the sample required to inhibit growth against the tested microorganisms. The synthesised nanoparticles (AgNPs 1, 2, and 3 %) were tested against gram-negative *K pneumoniae* and gram-positive *Staphylococcus aureu*s (*S. aureus).* While *neomycin* was used as a positive control. According to the results are given in Table *1.1*, all the synthesised silver nanoparticles were found to have antimicrobial activity against both *K. pneumonia* and *S. aureus*. This was probably because silver nanoparticles can change both the chemical and physical properties of the cell walls and cell membranes. This is achieved by attaching themselves onto the cell which is negatively charged and as a result disturbs the important functions such as respiration and osmoregulation (Sharma *et al*., 2009a). Further on

the synthesised nanoparticles causes damage within the bacteria cell by interacting with proteins and DNA after they permeate the bacteria cell wall (Ahn *et al*., 2019).

The synthesised nanoparticles and the *neomycin* which was used as a positive control were found to have higher antimicrobial activity against gram-negative *K. pneumonia* compared to the gram-positive *S. aureus*. Logeswari et al., (2015) also reported a similar trend when they synthesized silver nanoparticles using the *Citrus sinensis* peels extracts, their silver nanoparticles were found to have higher antimicrobial activity against gram-negative *K. pneumonia* compared to the *S. aureus*. The high activity that was observed against the gram-negative bacteria was attributed to the cell wall. Gram-negative bacteria are known to have thinner walls as compared to the gram-positive bacteria thus easier to permeate (Dakshayani et al., 2019; Vigneshwaran et al., 2007); On the other hand, silver nanoparticles cannot easily permeate and interact with gram-positive bacteria *S. aureus* due to the rigid structure that comes about the thick peptidoglycan which consists of peptides cross-linked together giving linear and chains of polysaccharides (Rashid *et al*., 2019). The synthesised silver nanoparticles gave better activity compared to the *neomycin* that was used as a positive control. The difference in activity was due to the fact that silver nanoparticles are known to be smaller in size and have a higher surface area. Therefore they have a higher adsorption capacity thus more likely to interact with bio-molecules (Ren et al., 2019; Sharma et al., 2009b).

According to Table 3.1 above, 3 % Ag nanoparticles gave the lowest MIC values of 0.06250 and 0.1250 mg/mL against *K. pneumoniae* and *S. Aureus* respectively. While 1% Ag nanoparticles gave 0.2500 mg/mL for both the *K. pneumoniae* and *S. aureus*. The high antimicrobial that was observed with 3 % AgNPs was due to the small size of the silver nanoparticles as shown in the TEM images in *Figure 3.4* compared to the other silver nanoparticles that were synthesized using 1 % and 2 % AgNPs at were found to be agglomerated (Hernández-morales. *et al*., 2019). Smaller nanoparticles are known to have high surface area thus can easily interact with the cell, permeate and destroy the cell (Jemilugba *et al.*, 2019).

Table 1.1: Antibacterial activity of silver nanoparticles synthesized using different concentrations of *Citrus sinensis* peels extract

Test organisms	Silver nanoparticles (mg/mL)			
	1% AgNPs-Cs	*2% AgNPs-Cs*	*3% AgNPs-Cs*	*Neomycin*
Staphylococcus aureus	*0.2500*	*0.2500*	*0.1250*	*2.5000*
Klebsiella pneumonia	0.2500	0.1250	0.0625	0.6250

3.3. Synthesis of cellulose nanocrystals (CNCs) from hemp fibres

In the previous section, green synthesized Ag nanoparticles showed desirable antibacterial activity towards both the bacterial strains, however, the reported toxicity of Ag nanoparticles when applied in their pure state cannot be ignored. The challenges that accompany the application of AgNPs in their pure state can be overcome by the incorporation of these AgNPs into polymer fibres. In this study, the synthesised AgNPs were incorporated into the PVA/CNC polymer fibres. In this section, cellulose was extracted from hemp fibres using an alkaline solution and bleach to remove the unwanted material. The extracted cellulose was further hydrolysed using sulphuric acid to prepare the cellulose nanocrystals.

3.3.1. Extraction of cellulose from hemp fibres

Schematic diagram 3:2 shows the images of the raw hemp fibres before and after treatment with NaOH, $NaClO_2$, to remove lignin, hemicellulose, and other impurities such as pectin. The raw hemp fibres exhibited a brownish/yellowish colour which changed to pale yellow after the alkaline treatment with sodium hydroxide and pure white after bleaching with $NaClO_2$. The change in colour during different stages of the treatment is due to the difference in chemical composition such as hemicellulose, lignin, and cellulose. Both the NaOH and $NaClO_2$ are known to remove all the impurities, lignin, hemicellulose, pectin and waxed as shown in the FTIR spectra *Figure 3.5* with the disappearances of peaks at around 1200 cm^{-1} and 1700 cm^{-1}, as the treatment progressed. The change in colour was due to the treatment with $NaClO_2$ which removed the phenolic compounds of the chromophore groups present in lignin through the oxidization of the quinoid and carbonyl structure of lignin (Wu *et al*., 2019)

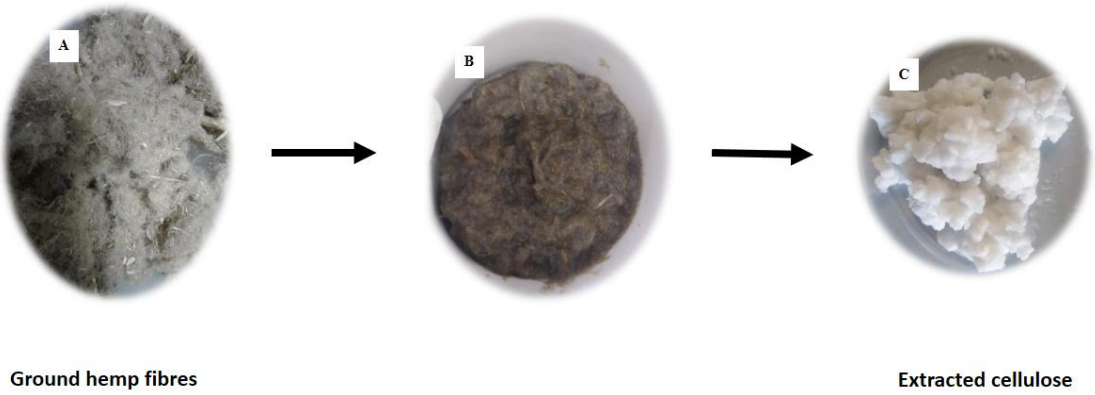

Scheme 3.3: Pictures showing the ground hemp fibres (A) after the alkaline treatment (B) and after bleaching (C)

(a) Scanning electron microscopic (SEM) analysis

SEM was used to demonstrate the effect treatment using the alkaline solution and bleach has on the morphology of the hemp fibres. According to *Figure 3.6* which shows the untreated raw hemp fibres, their strands were bound together in bundles with some smooth surface due to the presence of oils, waxes and other cementing material on the surface (Haghighatnia *et al*., 2017). The oil and waxes further cover the cellulose from interacting with any material. Treatment *Figure 3.6*. (B) resulted in a rougher surface and the diameter of the fibres was reduced which shows that some of the non-cellulosic material was removed (Sillard *et al*., 2017).

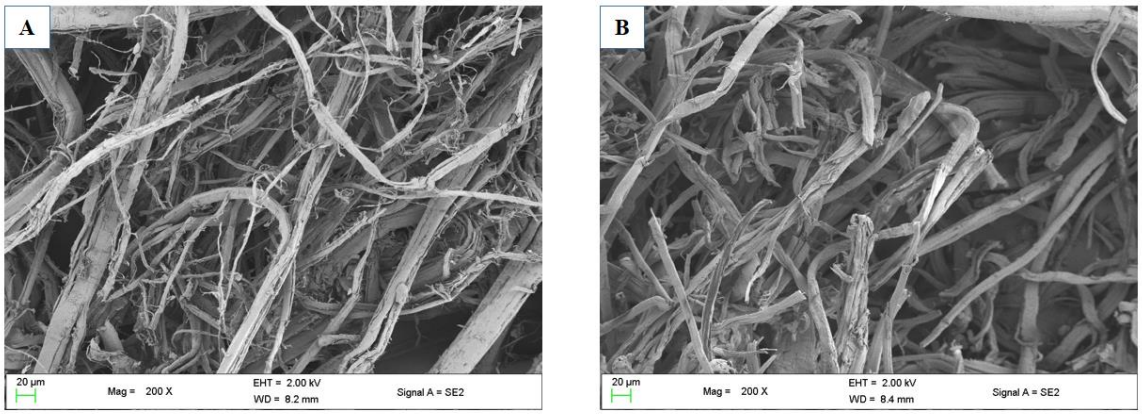

Figure 3.7: SEM images of hemp fibres before (A) and after treatment (B).

(b) FTIR spectroscopic analysis

FTIR spectroscopy was used to study the functional groups of hemp fibres, before and after treatment with NaOH and $NaClO_2$ and the results are shown in *Figure 3.7* below. Both the treated and untreated fibres showed characteristic peaks of cellulose. The broad peak observed at around 3500 cm^{-1} can be assigned to the stretching O-H group while the peak at 2900 and

1640 cm^{-1} can be assigned to the sp^3 C-H stretching vibration and the OH bending of the absorbed water respectively (Yang *et al*., 2020). The absorption band at around 1400 cm^{-1} can be assigned to the C-H_2 symmetric bending. The band at 1300 cm^{-1} can be assigned to the bending vibration of C-H and C-O groups of the aromatic ring in polysaccharides. Lastly, the peaks at around 1000 cm^{-1} can be attributed to C-O and OH (Kalpana & Perarasu, 2020).

There was a complete disappearance of an absorption band at around 1700 cm-^{1} which was present only in the pure hemp fibres following both the alkaline and bleaching treatment, the disappearance of the peak can be assigned to C=O of the ferulic and p-Coumaric acid of lignin and the hemicellulose or the acetyl group in hemicellulose. Thus the disappearance of this peaks indicates the removal of both the lignin and the hemicellulose (Gao *et al*., 2019),). Further on, the spectra showed the disappearance of another peak at around 1200 cm^{-1} which can be assigned to the C-O stretching of the aryl group in lignin and the CO-OR stretching vibration of hemicellulose (Gabriel *et al*., 2020; Melikoğlu *et al*., 2019). Another peak at around 820 cm^{-1} which can be assigned to the wagging vibration of the CH in the 1.4-substitutional aromatic ring in lignin was also found to have disappeared after treatment.

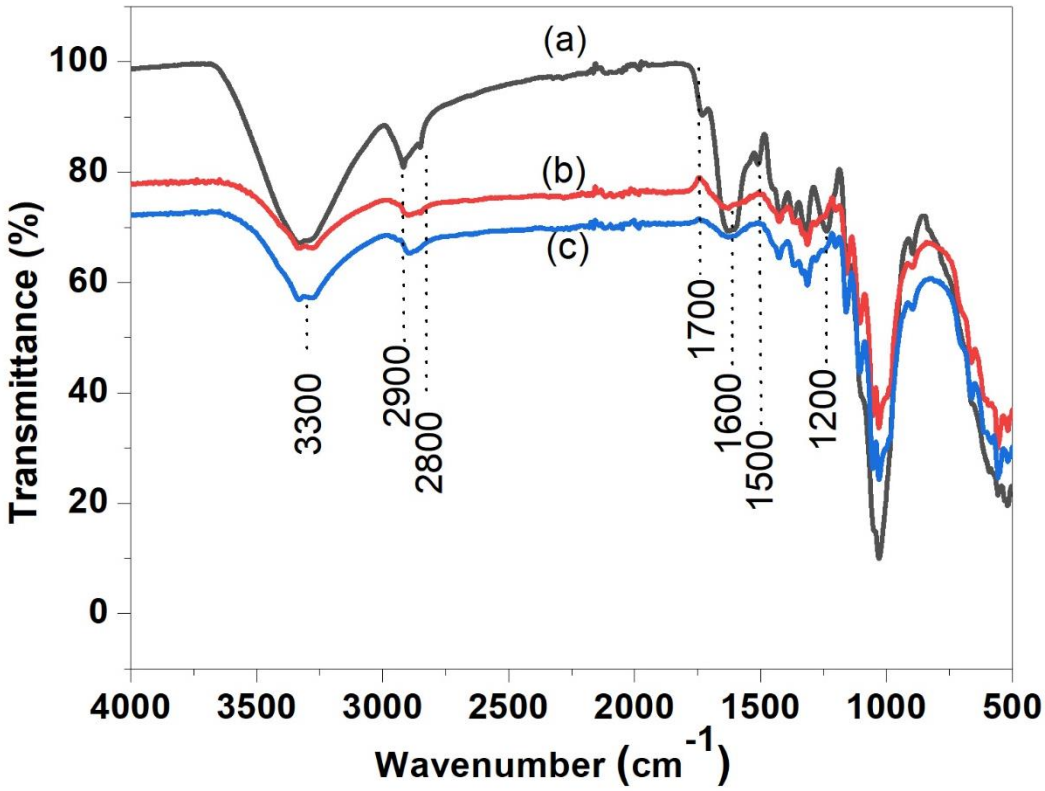

Figure 3.8: FTIR spectra of (a) untreated raw hemp fibres, (b) alkaline, and (b) bleached hemp fibres.

(c) XRD analysis

Powder XRD was used to establish the change in crystallinity of hemp fibres after treatment with NaOH and $NaClO_2$. The XRD patterns of the raw hemp fibres before and after treatment (alkaline and bleaching) are given in Figure 3.8. There are 4 peaks at around 2θ values of 15, 16 23, and 34. The peaks at 15 and 16 correspond to (110) and (110) the other peaks at 23 and 34 corresponds to (200) and (004) planes. The large distinct peak at 2θ value of 23 corresponds to the crystallographic planes of cellulose I (I_{200}) (Zhang *et al*., 2020). Significant changes can be observed regarding the intensity of the peaks from the raw hemp fibre, all the way to the bleached fibres. Further on, as the treatment progressed from alkaline to bleaching, the peak around 16 for which was observed with the untreated hemp fibres developed into two distinct peaks and this can be attributed to the high concentration of cellulose. Since when compared to the untreated hemp fibres, the peak at 16 $^{\circ}$ was broad and this was due to the amorphous material such as the amorphous cellulose, hemicellulose, and lignin. The XRD pattern corresponds with the FTIR spectra in *Figure 3.7* were the characteristic peaks of cellulose structure were observed in all the FTIR spectrum before and after treatment. The crystallinity index for the raw hemp fibres, alkali-treated fibres, and the bleached fibres was calculated according to the equation given in Equation *2.1* and it was found to be 28.97, 56.59, and 59.06, respectively. The increase in crystallinity as the treatment continued can be attributed to the relaxation of the cellulose chains and also better packing of the cellulose chains due to the removal of the amorphous constituents (John & Thomas, 2008). The increase in crystallinity index shows an improvement in chemical and thermal stability.

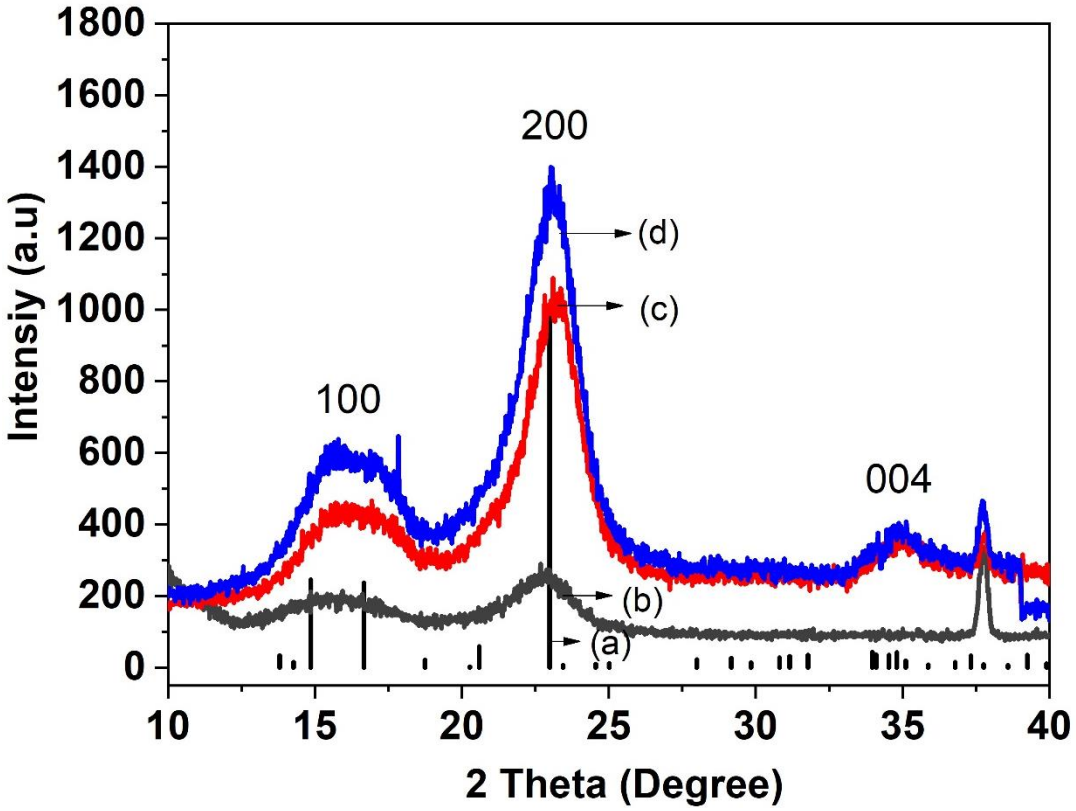

Figure 3.9: XRD patterns of the reference spectra of cellulose (a), raw hemp fibres (b) alkaline teated hemp fibers (c) and bleached hemp fibers (d) .

3.3.2. Synthesis of cellulose nanocrystals from the extracted cellulose

(a) FTIR spectroscopic analysis

The effect that hydrolysis has on the chemical structure and composition of the extracted cellulose (Bleached hemp fibres) was studied using FTIR spectroscopy and the results were compared to that of commercial cellulose. In general, no significant difference was observed between the FTIR spectra of the bleached fibres *Figure 3.8* cellulose nanocrystals (CNC), and commercial cellulose *Figure 3.9*. The absorption band at 3500 cm^{-1} can be assigned to the O-H stretching group of the intramolecular hydrogen bonds in cellulose (i). The bands between 2800-2900 cm^{-1} can be attributed to the asymmetric and symmetric aliphatic CH_2 and CH_3 stretching vibrations (Baskar *et al.*, 2018). The band at around 1600 cm^{-1} can be assigned to the bending mode of adsorbed moisture on the surface of the samples and as well as the carboxylate group (Wang & Zhao, 2021). The band at 1400 cm^{-1} can be attributed to the CH_2 asymmetric bending motion in cellulose. The absorption band at 1350 cm^{-1} was due to asymmetric C-H deformation and the band at 1300 cm^{-1} may be due to the CH_2 wagging. The band at around 1160 cm^{-1} can be assigned to C-O-C asymmetric bridge stretching vibration in

the cellulose structure (Singh *et al*., 2020). The peak at 1020 cm^{-1} was due to the C-C and C-O stretching in cellulose. This suggests that the cellulose nanocrystals were synthesised from the extracted cellulose (Ba, 2020).

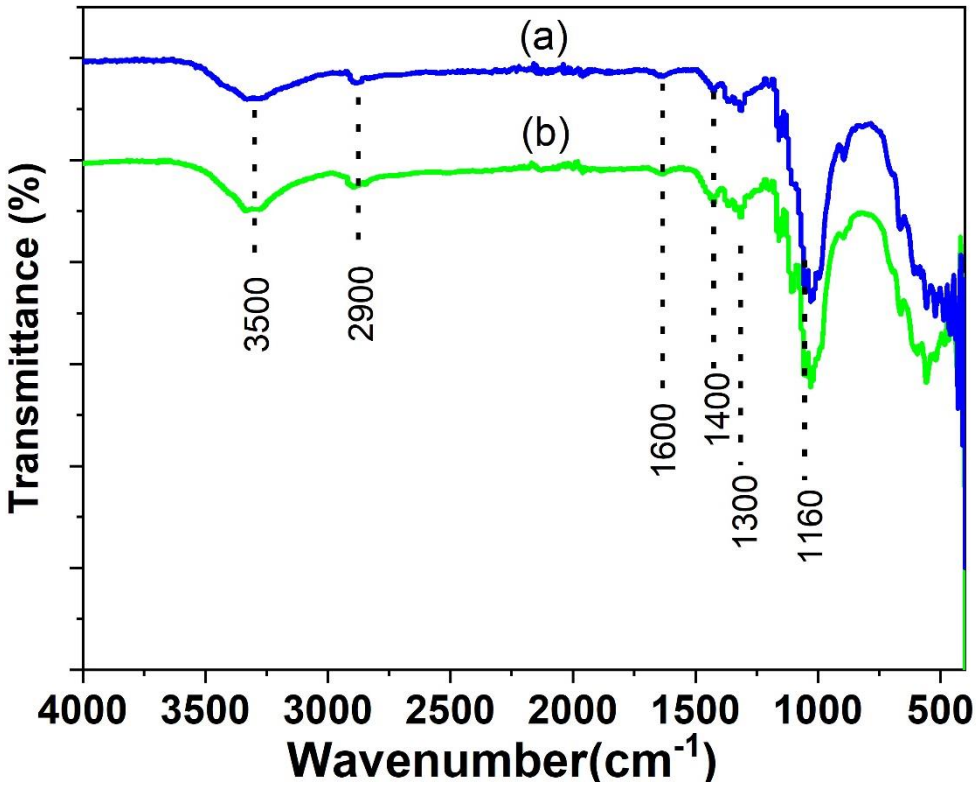

Figure 3.10: FTIR spectra of cellulose nanocrystals (a) synthesised by hydrolysing the extracted cellulose using sulphuric acid compared to the FTIR spectrum of commercial cellulose (b).

(b) XRD analysis

Figure 3.10 shows the XRD patterns of the cellulose nanocrystals (CNC's) isolated from the treated hemp fibres using sulphuric acid and commercial cellulose. The XRD pattern of the CNC's and the synthetic cellulose showed similar peaks at 16.5, 22.5, and 34.5 º which were also observed in *Figure 3.8*. This proves that the cellulose structure was still not destroyed after hydrolysis with the sulphuric (Bao *et al*., 2021; Khanjanzadeh *et al.*, 2019) The crystallinity index of the isolated CNC's was found to be 70.92. The increase in the crystallinity index was due to the release of the crystallites segments from the cellulose chains, which takes place when the hydronium ion (H_30^+) from the sulphuric acid penetrated readily into the amorphous region of the extracted cellulose to cause hydrolytic cleavage of the β-1,4-glycosidic linkages in the cellulose. The high crystallinity index also means high mechanical strength and also means better reinforcements for composites (Chougan *et al.*, 2020; Prasanna & Mitra, 2020; Verma *et al.*, 2021).

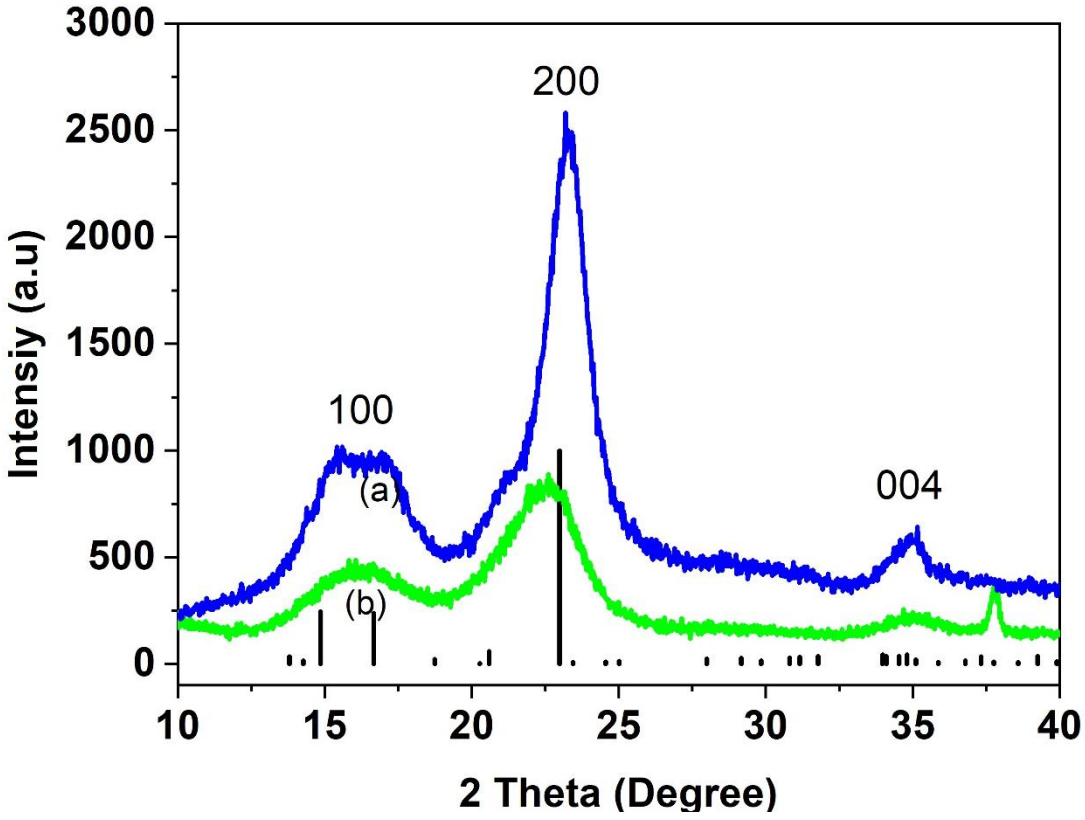

Figure 3.11: XRD patterns of synthesized cellulose nanocrystals (a) and pure cellulose (b)

(c) Transmission electron microscopic (TEM) analysis of CNC

The structure of the isolated CNC's from the hemp fibres was elucidated using transmission electron microscopy as shown in *Figure 3.11* below. According to the micrograph, the isolated CNC's presented needle-like structures with some degree of agglomeration. This shows that the sulphuric acid managed to hydrolyse the amorphous part of the cellulose leaving behind the crystalline part. The overlapping of the individual CNC's as shown in the TEM image made the accurate dimension measuring difficult. Tan *et al*., (2015) also observed similar results when they tried to isolate CNC's from cotton linters. According to their TEM results, some parts of the CNC's were found to be agglomerated white the other part were found to be separated. Evans *et al*., (2019) isolated CNC's from sugarcane bagasse and according to their results, the CNC's were found to be spherical and agglomerated.

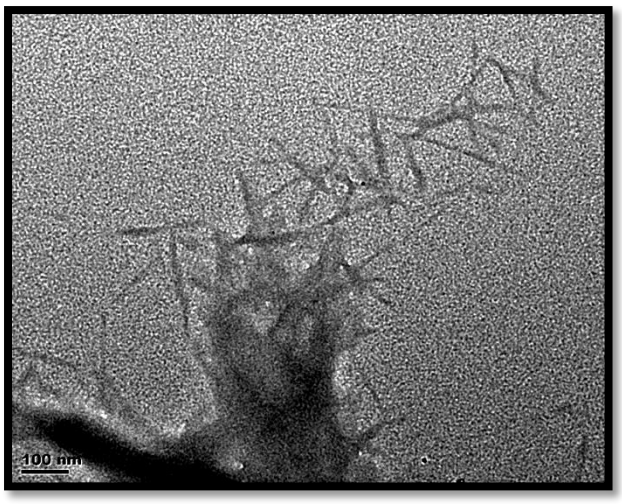

Figure 3.12: TEM micrograph of cellulose nanocrystals

3.3.3. Fabrication of PVA/CNC polymer fibres using the electrospinning technique.

In this study, the cellulose nanocrystals (CNCs) that were synthesized from the cellulose, was extracted from hemp fibres were blended with polyvinyl alcohol (PVA) to improve its conductivity and electro spinnability. The blending of PVA with CNC significantly improves the mechanical strength of PVA fibres, since CNC's are stiff and contain many hydroxyl groups which render good compatibility with PVA molecules The blended fibres were also compared with unblended PVA fibres and lower percentages of CNCs were used as a result of pure CNC solution inability to electrospun. The 10 % PVA was deemed optimum for use and combined with 3 % of CNC's.

3.3.3.1.Comparison of neat PVA fibres and PVA/CNC polymer fibres

(a) SEM of neat PVA and PVA/CNC

Figure 3.12 shows the morphology of the electrospun fibres of neat PVA and PVA loaded with cellulose nanocrystals (10 % PVA/3 % CNC). Pure CNC solution produced no fibres as the solution was spraying which resulted in the formation of droplets on the aluminium foil. PVA solution, in contrast, yielded flat-like beaded free fibres *Figure 3.12* (A). According to *Figure 3.12* (B) addition of CNC's to PVA resulted in the fabrication of cylindrical, uniform, and beaded free fibres. Any concentration above 3% CNC was difficult to electrospun. This is due to the phase separation between the PVA and CNC and also the high viscosity of the resultant solution. The fibre diameter of the neat PVA 186 (±36) nm increased with the addition of the CNC's 438 (±175) nm . The increase in fibre diameter was due to the increase in viscosity

when the cellulose nano-crystals were added to PVA (Zou *et al.*, 2020). Ago *et al.*, (2020) also observed an increase in the diameter of the fibres when they added lignin into PVA.

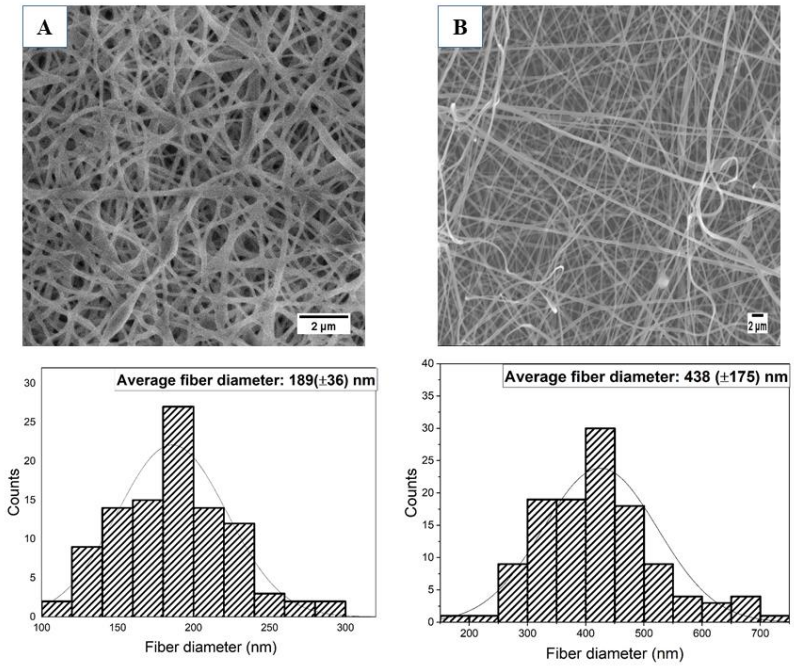

Figure 3.13: SEM images of A) Pure PVA and B) PVA/CNC

(b) FTIR spectroscopic analysis of PVA and PVA/CNC

The FTIR spectra of CNC, PVA, and the bio-composite of PVA and CNC is shown in *Figure 3.13* . The spectra show common bands at 3500, 2900, 1400, and 1300 cm^{-1}. The band at 3500 cm^{-1} can be attributed to the OH- stretching while the band at 2900, 1400, and 1300 can be assigned to bending, stretching, rocking, and wagging modes of C-H bands. The absorption band at 1700 cm^{-1} can be assigned to the C=O from the poly acetate residue which was used as a starting material to produce PVA (Kim *et al.*, 2019). The peak at 3500 cm^{-1}, which is attributed to the hydroxyl (OH) stretching due to the intermolecular and intramolecular bonds. The addition of CNC to PVA caused a slight shift in the OH bands and this was due to the interaction between the OH in PVA and the OH found on the surface of the Cellulose nano-crystals (Fortunati *et al.*, 2013). The band at 2900 cm^{-1} corresponds to the alkyl group –CH stretching. The addition of CNC resulted in the appearance of two additional peaks at 1170 cm^{-1} and 1030 cm^{-1}. The band at 1030 cm^{-1} can be attributed to the asymmetric ring breathing mode of cellulose while the band at 1170 cm^{-1} can be assigned to the C-OH bending vibrations of alcohol found in cellulose. The absorption band at 850 cm^{-1} can be assigned to the β-1,4-glycosidic linkages.

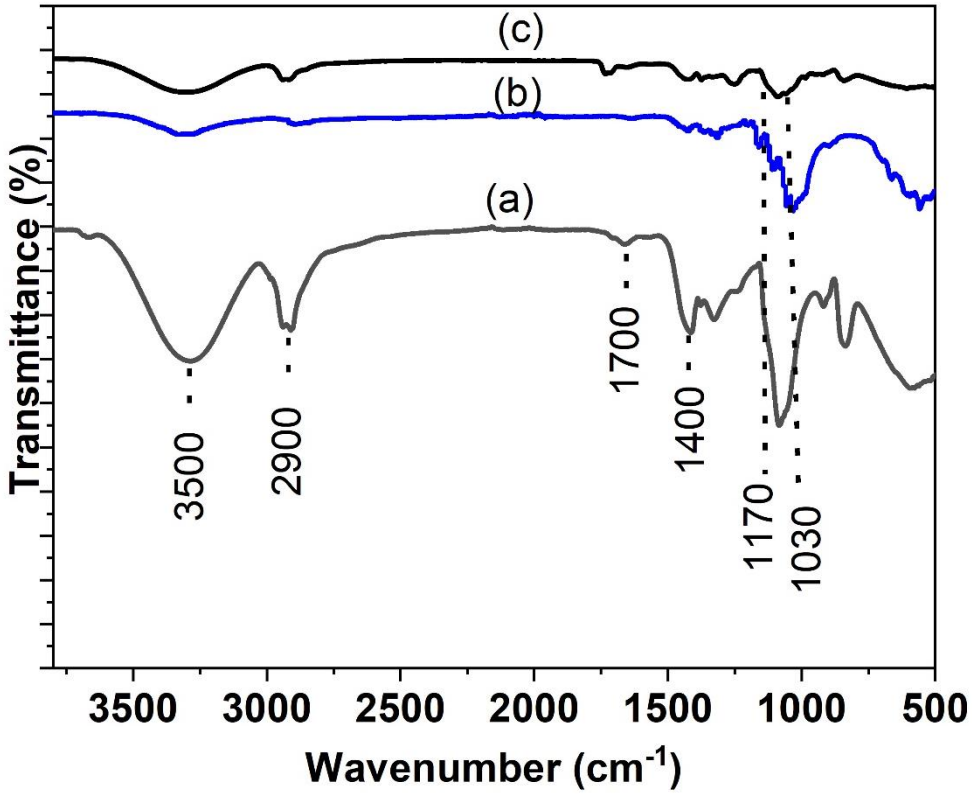

Figure 3.14: FTIR spectra of Pure PVA (a), CNC (b) and PVA/CNC (c).

(c) XRD analysis of PVA and PVA/CNC polymer fibres

XRD was used to study the crystallinity of PVA, CNC's, and the bio-composite of PVA/CNC. According to *Figure 3.14* the diffractogram for PVA shows a strong peak at 19.8 ° and a shoulder peak at 22 ° which can be attributed to its crystalline structure (Koosha *et al.*, 2019). PVA has another peak at 40 ° and that peak can be assigned to PVA's amorphous region thus confirming the semi-crystalline nature of PVA (Popescu, 2017). The XRD pattern for cellulose nanocrystals showed four distinct peaks at 14.8 °, 16.5 °, 20.4 °, and 22° assigned to 101, 101, 102, and 200 planes of cellulose respectively. The addition of CNC's to PVA increased the intensity of the characteristic peak of PVA at around 23 °. Adding CNC to PVA reduces the amorphous region of PVA in the bio-composite material. The incorporation of CNC's into PVA did not change the crystalline structure of PVA (Singh *et al.*, 2018). Sriupayo *et al.*, (2005) incorporated chitin whiskers into PVA nanocomposite films and according to their results, the nanocomposite became more crystalline as they increased the concentration of chitin whiskers.

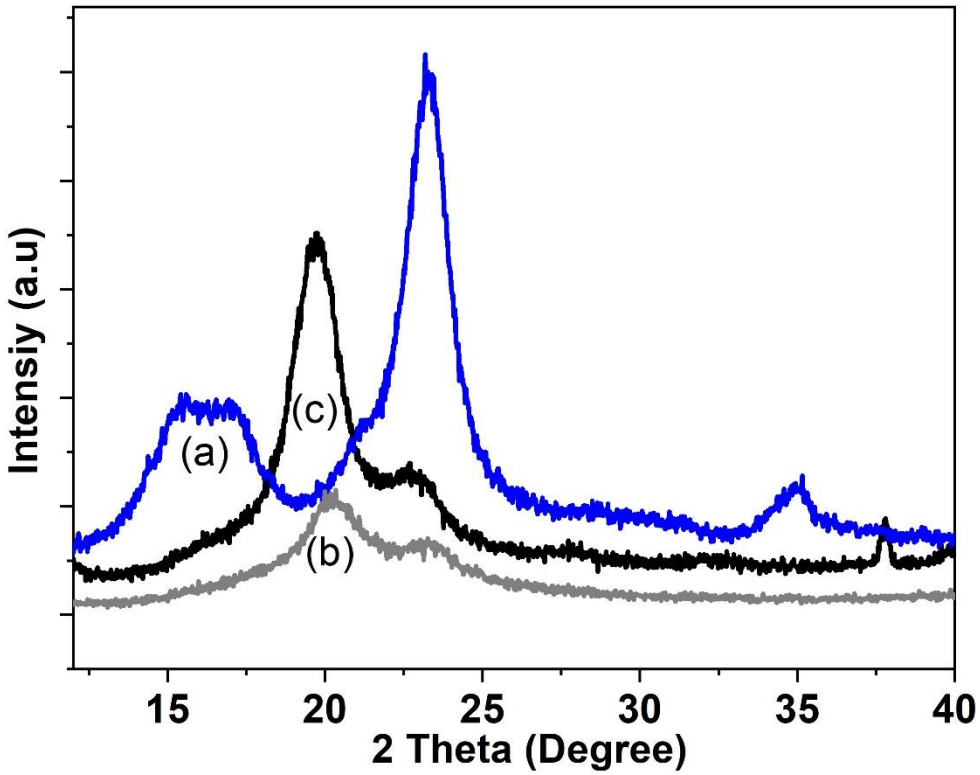

Figure 3.15: XRD pattern of CNC's (a), Pure PVA (b) and, PVA/CNC (c) polymer fibres.

3.3.3.2.Optimization of parameters

(a) Optimization of the concentration of CNC's (1, 2, and 3% m/v) in the PVA polymer fibres.

Figure 3.15 shows the SEM of pure PVA fibres and PVA/CNC polymer fibres loaded with increasing content of CNC's (1 %, 2 %, and 3 % m/v). According to the results, the fibres were more uniform compared to the pure PVA fibres. The improvement in the fibre structure may be due to better molecular interaction between PVA and CNC's which results in more entanglement and more uniform flow upon fibre formation (Peresin *et al*., 2014). No obvious beads were observed on the fibres. The addition of cellulose nanocrystals PVA resulted in a decreased fibre diameter from 454, 441, and 438 nm for 1 %, 2 %, and 3 % CNC's, respectively. This behaviour could be attributed to the increase in conductivity and viscosity. The increase in conductivity increases the electrostatic force which made it easier to overcome the surface tension of the polymer solution and allowing stretching of the polymer jet leading to homogeneous fibres. Cellulose nanocrystals are negatively charged due to the sulphate group present on the surface of the cellulose nanocrystals. Increasing concentration of CNC's enhanced the conductivity of the polymer solution resulting in a decrease in fibre diameter.

Patel et al., (2020) added cellulose nano-crystals poly (lactic acid) and the diameter of the fibres decreased. Sobolčiak *et al.*, (2017) also observed similar results when CNC was loaded into PVA polymers fibres. There was a decrease in diameter and this was due to an increase in conductivity. The PVA/CNC concentration of 3 % CNC's was taken as the optimum concentration due to the beadles' fibres with a lower diameter compared to the other PVA/CNC with 1 % and 2 % CNC content.

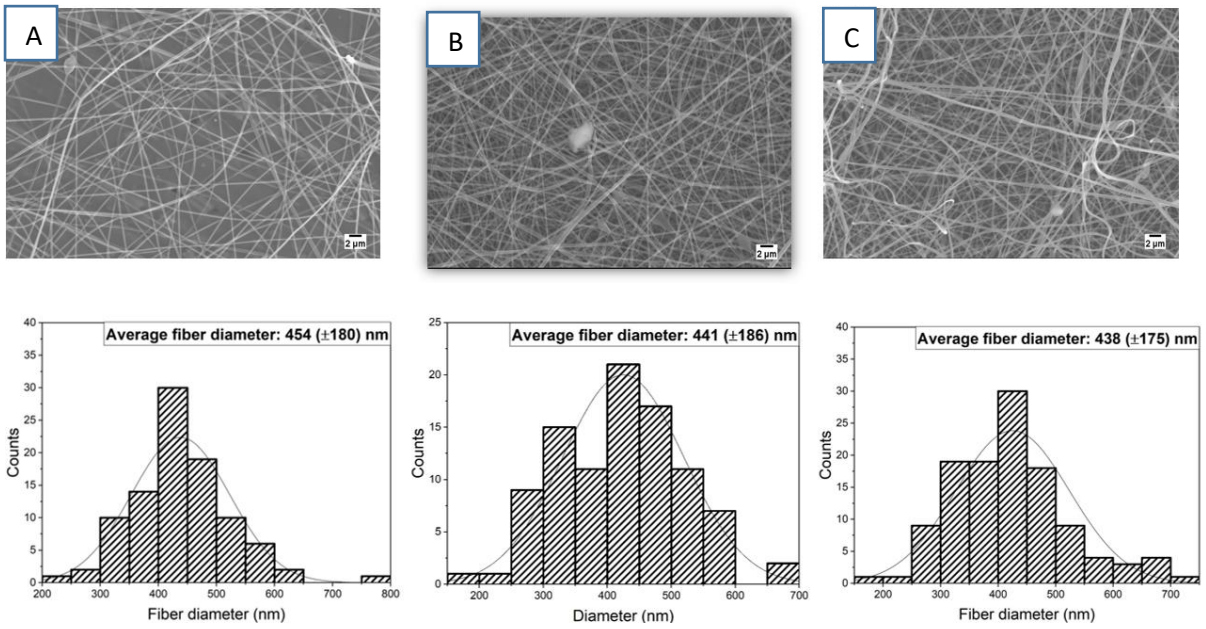

Figure 3.16: SEM images of the reinforced PVA nanofibres at different loading of CNC A) 1 %, B) 2 % and C) 3 % wt/wt. And their respective distribution curves.

(b) Optimization of the applied voltage

Error! Reference source not found. *Figure 3.16* shows the SEM images PVA/CNC polymer fibres. The concentration of PVA/CNC was 10:3 while the distance was kept constant at 10 cm. The voltage was varied between 17 and 21 kV. According to the SEM images, the diameter of the fibres decreased as the voltage increased. At high voltage the ejected jet experience greater stretching which results to decreased fibre diameter. The decrease in fibre diameter may also be due to the rapid evaporation of the solvent. More *et al*., (2015) also observed a similar trend, where the diameter of the fibre decreased when they electrospun PVP and the voltage was increased. Although the diameter of the fibres decreased as the voltage increased, the fibres obtained when 21 kV was used showed visible beads. Thus 20 kV was taken as the optimum voltage.

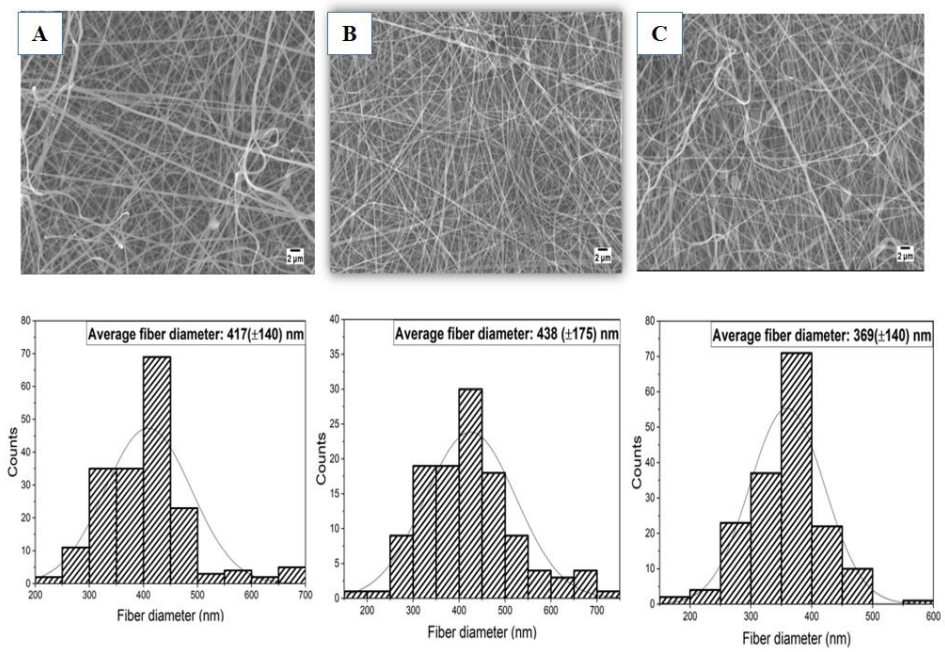

Figure 3.17: SEM images of PVA/CNC nanofibres at different voltages A) 17 kV, B) 20 kV and C) 21 kV and their distribution curves.

3.3.4. Incorporation of silver nanoparticles into PVA/CNC polymer fibres at increasing concentration

In this section, silver nanoparticles were incorporated into the PVA/CNC polymer fibres using the electrospinning technique to provide the controlled release of either the Ag^+ or the AgNPs at effective levels. further on the incorporation of the AgNPs into the PVA/CNC polymer fibres enabled the fabrication of functionalized nanofibrous composite by combining the unique properties of both the nanofibers and AgNPs. The antibacterial activity of the PVA/CNC incorporated with the AgNPs was evaluated using gram-positive *S. aureus* and gram-negative *K. Pneumonia*e as models.

*(a) Sc*anning electron microscopic (SEM) analysis

Figure 3.17 shows the SEM micrographs of PVA/CNC polymer fibres incorporated with increasing concentrations of silver nanoparticles (1 %, 2 %, and 3 % m/v). Uniform flat-like, beaded free fibres were obtained. The diameter of the fibres was found to decrease as the concentration of the silver nanoparticles loaded into the PVA/CNC polymer fibre was increased. The average fibre diameter was 385, 306, and 295 nm for 1, 2, and 3 % AgNPs respectively. The decrease in fibre diameter can be explained as follows; the Addition of silver nanoparticles into the PVA/CNC polymer solution increases the charge density of the ejected

jet thus strong elongation forces are exerted on the ejected jet resulting in fibres with a smaller diameter (Nguyen *et al.*, 2011). Ren *et al*., (2017) also observed a decrease in the fibre diameter of Polyacrylonitrile polymer fibres (129 nm) when they incorporated silver nanoparticles (118 nm).

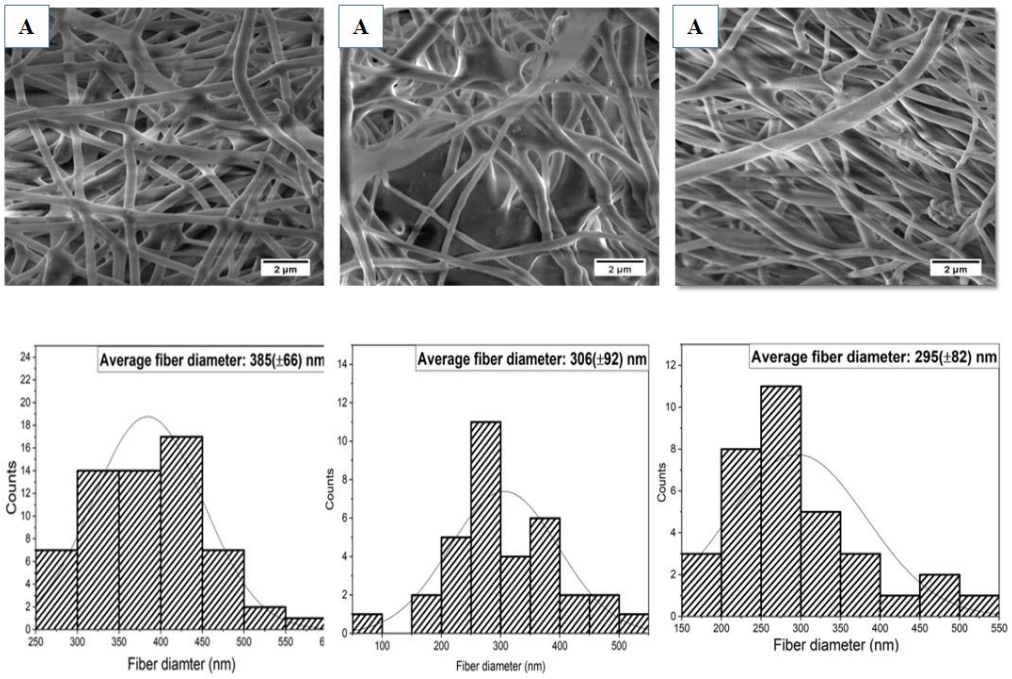

Figure 3.18: SEM image of variation of concentration of silver nanoparticles, 1 % (A), 2 % (B), and 3 % (C) incorporated into the PVA/CNC polymer fibres and their respective distribution curves.

(b) FTIR spectroscopic analysis

Figure 3.18 shows the FTIR spectra of PVA/CNC and PVA/CNC loaded with increasing concentrations of AgNPs (1 %, 2 %, and 3 % m/v). The spectra for all AgNPs-PVA/CNC showed all the PVA/CNC typical characteristic peaks at 3200, 900, 1400, and 1030 cm $^{-1}$. The peak at 3500 cm^{-1} is attributed to the presence of the OH group stretching, 2900 cm $^{-1}$: C-H, 1416 cm $^{-1}$: CH_2, and 1100 cm $^{-1}$ is related to the CH_2 scissoring and stretching C-O. According to the spectra, there was no obvious difference between the spectra of pure PVA/CNC fibres and the PVA/CNC loaded with AgNPs. However, the addition of the AgNPs into the PVA/CNC affected the PVA absorption bands at, 1244 and 1370 cm^{-1} which can be attributed to C-OH out-of-plane vibration and the coupling OH vibration, respectively. The change signifies interaction between the AgNPs and OH in PVA. Since no new peaks were observed, the FTIR spectra indicated that the addition of Ag nanoparticles does not affect the functional groups with the PVA/CNC (George *et al.*, 2014).

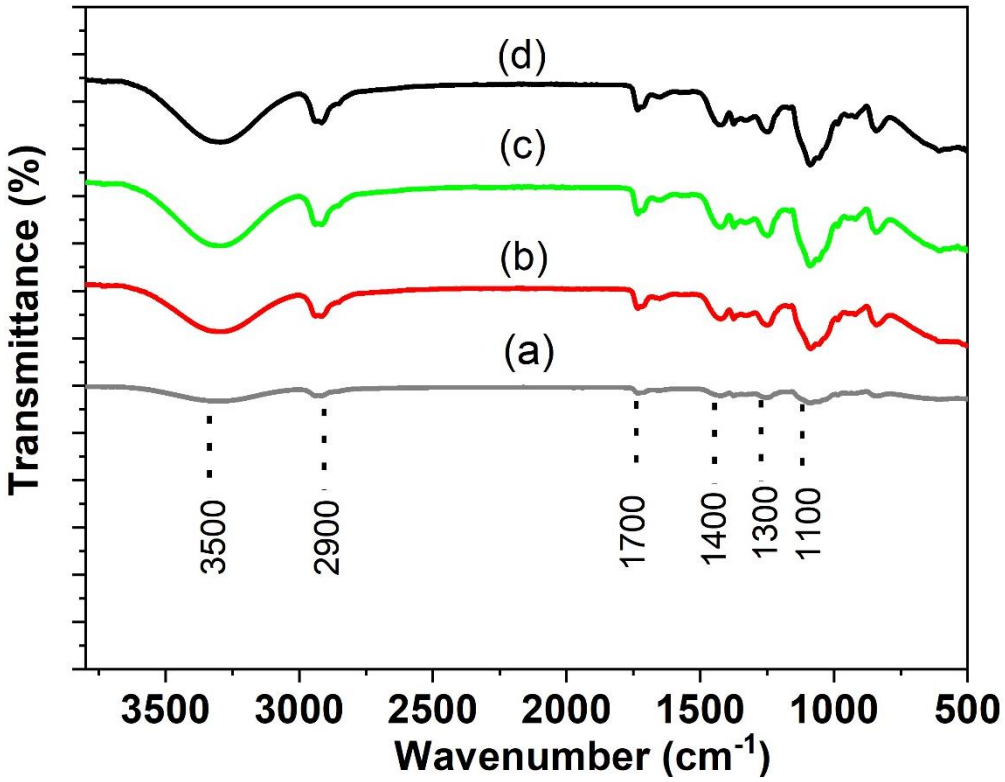

Figure 3.19: FTIR spectra of PVA/CNC (a) incorporated with AgNPs 1 % (b), 2 % (c) and 3 % wt/wt (d).

(c) XRD analysis

Figure 3.19 shows the XRD patterns of PVA/CNC polymers and PVA/CNC loaded with increasing content of silver nanoparticles (AgNPs-PVA/CNC). The diffraction pattern shows five distinct peaks. The peak at approximately 2 theta, 20 ^{o} can be assigned to the PVA/CNC while the other peaks at 38, 44 , 65 and 78 ^{o} can be attributed to the reflection plane 111, 200, 331, and 222 planes of metallic silver with a face-centred cubic lattice. Some of the peaks of AgNPs were not visible due to the resolution limit of XRD analysis (Abdel-Mohsen *et al.*, 2019). The XRD patterns of the PVA/CNC incorporated with the increasing amount of AgNPs were similar to that of the original synthesized nanoparticles before the incorporation *Figure 3.12* Which shows that the incorporation of the silver nanoparticles into the polymer fibres does not change the crystalline structure of the original synthesized silver nanoparticles. As the concentration of AgNPs increased, the main crystalline peak at 40 ° corresponding to the main plain at 111 increased. Augustine *et al.*, (2018a) observed a similar diffraction pattern when they incorporated silver nanoparticles into PVA polymer fibres.

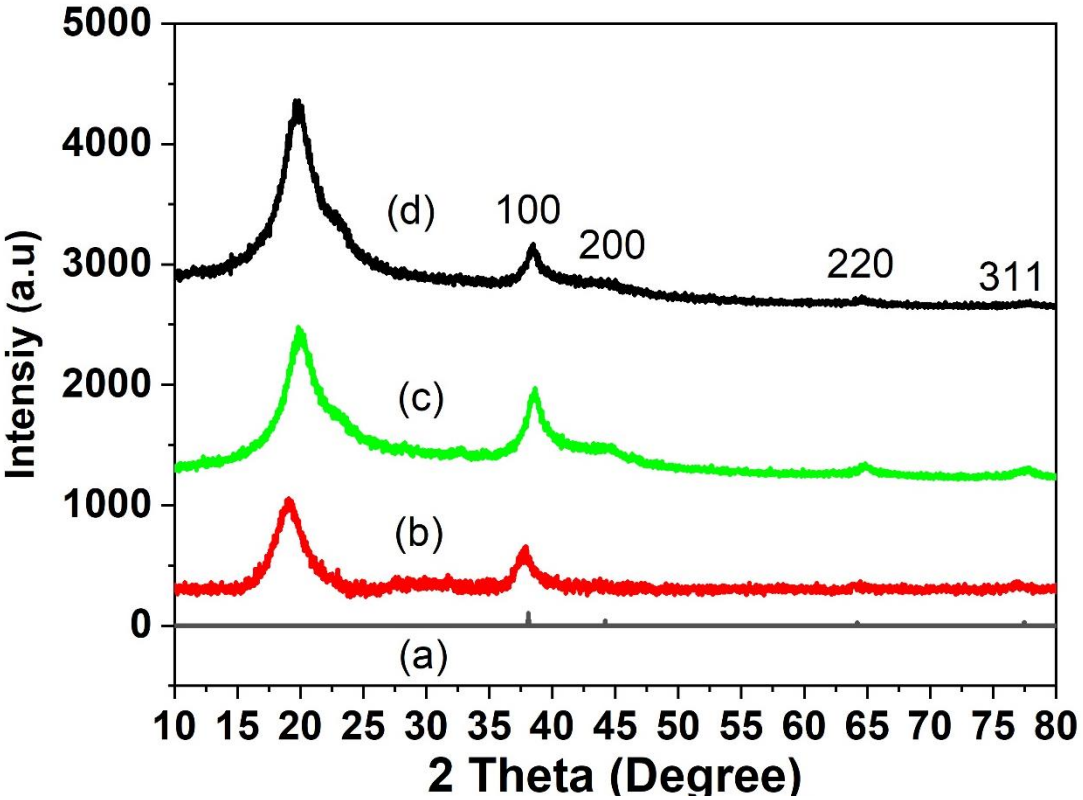

Figure 3.20: X-ray diffraction pattern of Ag reference spectra (a) and PVA/CNC incorporated 1 % (b), 2 % (c) and 3 % (d) AgNPs

(d) Antibacterial assay: Disk diffusion

The disk diffusion assay was used to study the antibacterial activity of PVA/CNC polymer fibres incorporated with increasing concentrations of AgNPs (1, 2, and 3 %). Gram-positive *S. aureus* and gram-negative *K. pneumoniae* were used as models. The disk diffusion assay was taken as a qualitative test, rather than a quantitative test since no defined halos were observed around the samples (Spagnol *et al.*, 2018). The zone of inhibition is influenced by the degree of leaching of the silver nanoparticles from the PVA/CNC polymer fibres. According to the digital images shown in *Figure 3.20*, all the AgNPs-PVA/CNC exhibited antibacterial activities towards both the bacteria. This was due to the interaction between the silver nanoparticles and the constituents on the cell wall of the bacteria which result in structural changes and degradation that eventually leading to cell death (Sondi & Salopek-sondi, 2004). further on, the highest AgNPs 3 %, exhibited higher antibacterial activity compared to the 1 % and 2 % AgNPs-PVA/CNC. According to Xu *et al*., (2013) silver nanoparticles that are less than 15nm in size have efficient antibacterial activity as they can easily penetrate through the cell wall of the bacteria and interact with the sulfur/phosphorous compound on the DNA thus causing more damage. The antibacterial efficiency that was observed can be linked to the TEM

images given in *Figure 3.4*. The Silver nanoparticles that were synthesized using 3 % *Citrus sinensis peels* extracts had an average particle size of 12 nm while the other (2 % and 1 %) were found to be agglomerated thus unable to penetrate the inside of the bacteria. Aadil et al., (2018) also observed similar antibacterial results when they loaded silver nanoparticles into PVA/Lignin and tested their antibacterial activity against gram-positive (*S. aureus*) and gram-negative (*B. Circulans*). The PVA/lignin polymer fibres loaded with the AgNPs were active against both the bacterial strains, however, the halos were also not defined thus the zone of inhibition could not be measured.

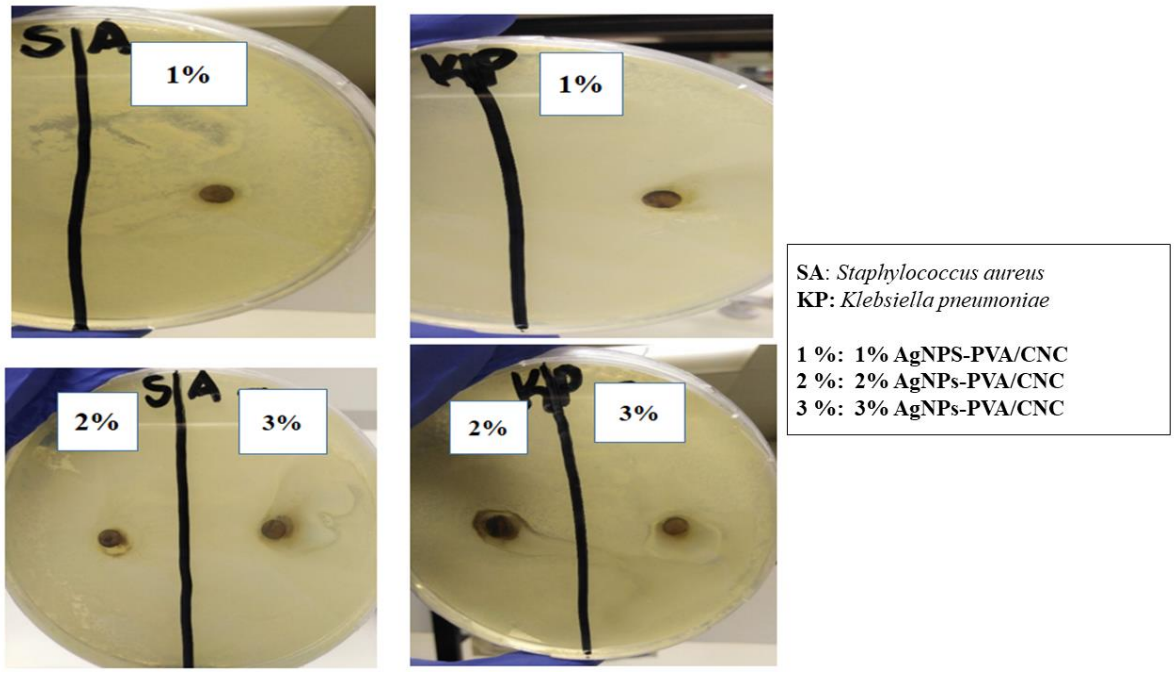

Figure 3.21: Digital images of petri-dishes of AgNPs-PVA/CNC inhibiting the growth of *S. aureus* and *K .pneumoniae*.

3.3.5. Incorporation of eucalyptus oil into PVA/CNC polymer fibres under various concentrations

Various types of essential oils such as the eucalyptus oil are derived from secondary metabolisms of some plants and are widely known for their broad antimicrobial activity. However pure essential oils tend to be volatile, sensitive to air/sunlight, and may impart their odours. To overcome the challenge, in this section; the eucalyptus oil was incorporated into PVA/CNC polymer fibres using the electrospinning technique and their antibacterial activity was evaluated using gram-positive *S. aureus* and gram-negative *K. pneumoniae.*

(a) Scanning electron microscopic (SEM) analysis

Figure 3.21 shows the SEM images of PVA/CNC loaded with the increasing amount of eucalyptus oil. The fibrous mats showed spindle-like beads. The beads were shown to increase as the concentration of the oil increased. The average fibre diameters were 280, 252, and 231 nm for 1, 2, and 3 % oil, respectively. The increase in the concentration of the oil promoted the formation of the beads and reduced the formation of the fibres. The presence of beads in polymer fibres materials compromises their unique properties. Balasubramanian & Kodam, (2014) reported a decrease in specific surface area with an increase beads. The change in morphology of the fibres from beaded free PVA/CNC polymer fibres to the resultant beaded fibres as the oil was added was is due to the difference in liquid phase properties between the oil, CNC, and the PVA. Amiri & Bahrami, (2014) reported that the change in morphology may also be attributed to the change in the entanglement of the polymer chains when the oil was added. The poor electrospinning behaviour may also be due to the low viscosity which results in the formation of an unstable Tyler cone. The reduction in the diameter of the fibres when eucalyptol was added may be attributed to the increase in conductivity of the solution when the oil was added which results in greater elongation forces exerted on the polymer jet thus causing a reduction in diameter of the fibres. Even though polymer fibres with 3 % eucalyptol oil had small diameter as compared to the others, 1 % was taken as the optimum since it had minimum beads.

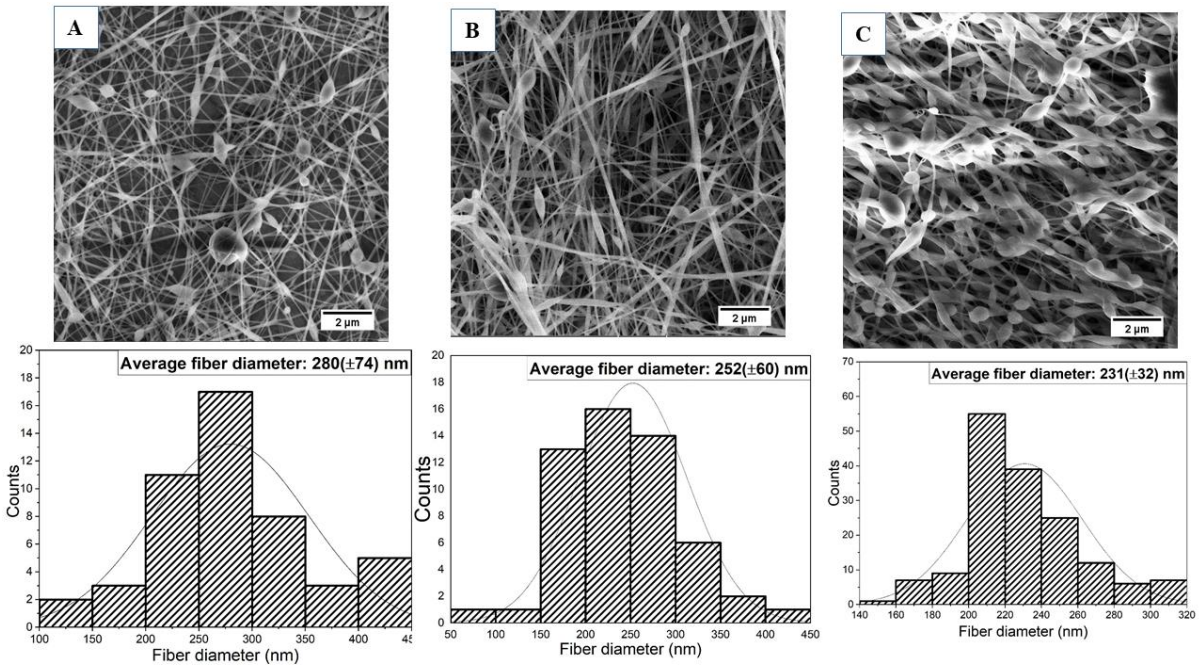

Figure 3.22: SEM image of PVA/CNC polymer fibres incorporated with increasing concentration of Eucalyptus oil A) 1 % B) 2 % and C) 3 % and their respective distribution curves.

(b) FTIR spectroscopic analysis

FTIR spectroscopy was used to study the interaction between the Eucalyptus oil and the PVA/CNC polymer fibres. *Figure 3.22* shows the FTIR spectra for pure PVA/CNC polymer fibres and Eucalyptus oil/PVA/CNC. The spectrum of the bio-composite showed all the typical peaks of PVA/CNC. The peak at 3500 cm^{-1} can be attributed to the O-H stretching vibrations, the absorption bands at 2900, 1400, and 1300 cm^{-1} can be assigned to bending, stretching, rocking, and wagging modes of C-H bands. According to Figure 3.22 (B) which shows the zoomed version of Figure 3.22(A), The Eucalyptol oil/PVA/CNC polymer fibres further showed additional peaks at around 990 cm^{-1} and 1049 cm^{-1} which can be assigned to the CH_2 and C-O-C of the γ-Terpene and 1.8-Cinoele, respectively (Hernández-lópez *et al*., 2019). Miletić *et al*., (2019) Observed a similar FTIR spectrum when they incorporated pomegranate seed oil into both poly (vinyl alcohol) and polyacrylic acid. The spectrum of pure polymer fibres was similar to that of the PVA/PVP incorporated with pomegranate seed oil.

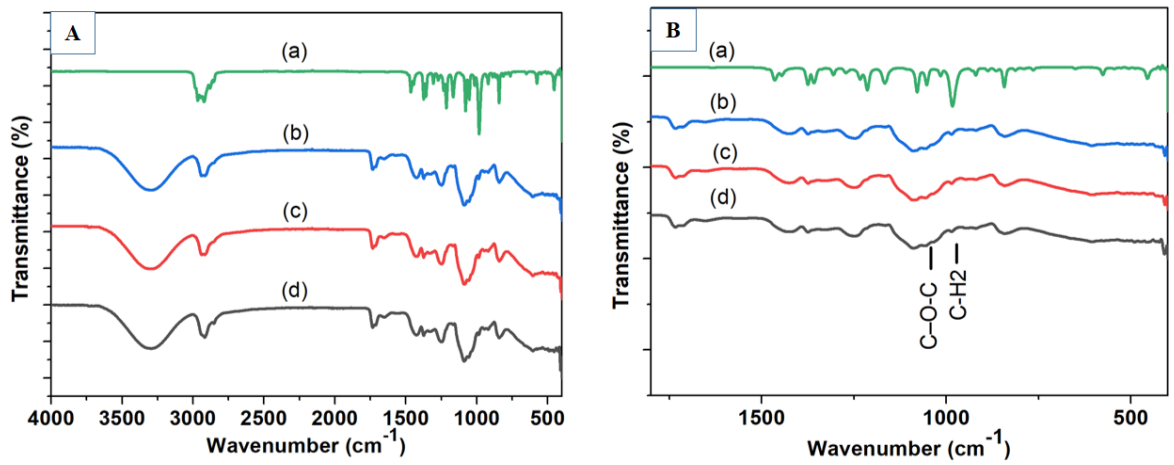

Figure 3.23: FTIR spectra of eucalyptus oil (a) and PVA/CNC incorporated with Eucalyptus oil 1 % (b), 2 % (c) and 3 % (d) And their respective FTIR spectra zoomed (B).

(c) XRD analysis

The XRD diffractogram of neat PVA/CNC polymer fibres compared to PVA/CNC polymer fibres incorporated with the increasing amount of eucalyptus oil is given in *Figure 3.23*. The diffractograms of both the neat PVA/CNC and the bio-composite (eucalyptus oil/PVA/CNC) were similar. The Addition of the eucalyptus oil in the PVA/CNC polymer solution did not influence the structure. However, the peaks became a bit wider as the concentration of the oil increased. According to (Bastos *et al.*, 2012) the peaks became broader due to the disorientation of the molecules in the composite. Krumreich *et al*., (2019) also observed slight changes in the XRD diffractograms of zein polymer fibres when they incorporated avocado oil into the fibres.

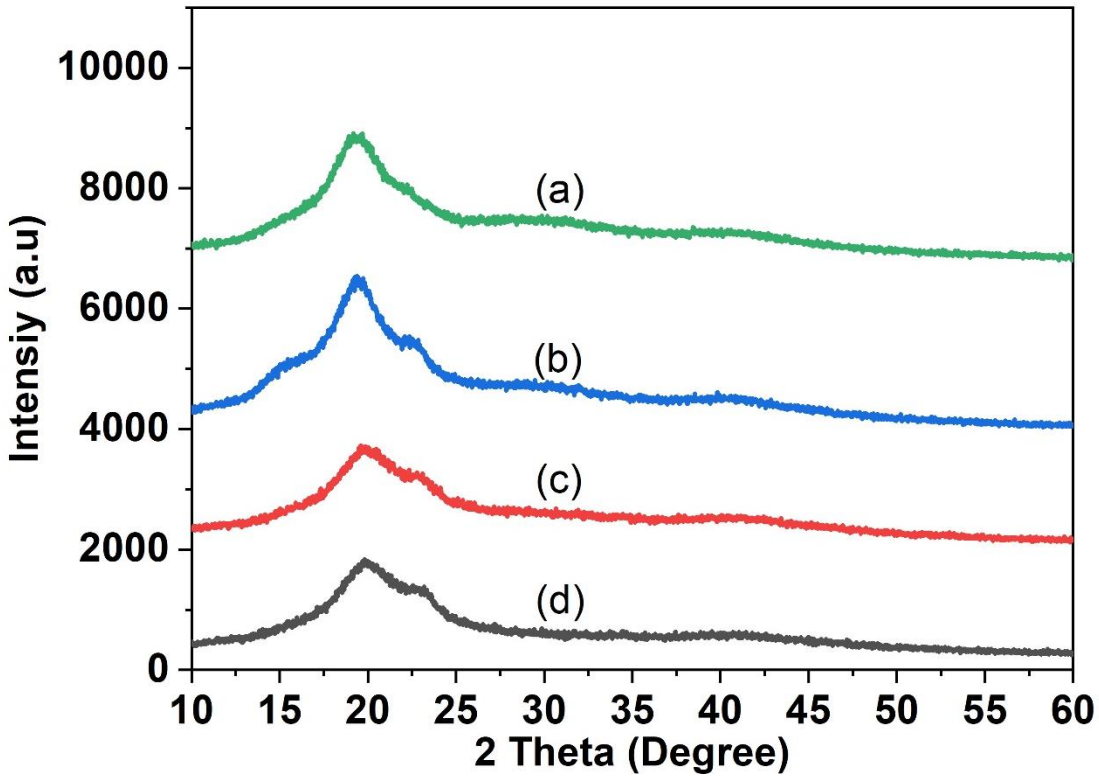

Figure 3.24: X-ray diffraction Patten of neat PVA/CNC (a) incorporated with Eucalyptus oil 1 % (b), 2 % (c) and 3 % (d).

(d) Antibacterial assay: Disk diffusion

The disk diffusion assay was used to study the antibacterial activity of the pure eucalyptus oil and PVA/CNC polymer fibres incorporated with increasing the concentration of the eucalyptus oil (1, 2, and 3 %). Gram-positive *S. aureus* and gram-negative *K. pneumoniae* were used as models. The disk diffusion assay was taken as a qualitative test, rather than a quantitative test since no defined halos were observed around the samples. According to the digital images given in *Figure 3.24,* Pure oil, exhibited a clear zone of inhibition with an undefined shape against gram-negative bacteria (*K. pneumoniae*) and no antibacterial activity against gram-positive bacteria *(s. aureus*) . In contrast, when the oil was incorporated into the PVA/CNC polymer fibres, a small halo which indicates possible inhibition of *S. aureus*, was observed around the polymer fibres. Also, the PVA/CNC incoparated with oil the inhibition of *K. pneumoniae.* The observed antibacterial activity may be due to the synergistic effect between the PVA/CNC and the oil. All the PVA/CNC polymer fibres incorporated with an increasing concentration of the eucalyptus oil exhibited antibacterial activity against both the bacterial strains. However not as good as the PVA/CNC incorporated with silver nanoparticles, *Figure 3.20*. Hafsa et al., (2016) observed similar results when they incorporated eucalyptus oil into

chitosan fibre, pure chitosan did not show any antibacterial activity, High antibacterial activity was exhibited against gram-negative *K. pneumoniae* and the lowest inhibition was observed against gram-positive *S. aureus*. The hydrophobic nature of the essential oils allows them to penetrate lipid layers of the bacterial cell membrane and disturb its structures (Tang *et al.*, 2019).

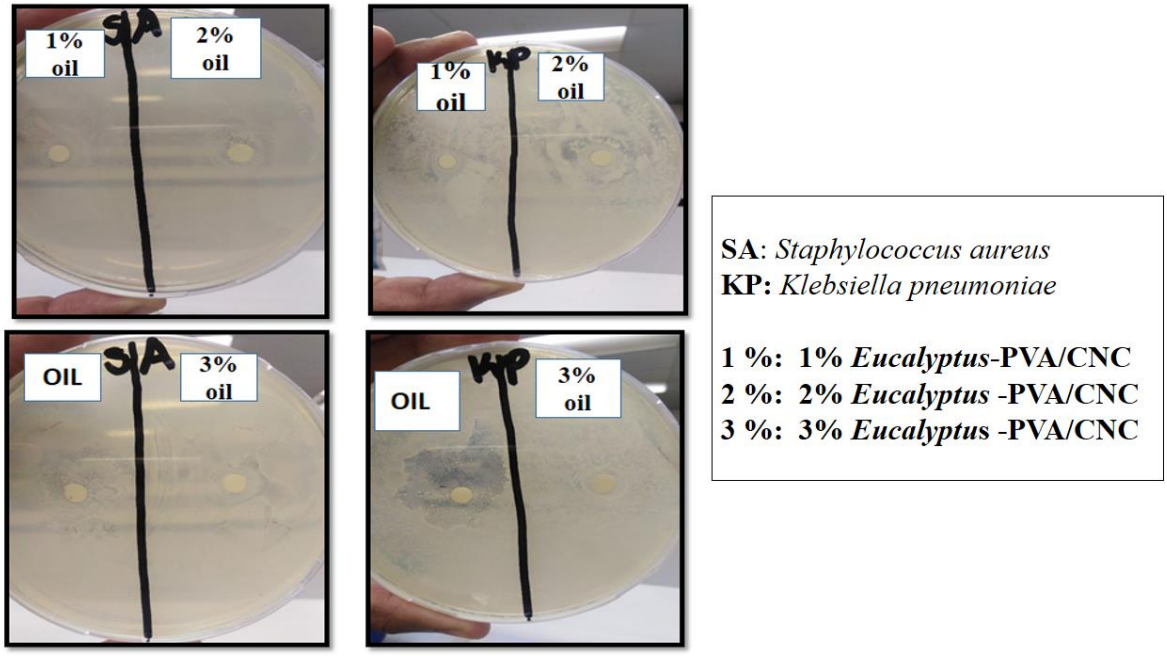

Figure 3.25: Digital images of petri-dishes of eucalyptus oil-PVA/CNC inhibiting the growth of *S. aureus* and *K. pneumoniae.*

3.3.6. Incorporation of AgNPs and eucalyptus oil into the PVA/CNC polymer fibres.

The antibacterial activity of the silver nanoparticles incorporated into the PVA/CNC polymer fibres and eucalyptus oil incorporated into PVA/CNC polymer fibres has been reported in the previous sections. This specific section focussed on the incorporation of both the silver nanoparticles and the eucalyptus oil into the PVA/CNC polymer fibres using the electrospinning technique and also to study their antibacterial synergistic effect against gram-positive (*S. aureus*) and gram-negative (*K. pneumoniae)* bacteria.

(a) Scanning electron microscopic (SEM) analysis

Figure 3.25 shows the SEM of pure PVA/CNC and the bio-composite of AgNPs/eucalyptus oil/ PVA/CNC and their respective distribution curves. The PVA/CNC polymer fibres presented no defects (beads) on the surface while the AgNPs/eucalyptus oil/ PVA/CNC bio-composite had a negligible number of beads on the surface. The beads observed in

AgNPs/oil/PVA/CNC polymer fibres were not as many as the beads on the PVA/CNC incorporated with the eucalyptol. Thus the addition of silver nanoparticles improved the morphology of the polymer fibres. Further on, the diameter of the pure PVA/CNC is 438 nm while the fibres incorporated with both the AgNPs and the eucalyptol oil showed a lower diameter of 260 nm. The reduction in diameter can be attributed to the increase in conductivity when both the AgNPs and the eucalyptol oil were added which resulted in larger elongation forces for the polymer jet.

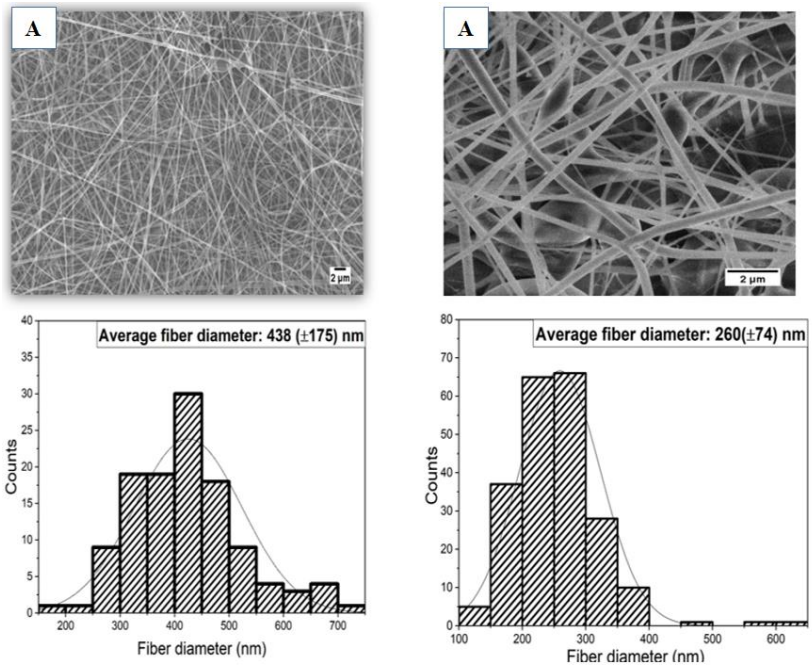

Figure 3.26: SEM image of neat PVA/CNC fibres (A) and AgNPs/ eucalyptus oil /PVA/CNC (B) polymer fibres with their respective distribution curves.

(b) FTIR spectroscopic analysis

FTIR spectroscopy was used to study the interaction between the green synthesised silver nanoparticles, Eucalyptus oil, and the PVA/CNC polymer fibres. *Figure 3.26* shows the FTIR spectra for pure PVA/CNC polymer fibres and bio-composite AgNPs/Eucalyptol oil/PVA/ CNC. The spectrum of the bio-composite showed all the typical peaks of PVA/CNC. The peak at 3500 cm^{-1} can be attributed to the O-H stretching vibrations, the peaks at 2900, 1400, and 1300 cm^{-1} can be assigned to bending, stretching, rocking, and wagging modes of C-H bands. The AgNPs/Eucalyptol oil/PVA/CNC polymer fibres gave additional peaks at around 990 cm^{-1} and 1049 cm^{-1} which can be assigned to the CH_2 and C-O-C of the γ-terpene and 1.8-Cinoele,

respectively thus proving the presence of the eucalyptus oil in the bio-composite

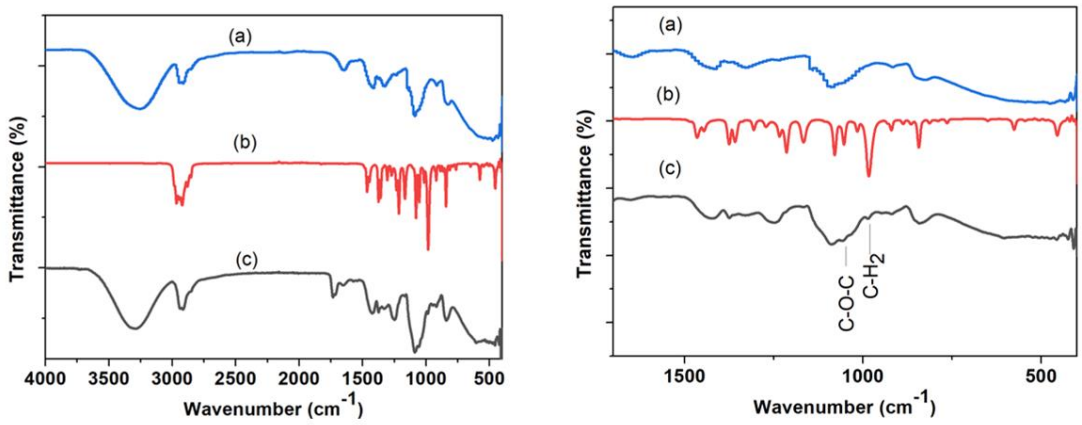

Figure 3.27: FTIR spectra of Pure PVA/CNC (a), Eucalyptus (b), and oil/AgNPs/PVA/CNC (c) and their respective FTIR spectra zoomed (B).

(c) XRD analysis

XRD pattern was used to study the presence of silver nanoparticles (AgNPs) in the bio-composite of AgNPs/Eucalyptol oil/PVA/CNC. The XRD pattern is shown in *Figure 3.27* below. The XRD pattern of AgNPs/Eucalyptol oil /PVA/CNC was similar to that of the AgNPs/PVA/CNC shown in *Figure 3.19*. The peak at 2 theta 20 ° can be attributed to PVA/CNC semi-crystalline peak while the other four peaks at 40 ° correspond to the (111), (111), (200) crystal planes of Ag. Sofi *et al*., (2019) observed a similar XRD pattern when they incorporated lavender oil and the silver nanoparticles into polyurethane polymer fibre. The XRD pattern of polyurethane incorporated with silver nanoparticles was similar to that of polyurethane fibres incorporated with both the silver nanoparticles and lavender oil.

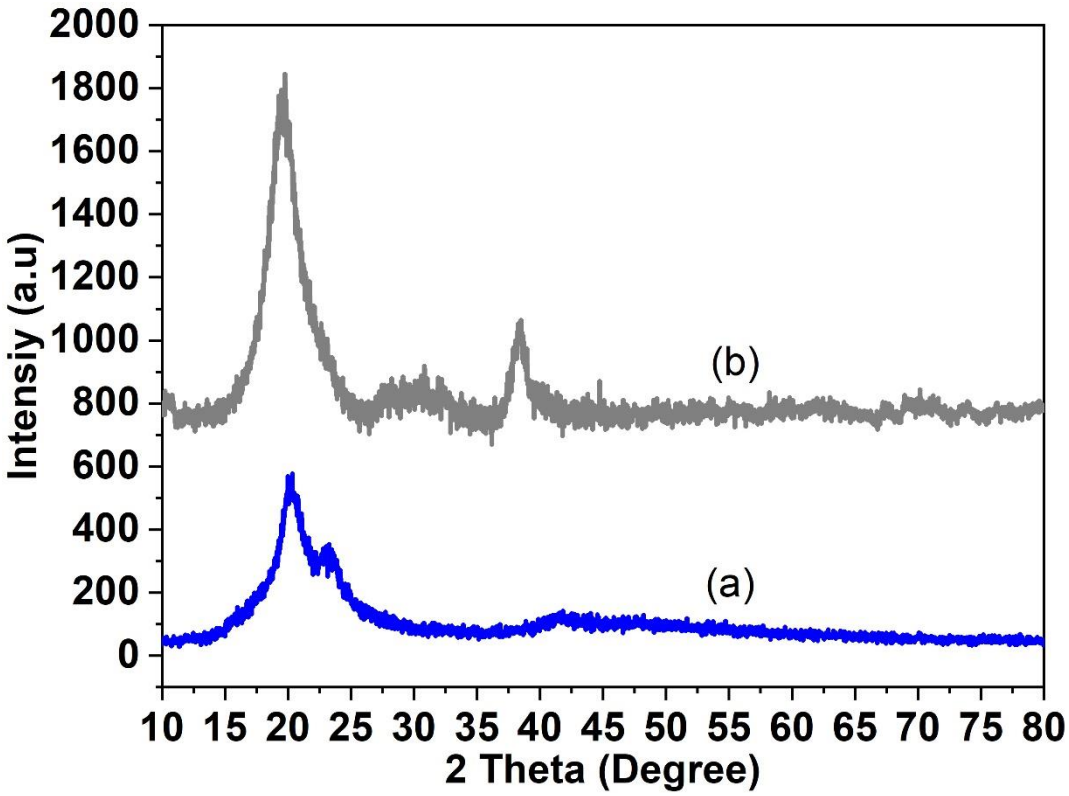

Figure 3.28: X-ray diffraction Patten of Pure PVA/CNC (a) and AgNPs/eucalyptus oil/PVA/CNC (b) polymer fibres.

(d) Antibacterial assay

The disk diffusion assay was used to study the synergistic effect of PVA/CNC incorporated with both the AgNPs and the eucalyptol oil (AgNPs/oil/PVA/CNC). *S. Aureus and K. Pneumoniae* were used as models. PVA/CNC polymer fibres showed no antibacterial activity against gram-positive *S. aureus*, however, a small halo was observed around the PVA/CNC on the petri dish containing the gram-negative bacteria *Figure 3.28*. This may be due to the difference in cell walls between the gram-positive and gram-negative bacteria. The minimum antibacterial activity that was observed was because the PVA/CNC cannot diffuse into the plate, thus only inhibits the growth of the bacteria that is in direct contact with the active site of PVA/CNC polymer fibres (Hafsa *et al.*, 2016). In contrast, the PVA/CNC incorporated with both the eucalyptol oil and the AgNPs was effective in inhibiting the growth of both the gram-positive *S. aureus* and gram-negative *K. pneumonia* as they showed a larger zone of inhibition compared to the PVA/CNC fibres containing AgNPs only *Figure 3.20,* and also the PVA/CNC fibres containing the eucalyptus oil. The observed synergistic effect can be attributed to the various antibacterial mechanisms of the essential oils and silver nanoparticles. The essential oil constituents can attacks the cell membrane through the phospholipids bilayer, disrupt the

enzyme systems which compromise the genetic material of bacteria. Thus forming fatty acid hydroperoxidases caused by oxygenation of unsaturated fatty acid. In case of the silver nanoparticles, there is controversy in antibacterial activity. Many studies have reported that various parameters such as the size, shape, stability, and concentration of the AgNPs influence the antibacterial activity. However in general the AgNPs interacts with the sulphur on the proteins located on the bacterial membrane. The interaction disrupts the membrane permeability causing the intercellular content to leak and compromising the respiration of the cell (Srikhao *et al.*, 2020).

According to the size of the zone of inhibition, the bio-composite was more active against gram-negative bacteria than the gram-positive. The difference in the inhibition of growth of the gram-positive bacteria and gram-negative bacteria can be linked to the difference in the structure of the cell walls and the thickness of the cell walls. Gram-negative bacteria have a thinner (7 – 8 nm) peptidoglycan layer when compared to the gram-positive strain, which has thicker peptidoglycan (20-80 nm). Peptidoglycan is a complex structure that is made of linear polysaccharides chains cross-linked together by peptides. Further on the gram-positive bacteria strains have a layer with strong negative charges from teichoic acids and lipoteichoic acid. This makes it difficult for both the essential oil and silver nanoparticles to penetrate the gram-positive cytoplasmic membrane cell death (Arqués *et al.*, 2008)

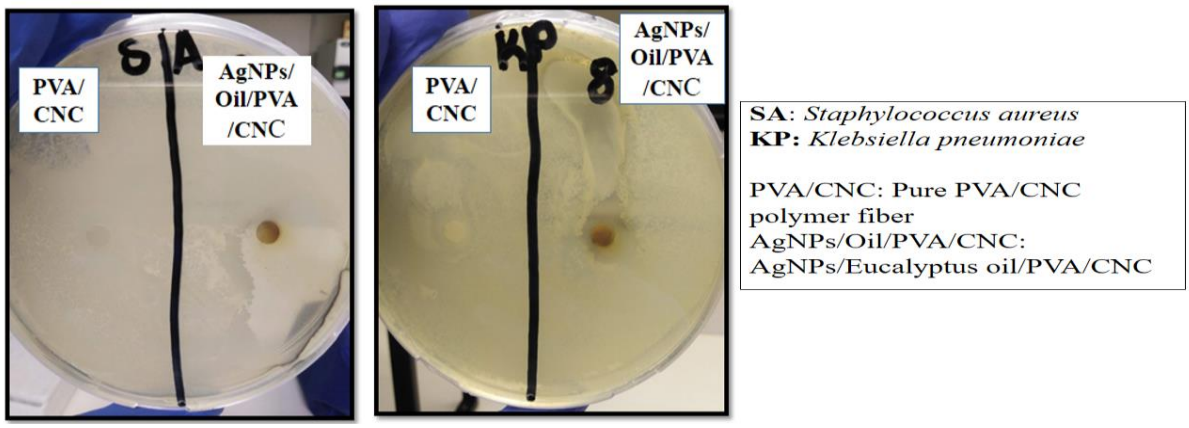

Figure 3.29: Images of petri-dishes of AgNPs/eucalyptus oil/ PVA/CNC inhibiting the growth of *S. aureus* and *K. pneumoniae.*

CHAPTER FOUR

4.1. CONCLUSIONS

Ag nanoparticles were synthesized using increasing concentrations of the aqueous extract of the *Citrus sinensis peels*. The total phenolic and flavonoid content in the plant extracts were found to have increased as the concentration of the crude extract increased from 1-3 %. The AgNPs were characterised using various techniques. According to the UV-Vis spectra, the synthesized Ag exhibited an SPR peak at around 420 nm confirming the successful synthesis of silver nanoparticles. XRD pattern of all the synthesized AgNPs indicated the crystalline structure having face centered cubic planes. FTIR analysis proved the presence of bio-chemicals which played a dual role of reducing Ag^{+} to Ag^{0} and stabilizing the AgNPs. TEM images showed that the nanoparticles that were synthesised using 1 and 2 % plant extracts were agglomerated, while 3 % resulted in the formation of polydispersed, spherical nanoparticles with an average particle size of 10 (±1.2) nm.

Pure cellulose was extracted from hemp fibres through alkalization using sodium hydroxide followed by bleaching using sodium hypochlorite. FTIR spectroscopy proved efficient removal of both hemicellulose and lignin and this can be seen by the disappearance of peaks at 1200 cm^{-1} and 1700 cm^{-1} while the structure of cellulose was maintained as the treatment progressed. Polymer blended fibres of PVA and CNC were fabricated using the electrospinning technique. SEM images showed that the addition of an increasing amount of CNC's into PVA resulted in straight-like fibres with an increased diameter as compared to the neat PVA polymer fibres. The change in morphology of the polymer fibres may be attributed to an increase in viscosity as the CNC's were added into the PVA polymer solution. Another parameter that was optimised was the voltage and according to the SEM images, as the voltage was increased from 17 -21 kV, a decrease in fibres diameter was observed.

The silver nanoparticles that were synthesized using increasing concentration of the aqueous extract of the *Citrus sinensis* peels were incorporated into the PVA/CNC polymer fibres using the electrospinning technique. SEM images showed that the incorporation of silver nanoparticles into the PVA/CNC polymer fibres resulted in flat-like fibres with reduced

diameter and this can be attributed to the increase in conductivity. XRD pattern proved the presence of the AgNPs in the PVA/CNC polymer composite.

Increasing concentrations of the eucalyptus oil were incorporated into the PVA/CNC fibres using the electrospinning technique. According to the SEM images, the addition of an increasing amount of the eucalyptus oil into the PVA/CNC polymer fibres resulted in spindle-like beaded fibres with a decreased diameter and this can be attributed to the decrease in viscosity of the polymer solution. FTIR spectroscopy confirmed the presence of the Eucalyptus oil in the PVA/CNC composites and this was due to the appearance of additional peaks at 990 and 1049 cm^{-1} which can be assigned to the CH_2 and C-O-C of the γ-terpene and 1.8-Cinoele, respectively.

Both the AgNPs and the eucalyptus oil were incorporated into the PVA/CNC polymer fibres. The SEM images showed a decrease in fibres diameter when both the AgNPs and the eucalyptus oil were incorporated into the PVA/CNC polymer fibres. FTIR proved the presence of the eucalyptus oil in the AgNPs/OIL/PVA/CNC composite and XRD proved the presence of silver in the composite. The synthesized silver nanoparticle showed antibacterial activity against both gram-positive and gram-negative bacteria. While Pure PVA/CNC polymer fibres showed no antibacterial activity. PVA/CNC incorporated with AgNPs and the eucalyptus oil showed effective inhibition of both the gram-positive and gram-negative bacteria that were used as models.

4.2. RECOMMENDATIONS

(a). As the concentration of the aqueous extract of the *Citrus sinensis* peels moved from 2 % to 3 %, the AgNPs became more distinct. Thus it is recommended that further optimization of the concentration of the aqueous extract of the *Citrus sinensis* may be conducted using a wider range. Since the shape and size of the synthesised nanoparticles depend on several parameters; it is also recommended to study the effect that other parameters such as the pH of the solution and the concentration of the precursor has on the morphology of the nanoparticles.

(b). The main ingredients of natural fibres are cellulose, lignin, hemicellulose, pectin and waxes thus the extraction of cellulose from the fibres depends on various factors. It is therefore recommended that the rate of reaction and the concentration of both the NaOH and NaOCl that was used to remove unwanted material be optimised.

(c). PVA is known to be highly soluble in water and also absorbs water due to the high amount of the hydroxyl groups thus is recommended to study the water absorption ability and also the solubility of PVA/CNC polymer fibre composite.

(d). The incorporation CNC's into PVA polymer fibres has been reported to improve the mechanical strength of the polymer fibre due to the stiffness of the CNC's. It is therefore recommended to study the tensile strength of the polymer fibres. Several studies have reported on the toxicity of silver nanoparticles when exposed to them at high concentrations. However, is reported that the incorporation of these silver nanoparticles into polymer fibres provides a slow release. It is therefore recommended to study the release study of the AgNPs/Ag^+ from the PVA/CNC polymer fibres.

(e). Essential oils are volatile and highly sensitive to air and light. The incorporation of essential oils into polymer fibres has also been reported to provide the slow release of the oil while protecting them from the external environment. Therefore, it is recommended to conduct the release study of the essential oil from the polymer fibres. The incorporation of the eucalyptus oil into the PVA/CNC polymer fibres resulted in the formation of beads on the surface of the polymer fibres thus compromising the surface area of the fibres. It is, therefore, recommended to add a surfactant to eliminate the formation of beads on the surface of the fibres.

(f). The antibacterial bacteria activity of the Ag nanoparticles, PVA/CNC polymer fibres incorporated with Ag nanoparticles, and also polymer fibres incorporated with eucalyptus oil has been reported in this study. Gram-positive bacterium *S. aureus* with gram-negative bacterium *K. pneumoniae* were used as models. It is recommended to further study the antibacterial activity of all the samples using more bacterial strains and the mechanism in which either the Ag nanoparticles or the eucalyptus oil exhibits antibacterial activity. Also, the toxicity of all the samples should be studied against different cell lines.

4.3. REFERENCES

Aadil, K. R., Mussatto, S. I., & Jha, H. (2018). Synthesis and characterization of silver nanoparticles loaded poly(vinyl alcohol)-lignin electrospun nanofibers and their antimicrobial activity. *International Journal of Biological Macromolecules*, *120*, 763–767.

Abbate, L., Tusa, N., Fatta Del Bosco, S., Strano, T., Renda, A., & Ruberto, G. (2012). Genetic improvement of Citrus fruits: New somatic hybrids from Citrus sinensis (L.) Osb. and Citrus limon (L.) Burm. F. *Food Research International*, *48*(1), 284–290.

Abdel-halim, E. S., & Al-deyab, S. S. (2011). Utilization of hydroxypropyl cellulose for green and efficient synthesis of silver nanoparticles. *Carbohydrate Polymers*, *86*(4), 1615–1622.

Abdel-Mohsen, A. M., Pavliňák, D., Čileková, M., Lepcio, P., Abdel-Rahman, R. M., & Jančář, J. (2019). Electrospinning of hyaluronan/polyvinyl alcohol in presence of in-situ silver nanoparticles: Preparation and characterization. *International Journal of Biological Macromolecules*, *139*, 730–739.

Ago, M., Jakes, J. E., & Rojas, O. J. (2013). *Thermal-Mechanical Properties of Lignin-based Electrospun Nanofibers and Films Reinforced with Cellulose Nanocrystals: A Dynamic Mechanical and Nanoindentation Study*. 5(22):11768-76

Ahmed, A. F., Attia, F. A. K., Liu, Z., Li, C., Wei, J., & Kang, W. (2019). Antioxidant activity and total phenolic content of essential oils and extracts of sweet basil (Ocimum basilicum L.) plants. *Food Science and Human Wellness*, *8*(3), 299–305.

Ahmed, M., Azizi, S., Alloin, F., Sanchez, J., & Dufresne, A. (2004). Cellulose nanocrystals reinforced poly (oxyethylene). *Polymer*. *45*, 4149–4157.

Ahn, E., Jin, H., & Park, Y. (2019). Materials Science & Engineering C Assessing the antioxidant , cytotoxic , apoptotic and wound healing properties of silver nanoparticles green-synthesized by plant extracts. *Materials Science & Engineering C*, *101*(August 2018), 204–216.

Ait-ouazzou, A., & Conchello, P. (2011). *Chemical composition and antimicrobial activity of essential oils of Thymus algeriensis , Eucalyptus globulus and Rosmarinus officinalis from Morocco ´ a Mohammed Bakkali , b*. *2010*, 2643–2651.

Aktürk, A., Erol Taygun, M., Karbancıoğlu Güler, F., Goller, G., & Küçükbayrak, S. (2019). Fabrication of antibacterial polyvinylalcohol nanocomposite mats with soluble starch coated silver nanoparticles. *Colloids and Surfaces A: Physicochemical and Engineering Aspects*, *562*, 255–262.

Albuquerque, B. R., Prieto, M. A., Barreiro, M. F., Rodrigues, A., Curran, T. P., Barros, L., & Ferreira, I. C. F. R. (2017). Catechin-based extract optimization obtained from Arbutus unedo L. fruits using maceration/microwave/ultrasound extraction techniques. *Industrial Crops and Products*, *95*, 404–415.

Ali, Y., Ahmed, J., Hiremath, N., Auras, R., & Joseph, A. (2017). Food Hydrocolloids properties of bionanocomposite fi lms based on fi sh skin gelatin and silver-copper nanoparticles. *Food Hydrocolloids*, *62*, 191–202.

Alipour, R., Khorshidi, A., Shojaei, A. F., Mashayekhi, F., & Moghaddam, M. J. M. (2019). Skin wound healing acceleration by Ag nanoparticles embedded in PVA/PVP/Pectin/Mafenide acetate composite nanofibers. *Polymer Testing*, *79*, 106022.

Amiri, P., & Bahrami, S. H. (2014). Electrospinning of poly(acrylonitrile-acrylic acid)/β cyclodextrin nanofibers and study of their molecular filtration characteristics. *Fibres and Textiles in Eastern Europe*, *103*(1), 14–21.

Andersson, D. I. (2003). Persistence of antibiotic resistant bacteria. *Current Opinion in Microbiology*, *6*(5), 452–456.

Andre, C. M., Hausman, J. F., & Guerriero, G. (2016). Cannabis sativa: The plant of the thousand and one molecules. *Frontiers in Plant Science*, *7*.

Ardekani, N. T., Khorram, M., Zomorodian, K., Yazdanpanah, S., Veisi, H., & Veisi, H. (2019). Evaluation of electrospun poly (vinyl alcohol)-based nanofiber mats incorporated with Zataria multiflora essential oil as potential wound dressing. *International Journal of Biological Macromolecules*, *125*, 743–750.

Arqués, J. L., Rodríguez, E., Nuñez, M., & Medina, M. (2008). Inactivation of Gram-negative pathogens in refrigerated milk by reuterin in combination with nisin or the lactoperoxidase system. *European Food Research and Technology*. 227, 77–82

Augustine, R., Hasan, A., Yadu Nath, V. K., Thomas, J., Augustine, A., Kalarikkal, N., Moustafa, A. E. Al, & Thomas, S. (2018a). Electrospun polyvinyl alcohol membranes

incorporated with green synthesized silver nanoparticles for wound dressing applications. *Journal of Materials Science: Materials in Medicine*, *29*(11).

Augustine, R., Hasan, A., Yadu Nath, V. K., Thomas, J., Augustine, A., Kalarikkal, N., Moustafa, A. E. Al, & Thomas, S. (2018b). Electrospun polyvinyl alcohol membranes incorporated with green synthesized silver nanoparticles for wound dressing applications. *Journal of Materials Science: Materials in Medicine*, *29*(11).

Awal, A., Sain, M., & Chowdhury, M. (2011). Preparation of cellulose-based nano-composite fibers by electrospinning and understanding the effect of processing parameters. *Composites Part B: Engineering*, *42*(5), 1220–1225.

Ba, G. (2020). Phragmites australis as a new cellulose source : Extraction , characterization and adsorption of methylene blue. *Journal of Molecular Liquids* 312 (2020) 113313

Bai, J., Li, Y., Yang, S., Du, J., Wang, S., Zheng, J., Wang, Y., Yang, Q., Chen, X., & Jing, X. (2007). A simple and effective route for the preparation of poly(vinylalcohol) (PVA) nanofibers containing gold nanoparticles by electrospinning method. *Solid State Communications*, *141*(5), 292–295.

Bakhsheshi-Rad, H. R., Ismail, A. F., Aziz, M., Akbari, M., Hadisi, Z., Khoshnava, S. M., Pagan, E., & Chen, X. (2020). Co-incorporation of graphene oxide/silver nanoparticle into poly-L-lactic acid fibrous: A route toward the development of cytocompatible and antibacterial coating layer on magnesium implants. *Materials Science and Engineering C*, *111*, 110812.

Balasubramanian, K., & Kodam, K. M. (2014). Encapsulation of therapeutic lavender oil in an electrolyte assisted polyacrylonitrile nano fi bres for antibacterial applications. *RSC Advances*, *4*, 54892–54901.

Balasundram, N., Sundram, K., & Samman, S. (2006). Phenolic compounds in plants and agri-industrial by-products: Antioxidant activity, occurrence, and potential uses. *Food Chemistry*, *99*(1), 191–203.

Bao, C., Chen, X., Liu, C., Liao, Y., Huang, Y., Hao, L., Yan, H., & Lin, Q. (2021). Extraction of cellulose nanocrystals from microcrystalline cellulose for the stabilization of cetyltrimethylammonium bromide-enhanced Pickering emulsions. *Colloids and*

Surfaces A: Physicochemical and Engineering Aspects, *608*, 125442.

Bar, H., Bhui, D. K., Sahoo, G. P., Sarkar, P., De, S. P., & Misra, A. (2009a). *Colloids and Surfaces A : Physicochemical and Engineering Aspects Green synthesis of silver nanoparticles using latex of Jatropha curcas*. *339*, 134–139.

Barba, F. J., Zhu, Z., Koubaa, M., Sant'Ana, A. S., & Orlien, V. (2016). Green alternative methods for the extraction of antioxidant bioactive compounds from winery wastes and by-products: A review. *Trends in Food Science and Technology*, *49*, 96–109.

Barberia-roque, L., Gámez-espinosa, E., Viera, M., & Bellotti, N. (2019). International Biodeterioration & Biodegradation Assessment of three plant extracts to obtain silver nanoparticles as alternative additives to control biodeterioration of coatings. *International Biodeterioration and Biodegradation*, *141*(December 2017), 52–61.

Basavegowda, N., & Rok Lee, Y. (2013). Synthesis of silver nanoparticles using Satsuma mandarin (Citrus unshiu) peel extract: A novel approach towards waste utilization. *Materials Letters*, *109*, 31–33.

Baskar, K., Sudha, V., Nattudurai, G., Ignacimuthu, S., Duraipandiyan, V., Jayakumar, M., Al-Dhabi, N. A., & Benelli, G. (2018). Larvicidal and repellent activity of the essential oil from Atalantia monophylla on three mosquito vectors of public health importance, with limited impact on non-target zebra fish. *Physiological and Molecular Plant Pathology*, *101*, 197–201.

Bastos, S., Gonc, P., Gomes, K., Araújo, D. L., Helena, M., & Leão, R. (2012). Microencapsulation of cashew apple (Anacardium occidentale , L .) juice using a new chitosan – commercial bovine whey protein isolate system in spray drying. *Food and Bioproducts Processing*, *90*, 683–692.

Bayar, N., Bouallegue, T., Achour, M., Kriaa, M., Bougatef, A., & Kammoun, R. (2017). Ultrasonic extraction of pectin from Opuntia ficus indica cladodes after mucilage removal: Optimization of experimental conditions and evaluation of chemical and functional properties. *Food Chemistry*, *235*, 275–282.

Behravan, M., Hossein, A., Naghizadeh, A., Ziaee, M., Mahdavi, R., & Mirzapour, A. (2019). International Journal of Biological Macromolecules Facile green synthesis of silver nanoparticles using Berberis vulgaris leaf and root aqueous extract and its

antibacterial activity. *International Journal of Biological Macromolecules*, *124*, 148–154.

Bhardwaj, N., & Kundu, S. C. (2010). Electrospinning: A fascinating fiber fabrication technique. *Biotechnology Advances*, *28*(3), 325–347.

Bhat, A. H., Khan, I., Usmani, M. A., Umapathi, R., & Al-Kindy, S. M. Z. (2019). Cellulose an ageless renewable green nanomaterial for medical applications: An overview of ionic liquids in extraction, separation and dissolution of cellulose. *International Journal of Biological Macromolecules*, *129*, 750–777.

Bhattacharya, S., Kim, D., Gopal, S., Tice, A., Lang, K., Dordick, J. S., Plawsky, J. L., & Linhardt, R. J. (2020). Antimicrobial effects of positively charged, conductive electrospun polymer fibers. *Materials Science and Engineering C*, *116*, 111247. 7

Bindhu, M. R., & Umadevi, M. (2013). Synthesis of monodispersed silver nanoparticles using Hibiscus cannabinus leaf extract and its antimicrobial activity. *Spectrochimica Acta - Part A: Molecular and Biomolecular Spectroscopy*, *101*, 184–190.

Bonadies, I., Longo, A., Androsch, R., & Di Lorenzo, M. L. (2019). Biodegradable electrospun PLLA fibers containing the mosquito-repellent DEET. *European Polymer Journal*, *113*, 377–384.

Börjesson, M., & Westman, G. (2015). Crystalline Nanocellulose — Preparation, Modification, and Properties. *Cellulose - Fundamental Aspects and Current Trends*.

Burt, S. (2004). Essential oils : their antibacterial properties and potential applications in foods — a review. *International Journal of Food Microbiology* 94 (2004) 223 – 253 .

Cappellari, L. del R., Santoro, M. V., Nievas, F., Giordano, W., & Banchio, E. (2013). Increase of secondary metabolite content in marigold by inoculation with plant growth-promoting rhizobacteria. *Applied Soil Ecology*, *70*, 16–22.

Cavassin, E. D., Francisco, L., Figueiredo, P. De, Otoch, J. P., Seckler, M. M., Oliveira, R. A. De, Franco, F. F., Marangoni, V. S., Zucolotto, V., Sara, A., Levin, S., & Costa, S. F. (2015). Comparison of methods to detect the in vitro activity of silver nanoparticles (AgNP) against multidrug resistant bacteria. *Journal of Nanobiotechnology*, 1–16.

Chahar, V., Sharma, B., Shukla, G., Srivastava, A., & Bhatnagar, A. (2018). Study of antimicrobial activity of silver nanoparticles synthesized using green and chemical

approach. *Colloids and Surfaces A*, *554*(February), 149–155.

Chahardoli, A., Karimi, N., & Fattahi, A. (2018). Nigella arvensis leaf extract mediated green synthesis of silver nanoparticles : Their characteristic properties and biological efficacy. *Advanced Powder Technology*, *29*(1), 202–210.

Chan, C. H., Yusoff, R., & Ngoh, G. C. (2014). Optimization of microwave-assisted extraction based on absorbed microwave power and energy. *Chemical Engineering Science*, *111*, 41–47.

Chemat, F., Rombaut, N., Sicaire, A. G., Meullemiestre, A., Fabiano-Tixier, A. S., & Abert-Vian, M. (2017). Ultrasound assisted extraction of food and natural products. Mechanisms, techniques, combinations, protocols and applications. A review. *Ultrasonics Sonochemistry*, *34*, 540–560.

Chen, Y. W., Lee, H. V., Juan, J. C., & Phang, S. M. (2016). Production of new cellulose nanomaterial from red algae marine biomass Gelidium elegans. *Carbohydrate Polymers*, *151*, 1210–1219.

Cheok, C. Y., Chin, N. L., Yusof, Y. A., Talib, R. A., & Law, C. L. (2012). Optimization of total phenolic content extracted from Garcinia mangostana Linn. hull using response surface methodology versus artificial neural network. *Industrial Crops and Products*, *40*(1), 247–253.

Chougan, M., Hamidreza, S., Al-kheetan, M. J., & Gecevicius, M. (2020). Industrial Crops & Products Wheat straw pre-treatments using eco-friendly strategies for enhancing the tensile properties of bio-based polylactic acid composites. *Industrial Crops & Products*, *155*(May), 112836.

Çomak, B., Bideci, A., & Salli Bideci, Ö. (2018). Effects of hemp fibers on characteristics of cement based mortar. *Construction and Building Materials*, *169*, 794–799.

Ćujić, N., Šavikin, K., Janković, T., Pljevljakušić, D., Zdunić, G., & Ibrić, S. (2016). Optimization of polyphenols extraction from dried chokeberry using maceration as traditional technique. *Food Chemistry*, *194*, 135–142.

Dakshayani, S. S., Marulasiddeshwara, M. B., Kumar, M. N. S., Ramesh, G., Kumar, P. R., Devaraja, S., & Hosamani, R. (2019). International Journal of Biological Macromolecules Antimicrobial , anticoagulant and antiplatelet activities of green

synthesized silver nanoparticles using Selaginella (Sanjeevini) plant extract. *International Journal of Biological Macromolecules*, *131*, 787–797.

Darben, T., Cominos, B., & Lee, C. T. (1998). Topical eucalyptus oil poisoning. *Australasian Journal of Dermatology*, *39*(4), 265–267.

Darezereshki, E., Alizadeh, M., & Bakhtiari, F. (2011). *A novel thermal decomposition method for the synthesis of ZnO nanoparticles from low concentration ZnSO 4 solutions*. *Applied Clay* . 54(1):107-111

Deng, J., Xu, Z., Xiang, C., Liu, J., Zhou, L., Li, T., Yang, Z., & Ding, C. (2017). Comparative evaluation of maceration and ultrasonic-assisted extraction of phenolic compounds from fresh olives. *Ultrasonics Sonochemistry*, *37*, 328–334.

Deniz, A. E., Vural, H. A., Ortaç, B., & Uyar, T. (2011). Gold nanoparticle/polymer nanofibrous composites by laser ablation and electrospinning. *Materials Letters*, *65*(19–20), 2941–2943.

Dhanavade, M. J., Jalkute, C. B., Ghosh, J. S., & Sonawane, K. D. (2011). Study Antimicrobial Activity of Lemon (Citrus lemon L .) Peel Extract Study Antimicrobial Activity of Lemon (Citrus lemon L .) Peel Extract. *British Journal of Pharmacology and Toxicology.* 2(3): 119-122, 2011

Dias Antunes, M., da Silva Dannenberg, G., Fiorentini, Â. M., Pinto, V. Z., Lim, L. T., da Rosa Zavareze, E., & Dias, A. R. G. (2017). Antimicrobial electrospun ultrafine fibers from zein containing eucalyptus essential oil/cyclodextrin inclusion complex. *International Journal of Biological Macromolecules*, *104*, 874–882.

Ding, B., Yamazaki, M., & Shiratori, S. (2005). Electrospun fibrous polyacrylic acid membrane-based gas sensors. *Sensors and Actuators, B: Chemical*, *106*(1 SPEC. ISS.), 477–483.

Dong, H., Lin, S., Zhang, Q., Chen, H., Lan, W., Li, H., He, J., & Qin, W. (2016). Effect of extraction methods on the properties and antioxidant activities of Chuanminshen violaceum polysaccharides. *International Journal of Biological Macromolecules*, *93*, 179–185.

Doshi, J., & Reneker, D. H. (1995). Electrospinning Process and Applications of Electrospun Fibers. *Journal of Electrostatics, 35, 151-160.*

El-baz, F. K., Darwesh, O. M., & Series, N. (2015). Antiviral – Antimicrobial and schistosomicidal activities of Eucalyptus camaldulensis essential oils. *International Journal of Pharmaceutical Sciences Review and Research,* 31, 262-268.

El Raey, M. A., El-Hagrassi, A. M., Osman, A. F., Darwish, K. M., & Emam, M. (2019). Acalypha wilkesiana flowers: Phenolic profiling, cytotoxic activity of their biosynthesized silver nanoparticles and molecular docking study for its constituents as Topoisomerase-I inhibitors. *Biocatalysis and Agricultural Biotechnology*, 20, 101243.

Elkhaoulani, A., Arrakhiz, F. Z., Benmoussa, K., Bouhfid, R., & Qaiss, A. (2013). Mechanical and thermal properties of polymer composite based on natural fibers: Moroccan hemp fibers/polypropylene. *Materials and Design*, *49*, 203–208.

Evans, S. K., Wesley, O. N., Nathan, O., & Moloto, M. J. (2019). Heliyon Chemically puri fi ed cellulose and its nanocrystals from sugarcane baggase : isolation and characterization. *Heliyon*, *5*, e02635.

Fortunati, E., Puglia, D., Monti, M., Santulli, C., Maniruzzaman, M., & Kenny, J. M. (2013). Cellulose nanocrystals extracted from okra fibers in PVA nanocomposites. *Journal of Applied Polymer Science*, *128*(5), 3220–3230.

Gabriel, T., Belete, A., Syrowatka, F., Neubert, R. H. H., & Gebre-Mariam, T. (2020). Extraction and characterization of celluloses from various plant byproducts. *International Journal of Biological Macromolecules*, *158*, 1248–1258.

Gao, A., Chen, H., Hou, A., & Xie, K. (2019). Efficient antimicrobial silk composites using synergistic effects of violacein and silver nanoparticles. *Materials Science and Engineering C*, *103*, 109821.

Garriga, R., Jurewicz, I., Seyedin, S., Tripathi, M., Pearson, J. R., Cebolla, V. L., Dalton, A. B., Razal, J. M., & Muñoz, E. (2019). Two-dimensional oligoglycine tectomer adhesives for graphene oxide fiber functionalization. *Carbon*, *147*, 460–475.

George, J., Kumar, R., Sajeevkumar, V. A., Ramana, K. V., Rajamanickam, R., Abhishek, V., Nadanasabapathy, S., & Siddaramaiah. (2014). Hybrid HPMC nanocomposites containing bacterial cellulose nanocrystals and silver nanoparticles. *Carbohydrate Polymers*, *105*(1), 285–292. \

Ghalem, B. R., & Mohamed, B. (2008). Antibacterial activity of leaf essential oils of

Eucalyptus globulus and Eucalyptus camaldulensis. *African Journal of Pharmacy and Pharmacology*, *2*(10), 211–215.

Gorinstein, S., Martín-Belloso, O., Park, Y. S., Haruenkit, R., Lojek, A., Íž, M., Caspi, A., Libman, I., & Trakhtenberg, S. (2001). Comparison of some biochemical characteristics of different citrus fruits. *Food Chemistry*, *74*(3), 309–315.

Govindrao, P., Ghule, N. W., Haque, A., & Kalaskar, M. G. (2019). Journal of Drug Delivery Science and Technology Metal nanoparticles synthesis : An overview on methods of preparation , advantages and disadvantages , and applications. *Journal of Drug Delivery Science and Technology*, *53*, 101174.

Greiner, A., & Wendorff, J. H. (2007). Electrospinning: A Fascinating Method for the Preparation of Ultrathin Fibers. A*ngewandte Chemie International Edition*, 46(30), 5670–5703.

Gullberg, E., Cao, S., Berg, O. G., Ilbäck, C., Sandegren, L., Hughes, D., & Andersson, D. I. (2011). Selection of resistant bacteria at very low antibiotic concentrations. *PLoS Pathogens*, *7*(7), 1–9.

Hafsa, J., Smach, M. ali, Ben Khedher, M. R., Charfeddine, B., Limem, K., Majdoub, H., & Rouatbi, S. (2016). Physical, antioxidant and antimicrobial properties of chitosan films containing Eucalyptus globulus essential oil. *LWT - Food Science and Technology*, *68*, 356–364.

Haghighatnia, T., Abbasian, A., & Morshedian, J. (2017). Hemp fiber reinforced thermoplastic polyurethane composite: An investigation in mechanical properties. *Industrial Crops and Products*, *108*, 853–863.

Haider, A., Haider, S., & Kang, I. K. (2018). A comprehensive review summarizing the effect of electrospinning parameters and potential applications of nanofibers in biomedical and biotechnology. In *Arabian Journal of Chemistry*. 11(8) 1165–1188).

Hajji, S., Salem, R. B. S. Ben, Hamdi, M., Jellouli, K., Ayadi, W., Nasri, M., & Boufi, S. (2017). Nanocomposite films based on chitosan–poly(vinyl alcohol) and silver nanoparticles with high antibacterial and antioxidant activities. *Process Safety and Environmental Protection*, *111*, 112–121.

Hamedi, S., & Shojaosadati, S. A. (2019). Rapid and Green Synthesis of Silver Nanoparticles

Using Diospyros lotus Extract : Evaluation of their Biological and Catalytic Activities. *Polyhedron*. 171 . 172–180

Hammi, K. M., Jdey, A., Abdelly, C., Majdoub, H., & Ksouri, R. (2015). Optimization of ultrasound-assisted extraction of antioxidant compounds from Tunisian Zizyphus lotus fruits using response surface methodology. *Food Chemistry*, *184*, 80–89.

Hashim, N., Paramasivam, M., Tan, J. S., Kernain, D., Hussin, M. H., Brosse, N., Gambier, F., & Raja, P. B. (2020). Green mode synthesis of silver nanoparticles using Vitis vinifera's tannin and screening its antimicrobial activity / apoptotic potential versus cancer cells. *Materials Today Communications*, 25, 101511.

Heleno, S. A., Diz, P., Prieto, M. A., Barros, L., Rodrigues, A., Barreiro, M. F., & Ferreira, I. C. F. R. (2016). Optimization of ultrasound-assisted extraction to obtain mycosterols from Agaricus bisporus L. by response surface methodology and comparison with conventional Soxhlet extraction. *Food Chemistry*, *197*, 1054–1063.

Hernández-lópez, M., Correa-pacheco, Z. N., Bautista-baños, S., Zavaleta-avejar, L., Benítez-jiménez, J. J., Sabino-gutiérrez, M. A., & Ortega-gudiño, P. (2019). Bio-based composite fibers from pine essential oil and PLA / PBAT polymer blend . Morphological , physicochemical , thermal and mechanical characterization. *Materials Chemistry and Physics*, *234*, 345–353.

Hernández-morales, L., Espinoza-gómez, H., Flores-lópez, L. Z., Sotelo-barrera, E. L., Núñez-rivera, A., Cadena-nava, R. D., Alonso-núñez, G., & Alejandra, K. (2019). Applied Surface Science Study of the green synthesis of silver nanoparticles using a natural extract of dark or white Salvia hispanica L . seeds and their antibacterial application. *Applied Surface Science*, *489*, 952–961.

Hosseinpour-mashkani, S. M., & Ramezani, M. (2014). Silver and silver oxide nanoparticles : Synthesis and characterization by thermal decomposition. *Materials Letters*, *130*, 259–262.

Ibrahim, H. M. M. (2015). Green synthesis and characterization of silver nanoparticles using banana peel extract and their antimicrobial activity against representative microorganisms. *Journal of Radiation Research and Applied Sciences*, *8*(3), 265–275.

Iravani, S., & Zolfaghari, B. (2013). *Green Synthesis of Silver Nanoparticles Using Pinus*

eldarica Bark Extract. BioMed Research International, 2013, 1–5.

Islam, M. S., Naz, A. N., Alam, M. N., Das, A. K., & Yeum, J. H. (2020). Electrospun poly(vinyl alcohol)/silver nanoparticle/carbon nanotube multi-composite nanofiber mat: Fabrication, characterization and evaluation of thermal, mechanical and antibacterial properties. *Colloids and Interface Science Communications*, *35*, 100247.

Jatoi, A. W. (2020). Polyurethane nanofibers incorporated with ZnAg composite nanoparticles for antibacterial wound dressing applications. *Composites Communications*, *19*, 103–107.

Jazmín Silvero, M. C., Rocca, D. M., Artur de la Villarmois, E., Fournier, K., Lanterna, A. E., Perez, M. F., Cecilia Becerra, M., & Scaiano, J. C. (2018). Selective photoinduced antibacterial activity of amoxicillin-coated gold nanoparticles: From one-step synthesis to in vivo cytocompatibility. *ACS Omega*, *3*(1), 1220–1230.

Jeevanandam, P., Srikanth, C. K., & Dixit, S. (2010). Synthesis of monodisperse silver nanoparticles and their self-assembly through simple thermal decomposition approach. *Materials Chemistry and Physics*, *122*(2–3), 402–407.

Jemilugba, O. T., Hadji, E., Sakho, M., & Parani, S. (2019). Green synthesis of silver nanoparticles using Combretum erythrophyllum leaves and its antibacterial activities. *Colloid and Interface Science Communications*,31, 100191.

Jiang, S., Liu, S., & Feng, W. (2011). PVA hydrogel properties for biomedical application. *Journal of the Mechanical Behavior of Biomedical Materials*, *4*(7), 1228–1233.

John, M. J., & Thomas, S. (2008). Biofibres and biocomposites. *Carbohydrate Polymers*, *71*(3), 343–364.

Jorge de Souza, T. A., Rosa Souza, L. R., & Franchi, L. P. (2019). Silver nanoparticles: An integrated view of green synthesis methods, transformation in the environment, and toxicity. *Ecotoxicology and Environmental Safety*, *171*, 691–700.

Jovanović, A. A., Đorđević, V. B., Zdunić, G. M., Pljevljakušić, D. S., Šavikin, K. P., Gođevac, D. M., & Bugarski, B. M. (2017). Optimization of the extraction process of polyphenols from Thymus serpyllum L. herb using maceration, heat- and ultrasound-assisted techniques. *Separation and Purification Technology*, *179*, 369–380.

Jridi, M., Boughriba, S., Abdelhedi, O., Nciri, H., Nasri, R., Kchaou, H., Kaya, M., Sebai, H.,

Zouari, N., & Nasri, M. (2019). Investigation of physicochemical and antioxidant properties of gelatin edible film mixed with blood orange (Citrus sinensis) peel extract. *Food Packaging and Shelf Life*, *21*.

Kaliamurthi, S., Selvaraj, G., Hou, L., Li, Z., & Wei, Y. (2019). Grain & Oil Science and Technology Synergism of essential oils with lipid based nanocarriers : emerging trends in preservation of grains and related food products. *Grain & Oil Science and Technology*, *2*(1), 21–26.

Kalpana, V. P., & Perarasu, V. T. (2020). Analysis on cellulose extraction from hybrid biomass for improved crystallinity. *Journal of Molecular Structure*, *1217*, 128350.

Kassab, Z., Syafri, E., Tamraoui, Y., Hannache, H., Qaiss, A. E. K., & El Achaby, M. (2020). Characteristics of sulfated and carboxylated cellulose nanocrystals extracted from Juncus plant stems. *International Journal of Biological Macromolecules*, *154*, 1419–1425.

Kaviya, S., Santhanalakshmi, J., Viswanathan, B., Muthumary, J., & Srinivasan, K. (2011). Biosynthesis of silver nanoparticles using citrus sinensis peel extract and its antibacterial activity. *Spectrochimica Acta - Part A: Molecular and Biomolecular Spectroscopy*, *79*(3), 594–598.

Khaleghnezhad, V., Yousefi, A. R., Tavakoli, A., & Farajmand, B. (2019). Interactive effects of abscisic acid and temperature on rosmarinic acid, total phenolic compounds, anthocyanin, carotenoid and flavonoid content of dragonhead (Dracocephalum moldavica L.). *Scientia Horticulturae*, *250*, 302–309.

Khan, M. K., Abert-Vian, M., Fabiano-Tixier, A. S., Dangles, O., & Chemat, F. (2010). Ultrasound-assisted extraction of polyphenols (flavanone glycosides) from orange (Citrus sinensis L.) peel. *Food Chemistry*, *119*(2), 851–858.

Khanjanzadeh, H., Behrooz, R., Bahramifar, N., Pinkl, S., & Gindl-Altmutter, W. (2019). Application of surface chemical functionalized cellulose nanocrystals to improve the performance of UF adhesives used in wood based composites - MDF type. *Carbohydrate Polymers*, *206*, 11–20.

Kim, B., Park, H., Lee, S. H., & Sigmund, W. M. (2005). Poly(a crylic acid) nanofibers by electrospinning. *Materials Letters*, *59*(7), 829–832.

Kim, H. J., Kim, Y.-H., Yang, Y.-H., Lee, S. H., Hong, J. H., Ahn, Y., & Kim, H. (2011). Electrospinning of lignocellulosic biomass using ionic liquid. *Carbohydrate Polymers*, *88*(1), 395–398.

Kim, J. W., Park, H., Lee, G., Jeong, Y. R., Hong, S. Y., Keum, K., Yoon, J., Kim, M. S., & Ha, J. S. (2019). Paper-Like, Thin, Foldable, and Self-Healable Electronics Based on PVA/CNC Nanocomposite Film. *Advanced Functional Materials*, *29*(50).

Konwarh, R., Gogoi, B., Philip, R., Laskar, M. A., & Karak, N. (2011). Biomimetic preparation of polymer-supported free radical scavenging, cytocompatible and antimicrobial "green" silver nanoparticles using aqueous extract of Citrus sinensis peel. *Colloids and Surfaces B: Biointerfaces*, *84*(2), 338–345.

Koosha, M., Raoufi, M., & Moravvej, H. (2019). One-pot reactive electrospinning of chitosan/PVA hydrogel nanofibers reinforced by halloysite nanotubes with enhanced fibroblast cell attachment for skin tissue regeneration. *Colloids and Surfaces B: Biointerfaces*, *179*, 270–279.

Kostic, M., Pejic, B., & Skundric, P. (2008). Quality of chemically modified hemp fibers. *Bioresource Technology*, *99*(1), 94–99.

Borges, C. D., Zavareze, E. R., & Zambiazi, R. C. (2019). *Avocado Oil Incorporated in Ultrafine Zein Fibers by Electrospinning*. 383–392.

Kumar, C. G., & Mamidyala, S. K. (2011). Colloids and Surfaces B : Biointerfaces Extracellular synthesis of silver nanoparticles using culture supernatant of Pseudomonas aeruginosa. *Colloids and Surfaces B: Biointerfaces*, *84*(2), 462–466.

Lee, K. D., & Nagajyothi, P. C. (2011). Synthesis of plant-mediated silver nanoparticles using dioscorea batatas rhizome extract and evaluation of their antimicrobial activities. *Journal of Nanomaterials*, *2011*, 1–7.

Lefsih, K., Giacomazza, D., Dahmoune, F., Mangione, M. R., Bulone, D., San Biagio, P. L., Passantino, R., Costa, M. A., Guarrasi, V., & Madani, K. (2017). Pectin from Opuntia ficus indica: Optimization of microwave-assisted extraction and preliminary characterization. *Food Chemistry*, *221*, 91–99.

Leidy, R., & Ximena, Q. M. (2019). *Trends in Food Science & Technology Use of electrospinning technique to produce nano fi bres for food industries : A perspective*

from regulations to characterisations. *85*, 92–106.

Li, S., Shen, Y., Xie, A., Yu, X., Qiu, L., Zhang, L., & Zhang, Q. (2007). Green synthesis of silver nanoparticles using Capsicum annuum L. extract. *Green Chemistry*, 9(8), 852.

Liakos, I. L., Holban, A. M., Carzino, R., Lauciello, S., & Grumezescu, A. M. (2017). Electrospun fiber pads of cellulose acetate and essential oils with antimicrobial activity. *Nanomaterials*, *7*(4).

Lianfu, Z., & Zelong, L. (2008). Optimization and comparison of ultrasound/microwave assisted extraction (UMAE) and ultrasonic assisted extraction (UAE) of lycopene from tomatoes. *Ultrasonics Sonochemistry*, *15*(5), 731–737.

Logeswari, P., Silambarasan, S., & Abraham, J. (2013). Ecofriendly synthesis of silver nanoparticles from commercially available plant powders and their antibacterial properties. *Scientia Iranica*, *20*(3), 1049–1054.

Logeswari, Peter, Silambarasan, S., & Abraham, J. (2015). Synthesis of silver nanoparticles using plants extract and analysis of their antimicrobial property. *Journal of Saudi Chemical Society*, *19*(3), 311–317.

Lopresto, C. G., Petrillo, F., Casazza, A. A., Aliakbarian, B., Perego, P., & Calabrò, V. (2014). A non-conventional method to extract D-limonene from waste lemon peels and comparison with traditional Soxhlet extraction. *Separation and Purification Technology*, *137*, 13–20.

Luque-García, J. L., & Luque De Castro, M. D. (2004). Ultrasound-assisted Soxhlet extraction: An expeditive approach for solid sample treatment - Application to the extraction of total fat from oleaginous seeds. *Journal of Chromatography A*, *1034*(1–2), 237–242.

Luque de Castro, M. D., & García-Ayuso, L. E. (1998). Soxhlet extraction of solid materials: An outdated technique with a promising innovative future. *Analytica Chimica Acta*, *369*(1–2), 1–10.

Luty-błocho, M., Fitzner, K., Hessel, V., Löb, P., Maskos, M., & Metzke, D. (2011). *Synthesis of gold nanoparticles in an interdigital micromixer using ascorbic acid and sodium borohydride as reducers*. *171*, 279–290.

Luzi, F., Fortunati, E., Puglia, D., Lavorgna, M., Santulli, C., Kenny, J. M., & Torre, L.

(2014). Optimized extraction of cellulose nanocrystals from pristine and carded hemp fibres. *Industrial Crops and Products*, *56*, 175–186.

Magiorakos, A., Srinivasan, A., Carey, R. B., Carmeli, Y., Falagas, M. E., Giske, C. G., Harbarth, S., & Hindler, J. F. (2012). Multidrug-resistant, extensively drug-resistant and pandrug-resistant bacteria: an international expert proposal for interim standard definitions for acquired resistance.*Clinical Microbiology and Infection*, 18(3), 268-281.

Majumdar, M., Khan, S. A., Biswas, S. C., Roy, D. N., Panja, A. S., & Misra, T. K. (2020). In vitro and in silico investigation of anti-biofilm activity of Citrus macroptera fruit extract mediated silver nanoparticles. *Journal of Molecular Liquids*, *302*, 112586.

Martins, N., Barros, L., Santos-Buelga, C., Silva, S., Henriques, M., & Ferreira, I. C. F. R. (2015). Decoction, infusion and hydroalcoholic extract of cultivated thyme: Antioxidant and antibacterial activities, and phenolic characterisation. *Food Chemistry*, *167*, 131–137.

Medeiros, E. S., Mattoso, L. H. C., Offeman, R. D., Wood, D. F., & Orts, W. J. (2008). Effect of relative humidity on the morphology of electrospun polymer fibers. *Canadian Journal of Chemistry*, *86*(6), 590–599.

Melikoğlu, A. Y., Bilek, S. E., & Cesur, S. (2019). Optimum alkaline treatment parameters for the extraction of cellulose and production of cellulose nanocrystals from apple pomace. *Carbohydrate Polymers*, *215*, 330–337.

Miletić, A., Pavlić, B., Ristić, I., Zeković, Z., & Pilić, B. (2019). Encapsulation of fatty oils into electrospun nanofibers for cosmetic products with antioxidant activity. *Applied Sciences* , *9*(15),2955.

Milić, P. S. P. S. ., Rajković, K. M. K. M. ., Stamenković, O. S. O. S. ., & Veljković, V. B. . V. B. (2013). Kinetic modeling and optimization of maceration and ultrasound-extraction of resinoid from the aerial parts of white lady's bedstraw (Galium mollugo L.). *Ultrasonics Sonochemistry*, *20*(1), 525–534.

Minghetti, M., & Schirmer, K. (2016). Effect of media composition on bioavailability and toxicity of silver and silver nanoparticles in fish intestinal cells (RTgutGC). *Nanotoxicology*, 10(10), 1526–1534.

Mochochoko, T., Oluwafemi, O. S., Jumbam, D. N., & Songca, S. P. (2013). Green synthesis

of silver nanoparticles using cellulose extracted from an aquatic weed; Water hyacinth. *Carbohydrate Polymers*, *98*(1), 290–294.

Modenbach, A. A., & Nokes, S. E. (2014). Effects of sodium hydroxide pretreatment on structural components of biomass. *Transactions of the ASABE*, *57*(4), 1187–1198.

Mohamed, M. A., Salleh, W. N. W., Jaafar, J., Ismail, A. F., Abd Mutalib, M., Mohamad, A. B., Zain, M. F., Awang, N. A., & Mohd Hir, Z. A. (2017). Physicochemical characterization of cellulose nanocrystal and nanoporous self-assembled CNC membrane derived from Ceiba pentandra. *Carbohydrate Polymers*, *157*, 1892–1902.

Montaño-Leyva, B., Rodriguez-Felix, F., Torres-Chávez, P., Ramirez-Wong, B., López-Cervantes, J., & Sanchez-Machado, D. (2011). Preparation and characterization of durum wheat (Triticum durum) straw cellulose nanofibers by electrospinning. *Journal of Agricultural and Food Chemistry*, *59*(3), 870–875.

More, D. S., Moloto, M. J., Moloto, N., & Matabola, K. P. (2015). TOPO-capped silver selenide nanoparticles and their incorporation into polymer nanofibers using electrospinning technique. *Materials Research Bulletin*, *65*, 14–22.

Mulyaningsih, S., Sporer, F., Reichling, J., & Wink, M. (2011). Antibacterial activity of essential oils from Eucalyptus and of selected components against multidrug-resistant bacterial pathogens. *Pharmaceutical Biology*, *49*(9), 893–899.

Narayanan, K. B., & Sakthivel, N. (2010). Biological synthesis of metal nanoparticles by microbes. *Advances in Colloid and Interface Science*, *156*(1–2), 1–13.

Nazzaro, F., Fratianni, F., De Martino, L., Coppola, R., & De Feo, V. (2013). Effect of essential oils on pathogenic bacteria. *Pharmaceuticals*, *6*(12), 1451–1474.

Nesrin, K., Yusuf, C., Ahmet, K., Ali, S. B., Muhammad, N. A., Suna, S., & Fatih, Ş. (2020). Biogenic silver nanoparticles synthesized from Rhododendron ponticum and their antibacterial, antibiofilm and cytotoxic activities. *Journal of Pharmaceutical and Biomedical Analysis*, *179*.

Ng, L. Y., Mohammad, A. W., Leo, C. P., & Hilal, N. (2013). Polymeric membranes incorporated with metal/metal oxide nanoparticles: A comprehensive review. In *Desalination*. 308. 15–33.

Nguyen, T. T. T., Tae, B., & Park, J. S. (2011). Synthesis and characterization of nanofiber

webs of chitosan/poly(vinyl alcohol) blends incorporated with silver nanoparticles. *Journal of Materials Science*, *46*(20), 6528–6537.

Oriez, V., Peydecastaing, J., & Pontalier, P.-Y. (2020). Lignocellulosic Biomass Mild Alkaline Fractionation and Resulting Extract Purification Processes: Conditions, Yields, and Purities. *Clean Technologies*, *2*(1), 91–115.

Panichpakdee, J., Larpkiattaworn, S., Nuchchapong, S., Naruepai, B., Leekrajang, M., & Somwongsa, P. (2019). Electrospinning of natural rubber latex-blended polyvinyl alcohol. *Materials Today: Proceedings*, *17*, 2020–2027.

Patel, D. K., Dutta, S. D., Hexiu, J., Ganguly, K., & Lim, K. T. (2020). Bioactive electrospun nanocomposite scaffolds of poly(lactic acid)/cellulose nanocrystals for bone tissue engineering. *International Journal of Biological Macromolecules*, *162*, 1429–1441.

Patil, S. D. (2013). *Synergistic action of cinnamaldehyde with silver nanoparticles against spore-forming bacteria : a case for judicious use of silver nanoparticles for antibacterial applications*. 4721–4731.

Pei, R. S., Zhou, F., Ji, B. P., & Xu, J. (2009). Evaluation of combined antibacterial effects of eugenol, cinnamaldehyde, thymol, and carvacrol against E. coli with an improved method. *Journal of Food Science*, *74*(7).

Pelipenko, J., Kristl, J., Janković, B., Baumgartner, S., & Kocbek, P. (2013). The impact of relative humidity during electrospinning on the morphology and mechanical properties of nanofibers. *International Journal of Pharmaceutics*, *456*(1), 125–134.

Peresin, M. S., Vesterinen, A. H., Habibi, Y., Johansson, L. S., Pawlak, J. J., Nevzorov, A. A., & Rojas, O. J. (2014). Crosslinked PVA nanofibers reinforced with cellulose nanocrystals: Water interactions and thermomechanical properties. *Journal of Applied Polymer Science*, *131*(11).

Pickering, K. L., Efendy, M. G. A., & Le, T. M. (2016). A review of recent developments in natural fibre composites and their mechanical performance. *Composites Part A: Applied Science and Manufacturing*, *83*, 98–112.

Popescu, M. C. (2017). Structure and sorption properties of CNC reinforced PVA films. *International Journal of Biological Macromolecules*, *101*, 783–790.

Popescu, M., Dogaru, B., Goanta, M., & Timpu, D. (2018). International Journal of

Biological Macromolecules Structural and morphological evaluation of CNC reinforced PVA / Starch biodegradable fi lms. *International Journal of Biological Macromolecules*, *116*, 385–393.

Prasad, K., Lekshmi, G. S., Ostrikov, K., Lussini, V., Blinco, J., Mohandas, M., Vasilev, K., Bottle, S., & Bazaka, K. (2017). Synergic bactericidal effects of reduced graphene oxide and silver nanoparticles against Gram- positive and Gram-negative bacteria. *Scientific Reports*, *April*, 1–11.

Prasanna, N. S., & Mitra, J. (2020). Isolation and characterization of cellulose nanocrystals from Cucumis sativus peels. *Carbohydrate Polymers*, *247*, 116706.

Rafiq, M., Hussain, T., Abid, S., Nazir, A., & Masood, R. (2018). *Development of Sodium Alginate/PVA Antibacterial Nanofibers by the Incorporation of Essential Oils*. *Materials Research Express*, 5(3), 035007.

Rafique, M., Sadaf, I., Tahir, M. B., Rafique, M. S., & Nabi, G. (2019). Materials Science & Engineering C Novel and facile synthesis of silver nanoparticles using Albizia procera leaf extract for dye degradation and antibacterial applications. *Materials Science & Engineering C*, *99*(February, 1313–1324.

Rashid, S., Azeem, M., Ali, S., & Maroof, M. (2019). *Colloids and Surfaces B : Biointerfaces Characterization and synergistic antibacterial potential of green synthesized silver nanoparticles using aqueous root extracts of important medicinal plants of Pakistan*. *179*, 317–325.

Ravindra, S., Murali Mohan, Y., Narayana Reddy, N., & Mohana Raju, K. (2010). Fabrication of antibacterial cotton fibres loaded with silver nanoparticles via " Green Approach." *Colloids and Surfaces A: Physicochemical and Engineering Aspects*, *367*(1–3), 31–40.

Ren, S., Dong, L., Zhang, X., Lei, T., Ehrenhauser, F., & Song, K. (2017). Electrospun Nanofibers Made of Silver Nanoparticles, Cellulose Nanocrystals, and Polyacrylonitrile as Substrates for Surface-Enhanced Raman Scattering. *Materials (Basel)*.10(1): 68.

Ren, Yan-yu, Yang, H., Wang, T., & Wang, C. (2019). Bio-synthesis of silver nanoparticles with antibacterial activity. *Materials Chemistry and Physics*, *235*, 121746.

Ren, Yan yu, Yang, H., Wang, T., & Wang, C. (2019). Bio-synthesis of silver nanoparticles

with antibacterial activity. *Materials Chemistry and Physics*, *235*, 121746.

Rezaei, A., Nasirpour, A., & Fathi, M. (2015). Application of cellulosic nanofibers in food science using electrospinning and its potential risk. *Comprehensive Reviews in Food Science and Food Safety*, *14*(3), 269–284.

Rieger, K. A., & Schiffman, J. D. (2014). Electrospinning an essential oil: Cinnamaldehyde enhances the antimicrobial efficacy of chitosan/poly(ethylene oxide) nanofibers. *Carbohydrate Polymers*, *113*, 561–568.

Rodríguez-Solana, R., Salgado, J. M., Domínguez, J. M., & Cortés-Diéguez, S. (2014). Characterization of fennel extracts and quantification of estragole: Optimization and comparison of accelerated solvent extraction and Soxhlet techniques. *Industrial Crops and Products*, *52*, 528–536.

Ruíz-baltazar, Á. D. J., Maya-cornejo, J., Rodríguez-morales, A. L., & Esparza, R. (2019). Results in Physics Alcoholic extracts from Paulownia tomentosa leaves for silver nanoparticles synthesis. *Results in Physics*, *12*, 1670–1679.

Sadhasivam, S., Vinayagam, V., & Balasubramaniyan, M. (2020). Recent advancement in biogenic synthesis of iron nanoparticles. In *Journal of Molecular Structure*,1217, 128372.

Sadlon, A. E., & Lamson, D. W. (2010). Immune-modifying and antimicrobial effects of eucalyptus oil and simple inhalation devices. *Alternative Medicine Review*, *15*(1), 33–47.

Sair, S., Oushabi, A., Kammouni, A., Tanane, O., Abboud, Y., & El Bouari, A. (2018). Mechanical and thermal conductivity properties of hemp fiber reinforced polyurethane composites. *Case Studies in Construction Materials*, *8*, 203–212.

Samrot, A. V., Raji, P., Jenifer Selvarani, A., & Nishanthini, P. (2018). Antibacterial activity of some edible fruits and its green synthesized silver nanoparticles against uropathogen – Pseudomonas aeruginosa SU 18. *Biocatalysis and Agricultural Biotechnology*, *16*, 253–270.

Sanchez-Prado, L., Garcia-Jares, C., Dagnac, T., & Llompart, M. (2015). Microwave-assisted extraction of emerging pollutants in environmental and biological samples before chromatographic determination. *TrAC - Trends in Analytical Chemistry*, *71*, 119–143.

Sati, P., Dhyani, P., Bhatt, I. D., & Pandey, A. (2018). Ginkgo biloba flavonoid glycosides in antimicrobial perspective with reference to extraction method. *Journal of Traditional and Complementary Medicine*, 1–9.

Scandorieiro, S., de Camargo, L. C., Lancheros, C. A. C., Yamada-Ogatta, S. F., Nakamura, C. V., de Oliveira, A. G., Andrade, C. G. T. J., Duran, N., Nakazato, G., & Kobayashi, R. K. T. (2016). Synergistic and additive effect of oregano essential oil and biological silver nanoparticles against multidrug-resistant bacterial strains. *Frontiers in Microbiology*, *7*, 1–14.

Sekar, A. D., Muthukumar, H., Chandrasekaran, N. I., & Matheswaran, M. (2018). Photocatalytic degradation of naphthalene using calcined Fe–ZnO/ PVA nanofibers. *Chemosphere*, *205*, 610–617.

Selvaraj, S., Thangam, R., & Fathima, N. N. (2018). Electrospinning of casein nanofibers with silver nanoparticles for potential biomedical applications. *International Journal of Biological Macromolecules*, *120*, 1674–1681.

Shahzad, A. (2012). Hemp fiber and its composites - A review. *Journal of Composite Materials*, *46*(8), 973–986.

Sharma, V. K., Yngard, R. A., & Lin, Y. (2009a). Silver nanoparticles: Green synthesis and their antimicrobial activities. *Advances in Colloid and Interface Science*, *145*(1–2), 83–96.

Sharma, V. K., Yngard, R. A., & Lin, Y. (2009b). Silver nanoparticles: Green synthesis and their antimicrobial activities. In *Advances in Colloid and Interface Science*.145(1-2),. 83–96).

Siddiqi, K. S., Husen, A., & Rao, R. A. K. (2018). A review on biosynthesis of silver nanoparticles and their biocidal properties. *Journal of Nanobiotechnology*, *16*(1).

Sill, T. J., & von Recum, H. A. (2008). Electrospinning: Applications in drug delivery and tissue engineering. *Biomaterials*, *29*(13), 1989–2006.

Sillard, J. T. C., Szabo, D. P. P., & Daugaard, J. B. A. E. (2017). Chemically extracted nanocellulose from sisal fibres by a simple and industrially relevant process. *Cellulose*, *24*(1), 107–118.

Singh, S., Gaikwad, K. K., & Lee, Y. S. (2018). Antimicrobial and antioxidant properties of

polyvinyl alcohol bio composite films containing seaweed extracted cellulose nano-crystal and basil leaves extract. *International Journal of Biological Macromolecules*, *107*, 1879–1887.

Singh, S. S., Lim, L. T., & Manickavasagan, A. (2020). Ultrasound-assisted alkali-urea pre-treatment of Miscanthus × giganteus for enhanced extraction of cellulose fiber. *Carbohydrate Polymers*, *247*, 116758.

Slavutsky, A. M., & Bertuzzi, M. A. (2014). Water barrier properties of starch films reinforced with cellulose nanocrystals obtained from sugarcane bagasse. *Carbohydrate Polymers*, *110*, 53–61.

Smitha, S. L., Nissamudeen, K. M., Philip, D., & Gopchandran, K. G. (2008). Studies on surface plasmon resonance and photoluminescence of silver nanoparticles. *Spectrochimica Acta - Part A: Molecular and Biomolecular Spectroscopy*, *71*(1), 186–190.

Sobolčiak, P., Ali, A., Hassan, M. K., Helal, M. I., Tanvir, A., Popelka, A., Al-Maadeed, M. A., Krupa, I., & Mahmoud, K. A. (2017). 2D Ti3C2Tx (MXene)-reinforced polyvinyl alcohol (PVA) nanofibers with enhanced mechanical and electrical properties. *PLoS ONE*, 12(8), e0183705.

Sofi, H. S., Akram, T., Tamboli, A. H., Majeed, A., Shabir, N., & Sheikh, F. A. (2019). Novel lavender oil and silver nanoparticles simultaneously loaded onto polyurethane nanofibers for wound-healing applications. *International Journal of Pharmaceutics*, 569, 118590

Sondi, I., & Salopek-sondi, B. (2004). Silver nanoparticles as antimicrobial agent : a case study on E . coli as a model for Gram-negative bacteria. *J Colloid Interface Sci*.275(1):177-82.

Soto, K. M., Quezada-Cervantes, C. T., Hernández-Iturriaga, M., Luna-Bárcenas, G., Vazquez-Duhalt, R., & Mendoza, S. (2019). Fruit peels waste for the green synthesis of silver nanoparticles with antimicrobial activity against foodborne pathogens. *LWT - Food Science and Technology*, *103*, 293–300.

Spagnol, C., Fragal, E. H., Pereira, A. G. B., Nakamura, C. V., Muniz, E. C., Follmann, H. D. M., Silva, R., & Rubira, A. F. (2018). Cellulose nanowhiskers decorated with silver

nanoparticles as an additive to antibacterial polymers membranes fabricated by electrospinning. *Journal of Colloid and Interface Science*, *531*, 705–715.

Sriupayo, J., Supaphol, P., Blackwell, J., & Rujiravanit, R. (2005). Preparation and characterization of α-chitin whisker-reinforced poly(vinyl alcohol) nanocomposite films with or without heat treatment. *Polymer*, *46*(15), 5637–5644.

Subbiah, T., Bhat, G. S., Tock, R. W., Parameswaran, S., & Ramkumar, S. S. (2004). Electrospinning of Nanofibers. *Journal of Applied Polymer Science*, 96, 557–569

Syafiq, R., Sapuan, S. M., Zuhri, M. Y. M., Ilyas, R. A., Nazrin, A., Sherwani, S. F. K., & Khalina, A. (2020). Antimicrobial activities of starch-based biopolymers and biocomposites incorporated with plant essential oils: A review. *Polymers*, *12*(10), 1–26.

Syed, A., & Ahmad, A. (2012). Colloids and Surfaces B : Biointerfaces Extracellular biosynthesis of platinum nanoparticles using the fungus Fusarium oxysporum. *Colloids and Surfaces B: Biointerfaces*, *97*, 27–31.

Symington, M. C., Banks, W. M., West, O. D., & Pethrick, R. A. (2009). Tensile testing of cellulose based natural fibers for structural composite applications. *Journal of Composite Materials*, *43*(9), 1083–1108.

Tan, S. H., Inai, R., Kotaki, M., & Ramakrishna, S. (2005). Systematic parameter study for ultra-fine fiber fabrication via electrospinning process. *Polymer*, *46*(16), 6128–6134.

Tan, X. Y., Abd Hamid, S. B., & Lai, C. W. (2015). Preparation of high crystallinity cellulose nanocrystals (CNCs) by ionic liquid solvolysis. *Biomass and Bioenergy*, *81*, 584–591.

Tang, Y., Lan, X., Liang, C., Zhong, Z., Xie, R., Zhou, Y., Miao, X., Wang, H., & Wang, W. (2019). Honey loaded alginate/PVA nanofibrous membrane as potential bioactive wound dressing. *Carbohydrate Polymers*, *219*, 113–120.

Tarabet, L., Loubar, K., Lounici, M. S., Hanchi, S., & Tazerout, M. (2012). Eucalyptus biodiesel as an alternative to diesel fuel: Preparation and tests on di diesel engine. *Journal of Biomedicine and Biotechnology*, *2012*.

Thakkar, K. N., Mhatre, S. S., & Parikh, R. Y. (2010). Biological synthesis of metallic nanoparticles. *Nanomedicine: Nanotechnology, Biology, and Medicine*, *6*(2), 257–262.

Thomas, B., Mary, S., Vithiya, B., & Arul, T. A. (2019). ScienceDirect Antioxidant and

Photo Catalytic Activity Of Aqueous Leaf Extract Mediated Green Synthesis Of Silver Nanoparticles Using Passiflora Edulis F . Flavicarpa. *Materials Today: Proceedings*, *14*, 239–247.

Vasileva, P., Donkova, B., Karadjova, I., & Dushkin, C. (2011). Synthesis of starch-stabilized silver nanoparticles and their application as a surface plasmon resonance-based sensor of hydrogen peroxide. *Colloids and Surfaces A: Physicochemical and Engineering Aspects*, *382*(1–3), 203–210.

Verma, C., Chhajed, M., Gupta, P., Roy, S., & Maji, P. K. (2021). International Journal of Biological Macromolecules Isolation of cellulose nanocrystals from different waste bio-mass collating their liquid crystal ordering with morphological exploration. *International Journal of Biological Macromolecules*, *175*, 242–253.

Vieira, V., Prieto, M. A., Barros, L., Coutinho, J. A. P., Ferreira, O., & Ferreira, I. C. F. R. (2017). Optimization and comparison of maceration and microwave extraction systems for the production of phenolic compounds from Juglans regia L. for the valorization of walnut leaves. *Industrial Crops and Products*, *107*, 341–352.

Vigneshwaran, N., Ashtaputre, N. M., Varadarajan, P. V, Nachane, R. P., Paralikar, K. M., & Balasubramanya, R. H. (2007). *Biological synthesis of silver nanoparticles using the fungus Aspergillus flavus*. Materials Letters, *61(6)*, 1413–1418.

Vilela, D., Stanton, M. M., & Parmar, J. (2017). Microbots decorated with silver nanoparticles kill bacteria in aqueous media. A*CS Appl Mater Interfac*es

.9(27).22093-22100.

Vinatoru, M. (2001). An overview of the ultrasonically assisted extraction of bioactive principles from herbs. *Ultrasonics Sonochemistry*, *8*(3), 303–313.

Wang, S., Chen, F., Wu, J., Wang, Z., Liao, X., & Hu, X. (2007). Optimization of pectin extraction assisted by microwave from apple pomace using response surface methodology. *Journal of Food Engineering*, *78*(2), 693–700.

Wang, T., & Zhao, Y. (2021). Optimization of bleaching process for cellulose extraction from apple and kale pomace and evaluation of their potentials as film forming materials. *Carbohydrate Polymers*, *253*, 117225.

Worthington, R. J., & Melander, C. (2013). Combination approaches to combat multidrug-

resistant bacteria. *Trends in Biotechnology*, *31*(3), 177–184.

Wu, J., Liu, H., Ge, S., Wang, S., Qin, Z., Chen, L., Zheng, Q., Liu, Q., & Zhang, Q. (2015). The preparation, characterization, antimicrobial stability and invitro release evaluation of fish gelatin films incorporated with cinnamon essential oil nanoliposomes. *Food Hydrocolloids*, *43*, 427–435.

Wu, Y., Wu, J., Yang, F., Tang, C., & Huang, Q. (2019). Effect of H2O2 bleaching treatment on the properties of finished transparent wood. *Polymers*, *11*(5), 1–13.

Xing, L., Hu, C., Zhang, W., Guan, L., & Gu, J. (2020). Transition of cellulose supramolecular structure during concentrated acid treatment and its implication for cellulose nanocrystal yield. *Carbohydrate Polymers*, *229*, 115539.

Xu, D. P., Zheng, J., Zhou, Y., Li, Y., Li, S., & Li, H. Bin. (2017). Ultrasound-assisted extraction of natural antioxidants from the flower of Limonium sinuatum: Optimization and comparison with conventional methods. *Food Chemistry*, *217*, 552–559.

Xu, X., Yang, Y., Xing, Y., Yang, J., & Wang, S. (2013). *P*roperties of novel polyvinyl alcohol / cellulose nanocrystals / silver nanoparticles blend membranes. *Carbohydrate Polymers*, 98(2):1573-1577

Yang, J., Lu, X., Zhang, Y., Xu, J., Yang, Y., & Zhou, Q. (2020). A facile ionic liquid approach to prepare cellulose fiber with good mechanical properties directly from corn stalks. *Green Energy and Environment*, *5*(2), 223–231.

Yang, S., Jin, X., Liu, K., & Jiang, L. (2013). Nanoparticles assembly-induced special wettability for bio-inspired materials. *Particuology*, *11*(4), 361–370.

Yeshchenko, O. A., Dmitruk, I. M., Alexeenko, A. A., Kotko, A. V., Verdal, J., & Pinchuk, A. O. (2012). Size and Temperature Effects on the Surface Plasmon Resonance in Silver Nanoparticles. *Plasmonics*, *7*(4), 685–694.

Yolmeh, M., Habibi Najafi, M. B., & Farhoosh, R. (2014). Optimisation of ultrasound-assisted extraction of natural pigment from annatto seeds by response surface methodology (RSM). *Food Chemistry*, *155*, 319–324.

Zargham, S., Bazgir, S., Tavakoli, A., Rashidi, A. S., & Damerchely, R. (2012). The effect of flow rate on morphology and deposition area of electrospun nylon 6 nanofiber. *Journal of Engineered Fibers and Fabrics*, *7*(4), 42–49.

Zhang, H., Chen, Y., Wang, S., Ma, L., Yu, Y., Dai, H., & Zhang, Y. (2020). Extraction and comparison of cellulose nanocrystals from lemon (Citrus limon) seeds using sulfuric acid hydrolysis and oxidation methods. *Carbohydrate Polymers*, *238*(2), 116180.

Zhang, X., Yan, S., Tyagi, R. D., & Surampalli, R. Y. (2011). Chemosphere Synthesis of nanoparticles by microorganisms and their application in enhancing microbiological reaction rates. *Chemosphere*, *82*(4), 489–494.

Zimniewska, M., Wladyka-przybylak, M., & Mankowski, J. (2011). Cellulose Fibers: Bio- and Nano-Polymer Composites. *Cellulose Fibers: Bio- and Nano-Polymer Composites*. 97-119.

Zou, Y., Zhang, C., Wang, P., Zhang, Y., & Zhang, H. (2020). Electrospun chitosan / polycaprolactone nanofibers containing chlorogenic acid-loaded halloysite nanotube for active food packaging. *Carbohydrate Polymers*, *247*, 116711.